Minimum BER Block Precoders for Zero-forcing Equalization

MASTER OF ENGINEERING (2001) MCMASTER UNIVERSITY

(Electrical and Computer Engineering) Hamilton, Ontario

TITLE: **Minimum BER Block Precoders for Zero-forcing Equalization**

AUTHOR: Yanwu Ding

Diploma Eng. (Electrical)

Northern Jiaotong University, Beijing, China, 1992

SUPERVISOR: Dr. K. Max Wong

CO-SUPERVISOR: Dr. Timothy N. Davidson

NUMBER OF PAGES: xi, 91

Dedications:

To my loving son

Abstract

In this thesis the linear precoder which minimizes the bit error rate (BER) is derived for block transmission systems in which zero forcing (ZF) equalization and threshold detection are applied. Because the bit error rate for block transmission is a highly non-linear function of the precoder parameters, its minimization has been regarded as being difficult to implement. Therefore designers have attempted to find low BER precoders indirectly by optimizing alternative objectives, such as minimizing the Mean Square Error (MMSE), or maximizing the received signal-to-noise ratio (SNR). However, these precoders do not minimize the BER directly, and it is this problem which is the subject of the thesis.

The block transmission systems considered in this thesis employ block by block processing at the receiver, and therefore elimination of inter-block interference (IBI) is desirable. We will design Minimum BER (MBER) precoders for two schemes which eliminate IBI, namely zero padding (ZP) and cyclic prefix (CP). Based on the bit error rate formula derived in the thesis, an analytic solution for the MBER precoder at moderate-to-high SNRs is derived via a two-stage optimization process using Jensen's inequality. At moderate-to-high SNRs, the bit error rate is a convex function of the autocorrelation matrix which is, itself, a function of the precoder matrix because of the use of a zero-forcing equalizer. Simulations and analyses are given to the two sets of precoders based on ZP and CP respectively to verify the optimal precoders derived. The BER improvement of the ZP-MBER/CP-MBER precoders over other ZP/CP precoders is substantial, and the ZP-MBER precoder is superior to the CP-MBER precoder in performance. The latter also outperforms the scheme of discrete multi-tone (DMT) with water filling power loading, and cyclic prefix orthogonal frequency division multiplexing (CP-OFDM). The CP-MBER precoder is shown to be a two-stage modification

of the transmitting scheme for standard DMT. Firstly the water filling algorithm is replaced by the MMSE power loading algorithm suggested in the thesis, and secondly, the power loading is augmented by multiplication with a DFT matrix. It is shown that the CP-MBER precoder does not require more power to transmit a cyclic prefix than the CP-OFDM or water-filling DMT precoder.

A simple test which determines whether the SNR is high enough for our MBER precoder design to be optimal is provided. Furthermore, methods to guarantee sufficient SNR are suggested. One can either increase the transmitting power, or drop sub-channels and hence avoid transmission on the sub-channels which correspond to the small eigen-values of the channel. The MBER precoder design after dropping sub-channels is also discussed.

For the precoders which are characterized by an arbitrary unitary matrix in their solutions, the optimal unitary matrix which minimizes the BER is designed. Therefore, minimization of BER is achieved within the optimal solution set of the precoders. Applications of the design are discussed. Simulations and analytic evaluations are presented to show the BER improvement provided by the optimal unitary matrix.

Acknowledgements

The two year graduate study at McMaster University is a most valuable memory in my life, not only because I have been led to an exciting field, digital signal processing and communication systems which were totally new to me before, but also I have got the opportunity to learn the state-of-the-art technologies under the supervisions of excellent professors in the Advanced Signal Processing for Communications Group, Dept. of Electrical Computer Engineering.

I would like to thank my supervisor Dr. K. M. Wong and co-supervisor Dr. T. N. Davidson for their consistent supervision and encouragement throughout my study and research, their patient guidance on improving my skills of writing and presentation.

My warmest thanks also go to Dr. J. Zhang who helped me in the mathematical model formulation of my project, Dr. J. P. Reilly who helped me on the problems I have about matrix computation, and Dr. T. Luo who contributed comments and suggestions on the results of my research.

I am most grateful to C. Gies and H. Jachna, the secretaries of Dept. of ECE, their constant willingness to help makes my graduate study a very enjoyable experience.

I would also like to thank my friend, H. Tang, a graduate student in the Advanced Signal Processing for Communications Group, for reading part of my thesis, her suggestions and comments are really appreciated.

Acronyms

ADSL	Asymmetric Digital Subscriber Lines
BER	Bit Error Rate
BPSK	Binary Phase Shift Keying
CDMA	Code Division Multiple Access.
CP	Cyclic Prefix
DAB/DVB	Digital Audio and Video Terrestrial Broadcasting
DF	Decision-Feedback
DMT	Discrete Multi-Tone
FDMA	Frequency Division Multiple Access
HDSL	High bit rate Digital Subscriber Lines
IBI	Inter-Block Interference (IBI)
ISI	Inter-Symbol Interference
LTI	Linear Time Invariant
LZ	Leading Zero
MBER	Minimum BER
MLSE	Maximum-Likelihood Sequence Estimation
MMSE	Minimum Mean Square Error
MSE	Mean Square Error
OFDM	Orthogonal Frequency Division Multiplexing
QPSK	Quadrature Phase Shift Keying
SNR	Signal-to-Noise Ratio
TDMA	Time Division Multiple Access

ZFE	Zero-Forcing Equalization
ZP	Zero Padding

Notations

$\boldsymbol{A}$	Matrix $\boldsymbol{A}$
$\boldsymbol{a}$	Vector $\boldsymbol{a}$
$\lvert\cdot\rvert$	Determinate of matrix
$tr(\cdot)$	Trace of matrix
$E\{\cdot\}$	Expectation
$[\cdot]_{ij}$	The i,jth element
$\boldsymbol{A}^{\dagger}$	Pseudo-inverse of $\boldsymbol{A}$
$\boldsymbol{A}^{H}$	Hermitian $\boldsymbol{A}$
$\boldsymbol{A}^{*}$	Conjugate of $\boldsymbol{A}$
$\boldsymbol{A}^{T}$	Transpose of $\boldsymbol{A}$

List of Figures

Chapter 1

Introduction

1.1 Performance of the transmission system and precoding

Two important performance measures for a communication system are the transmission rate and the bit error rate. These measures capture the efficiency/capability and reliability of the transmission system. High transmission rate and low bit error rate are two pursuits for communication systems. In practice the two goals may be conflicting — a higher transmission rate may result in an increase in the bit error rate. The reason is that high-speed digital communication systems require that the channel has a bandwidth large enough to accommodate the essential frequency content of the data stream which has a broad spectrum, and the width of this spectrum increases at higher rates. Typically, however, the channel in practical communication systems is band-limited and dispersive, and thus introduces distortions in the received signal. In such circumstances, one bit in a data sequence is affected by other bits at the receiving terminal — an effect which is called intersymbol interference (ISI). Because ISI causes errors in the reconstruction of the transmitted data at receiver, it is desired to eliminate it or make it as small as possible in order to have a reliable high-speed data transmission. Efforts to combat ISI have been made at the receiver or the transmitter, or both. A classical technique employed at the receiver is equalization. Equalizers can be classified as linear and nonlinear. The standard zero-forcing (ZF) equalizer and minimum mean

square error (MMSE) equalizer are linear ones, while the decision-feedback (DF) equalizer and maximum-likelihood sequence estimation (MLSE) equalizer are nonlinear ones. Nonlinear equalizers can provide better performance but demand more computational budget, while linear ones are attractive because of their simple structure and low computational cost. Equalization can also be used at the transmitter, which has been known as pre-equalization or precoding [13], [29]. It has been shown to be an effective technique for approaching the capacity of high-SNR band limited channels [10], in addition to being a method to overcome ISI.

1.2 Block transmission and precoding

Block transmission is commonly used for communicating over dispersive channels affected by ISI [27], because it reduces the complexity of the equalization required to achieve a given level of performance. It can also reduce the susceptibility to most forms of impulse noise [1]. Examples of block transmission include orthogonal frequency division multiplexing (OFDM) and discrete multitone (DMT) [32]. OFDM has been selected as the standard modulation schemes for digital audio and video terrestrial broadcasting (DAB/DVB) in Europe, and DMT [6] has been applied in wireline modems, high bit rate digital subscriber lines (HDSL) and asymmetric digital subscriber lines (ADSL). In block transmission the transmitted data stream is divided into consecutive blocks usually with equal size. Because the channel is dispersive, one data block may be affected by other blocks at receiver, therefore interblock interference (IBI) is introduced. For better reconstruction of the transmitting blocks at receiver, it is desired to eliminate IBI. This can be realized by a precoder which introduces a certain amount of redundancy. Furthermore, the precoder can be designed to achieve various criteria of optimality such as maximum information rate, minimum mean square error or maximum received signal-to-noise ratio (SNR) [27], [28]. In this thesis, the precoder is to be designed to reach minimum BER.

1.3 Motivation for the work

Because of the potential of precoders in block transmission, much attention has been given to their optimal designs towards the two goals for communication systems, namely high transmission rate and low bit error rate. To reach the first goal an optimal precoder is designed by maximizing information rate or channel capacity [27]. As for the second goal, since the minimization of the bit error rate in block transmission is difficult to deal with due to its high nonlinearity, precoders to minimize BER directly have rarely been tackled in the literature. However alternative criteria have been proposed such as minimizing the mean square error at receiver, or maximizing the received SNR [28], [19]. In [28] the MMSE precoders are designed for ZF and MMSE equalizers respectively assuming the exact channel knowledge is available. In [19] the MMSE precoder is designed for ZF equalization under the assumption that the exact channel information is not known but its second-order statistics are known by the precoder. Because these precoders are not designed directly for minimizing BER, minimum bit error rate can not be guaranteed. This motivates us to explore the challenging problem to design the optimal precoder by minimizing BER directly.

1.4 Contributions of the thesis

The thesis focuses on the design of precoders which minimize BER for block transmission systems in which zero-forcing equalization and threshold detection are employed. The inter-block interference (IBI) is eliminated by zero padding (ZP) or by adding a cyclic prefix (CP). The main contributions of thesis are:

- An analytic solution for the minimum BER (MBER) precoder is derived and a simple test for its validity is suggested.
- A flexible scheme for dropping sub-channels based on the SNR and the corresponding MBER precoders are proposed.
- The factors that affect the BER performance of a precoder are studied and the relationship of MBER precoder and MMSE precoder is revealed.

- A comparison between the structure of the MBER precoder for CP systems and the standard DMT precoder is provided. The extra power spent on transmitting cyclic prefix for CP systems is also evaluated.
- For the precoders which are characterized by an arbitrary unitary matrix in their solutions, the optimal unitary matrix which minimizes BER is derived.

1.5 Structure of the thesis

The thesis is organized as follows. The block transmission model, assumptions made in the thesis, and the schemes to eliminate IBI are presented in Chapter 2. Chapter 3 explores the MBER precoder design based on the BER formula derived. The analytic solutions are derived for the two schemes of eliminating IBI based on the Jensen's inequality. A simple test for the validity of the analytic solutions and ways to ensure it are described. A flexible scheme of dropping sub-channels and the corresponding MBER precoders are proposed. The relationship between MBER and MMSE precoders, and in particular, the comparison between the CP-MBER precoder and the standard DMT precoder is discussed. The extra power spent on transmitting cyclic prefix in CP-MBER, CP-OFDM and water-filling DMT precoders are evaluated. Analytical evaluations and analyses of the BER performance of the various schemes are given. For the class of precoders whose solutions include an arbitrary unitary matrix, the optimal unitary matrix is designed by minimizing BER in Chapter 4, with the applications of the design. Conclusions are provided in Chapter 5, along with the discussion of future work. Some mathematical derivations such as the block BER formula, complex matrix derivative, the extra power spent on transmitting cyclic prefix in CP-MBER precoder are found in the Appendices.

Chapter 2

Block Transmission System

In this chapter the model for block transmission system used in the thesis and the schemes to mitigate IBI are described.

2.1 Multirate discrete-time transceiver model

The model for the block transmission system we use in the thesis is the baseband multirate discrete-time transmitter/channel/receiver model proposed in [28]. It is regarded as a general baseband transmission/reception model for block transmission system because it provides a unifying framework that encompasses not only many existing block transmission schemes such as OFDM, DMT, but also many multiple access techniques, including time division multiple access (TDMA), frequency division multiple access (FDMA), and code division multiple access (CDMA).

The model is illustrated in Figure 2.1. The serial transmitting data stream is converted to M-parallel substreams by downsampling of M. The substreams are then upsampled by P (inserting $P-1$ zeros between samples) and filtered by the transmitter filterbank which is also known as the precoder with impulse response denoted by $\{f_m(n)\}$, $m = 0, \cdots, M-1$. The upsampling rate P is chosen to be greater than M, and hence redundancy is introduced with a redundancy rate $(P-M)/P$. The parallel streams are converted to a serial sequence $u(n)$ by summing up the precoder outputs. The precoded sequence $u(n)$ is then launched

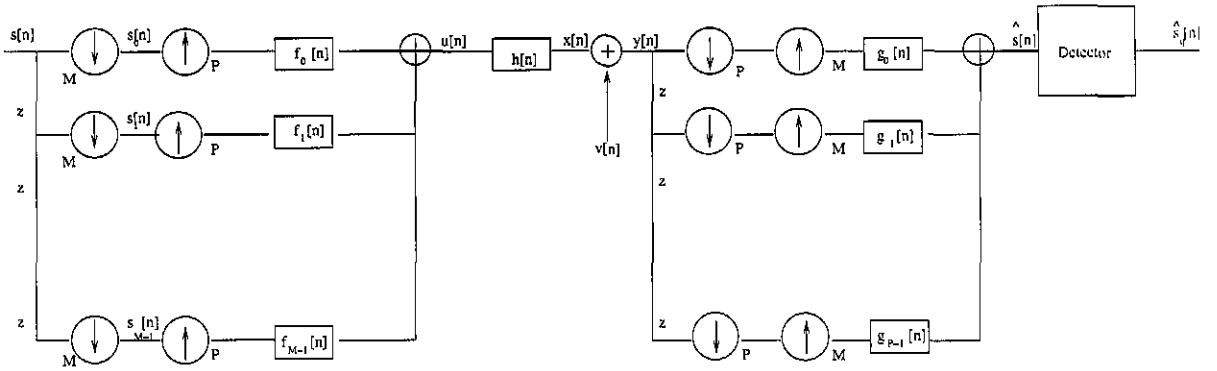

Figure 2.1: The baseband redundant multirate filter bank transceiver model

through the channel where additive Gaussian noise is present. At the receiver, downsampling by P performs the conversion of the serial received signal to a parallel bank of signals, each of which is then upsampled by M. The signals are then passed through the receiver filterbank which is also referred as the equalizer with impulse response denoted by $\{g_p(n)\}$, $p = 0, \cdots, P-1$. Because of the symmetric of up/down sampling rates at the transmitting and receiving parts the overall rate remains unchanged. The output of the receiving filterbank $\hat{s}(n)$ is then passed through a detector for decision.

Let the M-dimensional vectors $\boldsymbol{s}(n)$ and $\hat{\boldsymbol{s}}(n)$ denote the nth transmitting and received block respectively,

$$\begin{aligned}
\boldsymbol{s}(n) &= [s_0(n), s_1(n), \cdots, s_{M-1}(n)]^T \\
&= [s(nM), s(nM+1), \cdots, s(nM+M-1)]^T, \\
\hat{\boldsymbol{s}}(n) &= [\hat{s}_0(n), \hat{s}_1(n), \cdots, \hat{s}_{M-1}(n)]^T \\
&= [\hat{s}(nM), \hat{s}(nM+1), \cdots, \hat{s}(nM+M-1)]^T.
\end{aligned}$$

It can be shown [28] that

$$\hat{\boldsymbol{s}}(n) = \sum_{i=-\infty}^{\infty} \sum_{j=-\infty}^{\infty} \sum_{l=-\infty}^{\infty} \boldsymbol{G}_j \boldsymbol{H}_l \boldsymbol{F}_i \boldsymbol{s}(n-l-i-j) + \sum_{j=-\infty}^{\infty} \boldsymbol{G}_j \boldsymbol{v}(n-j), \tag{2.1}$$

where $\boldsymbol{F}_i$ are $P \times M$, $\boldsymbol{G}_j$ are $M \times P$, and $\boldsymbol{H}_l$ are $P \times P$ matrices given by

$$\boldsymbol{F}_i = \begin{pmatrix} f_0(iP) & f_1(iP) & \cdots & f_{M-1}(iP) \\ f_0(iP+1) & f_1(iP+1) & \cdots & f_{M-1}(iP+1) \\ \vdots & \vdots & \cdots & \vdots \\ f_0(iP+P-1) & f_1(iP+P-1) & \cdots & f_{M-1}(iP+P-1) \end{pmatrix}, \tag{2.2}$$

$$\boldsymbol{G}_j = \begin{pmatrix} g_0(jM) & g_1(jM) & \cdots & g_{P-1}(jM) \\ g_0(jM+1) & g_1(jM+1) & \cdots & g_{P-1}(jM+1) \\ \vdots & \vdots & \cdots & \vdots \\ g_0(jM+M-1) & g_1(jM+M-1) & \cdots & g_{P-1}(jM+M-1) \end{pmatrix}, \tag{2.3}$$

$$\boldsymbol{H}_l = \begin{pmatrix} h(lP) & h(lP-1) & \cdots & h(lP-P+1) \\ h(lP+1) & h(lP) & \ddots & h(lP-P+2) \\ \vdots & \ddots & \ddots & \vdots \\ h(lP+P-1) & h(lP+P-2) & \cdots & h(lP) \end{pmatrix}, \tag{2.4}$$

with $\{f_m(n)\}$, $m = 0, \cdots, M-1$, being the impulse response of the precoder, $\{g_p(n)\}$, $p = 0, \cdots, P-1$, the impulse response of the receiver, $h(n)$ the impulse response of the channel, and $\boldsymbol{v}$ the noise vector of length P.

2.2 Inter-block interference

Eq (2.1) indicates that the nth received block $\hat{\boldsymbol{s}}(n)$ contains components of not only the current transmitted block $\boldsymbol{s}(n)$, but other blocks $\boldsymbol{s}(n-1), \boldsymbol{s}(n-2), \cdots$ as well, due to the dispersive nature of the channel. The contribution made by these additional blocks is called inter-block interference (IBI). To better analyze IBI, we make the following assumptions about the model,

A1) The channel is a slowly varying FIR channel of order at most L, with $h(0) \neq 0$. Slowly varying means that the channel does not change within the transmission of one block. In other words, the channel is linear time invariant (LTI) in one block duration.

A2) The parameters M, and P are chosen such that $P = M + L$.

A3) The transmitter filters $\{f_m(n)\}$, $m = 0, \cdots, M-1$, are of order at most P, and the receiver filters $\{g_p(n)\}$, $p = 0, \cdots, P-1$, are of order at most M.

From Assumption A3), we have

$$\boldsymbol{F}_i = \begin{cases} \boldsymbol{F}_0 & \text{for } i = 0 \\ 0, & \text{otherwise} \end{cases}$$

$$\boldsymbol{G}_j = \begin{cases} \boldsymbol{G}_0 & \text{for } j = 0 \\ 0, & \text{otherwise.} \end{cases}$$

Also, from Assumption A1) and A2), since $P > L$, the IBI due to the channel entails no more than two successive blocks. The nth received block $\hat{\boldsymbol{s}}(n)$ can be expressed as a function of the current transmitting block $\boldsymbol{s}(n)$, the previous block $\boldsymbol{s}(n-1)$ and noise, such that

$$\hat{\boldsymbol{s}}(n) = \boldsymbol{G}_0\boldsymbol{H}_0\boldsymbol{F}_0\boldsymbol{s}(n) + \boldsymbol{G}_0\boldsymbol{H}_1\boldsymbol{F}_0\boldsymbol{s}(n-1) + \boldsymbol{G}_0\boldsymbol{v}(n), \tag{2.5}$$

where $\boldsymbol{F}_0$ is $P \times M$, $\boldsymbol{G}_0$ is $M \times P$, $\boldsymbol{H}_0$ and $\boldsymbol{H}_1$ are $P \times P$ matrices obtained from Eq (2.4) by having $l = 0, 1$ respectively. The first term in the right side of Eq (2.5) contains the desired block, and the latter two terms, which are inter-block interference and noise interference respectively, are not desired because they cause errors in the reconstruction of the desired block at the receiver. The IBI in Eq (2.5) can be mitigated if $\boldsymbol{G}_0\boldsymbol{H}_1\boldsymbol{F}_0 = \boldsymbol{0}$. Due to Assumption 1), the matrix $\boldsymbol{H}_1$ has non-zero elements only in its $L \times L$ top right matrix. This leads to two options to eliminate IBI, namely zero padding (ZP) and leading zeros (LZ) methods [28].

2.2.1 Zero padding

One way to cancel IBI is zero padding which is realized by forcing the last L samples of the transmit filters to be zero, $\boldsymbol{F}_0$ has the form of $\boldsymbol{F}_0 = \begin{pmatrix} \boldsymbol{F}_{zp} \\ \boldsymbol{0} \end{pmatrix}$, where $\boldsymbol{F}_{zp}$ is an $M \times M$ full rank matrix, $\boldsymbol{0}$ is an $L \times M$ null matrix, and $\boldsymbol{G}_0 = \boldsymbol{G}_{zp}$ is an $M \times P$ full row rank "fat"

matrix by linear equalization, $\boldsymbol{H}_0 = \boldsymbol{H}_{zp}$ is a $P \times M$ full column rank Toeplitz "tall" matrix given below,

$$\boldsymbol{H}_0 = \boldsymbol{H}_{zp} = \begin{pmatrix} h(0) & 0 & \cdots & 0 \\ \vdots & \ddots & \ddots & \vdots \\ h(L) & \ddots & \ddots & \vdots \\ 0 & \ddots & \ddots & h(0) \\ \vdots & \ddots & \ddots & \vdots \\ 0 & 0 & \cdots & h(L) \end{pmatrix}. \tag{2.6}$$

The output block $\hat{\boldsymbol{s}}$ (we have dropped (n) for the simplicity of the notation) is expressed as,

$$\hat{\boldsymbol{s}}_{zp} = \boldsymbol{G}_{zp}\boldsymbol{H}_{zp}\boldsymbol{F}_{zp}\boldsymbol{s} + \boldsymbol{G}_{zp}\boldsymbol{v}. \tag{2.7}$$

2.2.2 Leading zeros and cyclic prefix

Another way of mitigating IBI is leading zeros (LZ) that is implemented by forcing the first L filters of the receiver filterbank to be zero, i.e., $\boldsymbol{G}_0$ is chosen such that $\boldsymbol{G}_0 = \left(0, \boldsymbol{G}_{lz}\right)$, where $\boldsymbol{G}_{lz}$ is an $M \times M$ matrix, $\mathbf{0}$ is an $M \times L$ null matrix, and $\boldsymbol{F}_0 = \boldsymbol{F}_{lz}$ is a $P \times M$ full column rank "tall" matrix, $\boldsymbol{H}_0 = \boldsymbol{H}_{lz}$ is an $M \times P$ full row rank Toeplitz "fat" matrix given by,

$$\boldsymbol{H}_0 = \boldsymbol{H}_{lz} = \begin{pmatrix} h(L) & \cdots & h(0) & 0 & \cdots & 0 \\ 0 & \ddots & \ddots & \ddots & \cdots & \vdots \\ \vdots & \vdots & \ddots & \ddots & \ddots & 0 \\ 0 & \cdots & 0 & h(L) & \cdots & h(0) \end{pmatrix}. \tag{2.8}$$

The output block $\hat{\boldsymbol{s}}$ is expressed as,

$$\hat{\boldsymbol{s}}_{lz} = \boldsymbol{G}_{lz}\boldsymbol{H}_{lz}\boldsymbol{F}_{lz}\boldsymbol{s} + \boldsymbol{G}_{lz}\boldsymbol{v}. \tag{2.9}$$

It can be shown that the popular technique of cyclic prefix which is employed in orthogonal frequency division multiplexing (OFDM) and discrete multitone (DMT) transmission schemes falls into the category of LZ schemes. In OFDM and DMT, a cyclic prefix is introduced at transmitter such that the last L out of M symbols in given block are transmitted at both ends of the block. At the receiver, the cyclic prefix is removed by discarding the first L received data. This can be described mathematically by,

$$\boldsymbol{F}_0 = \boldsymbol{T}_{cp}\boldsymbol{F}_{cp},$$
$$\boldsymbol{G}_0 = \boldsymbol{G}_{cp}\boldsymbol{R}_{cp},$$

where

$$\boldsymbol{T}_{cp} = \begin{pmatrix} \boldsymbol{0}_{L\times(M-L)} & \boldsymbol{I}_{L\times L} \\ & \boldsymbol{I}_{M\times M} \end{pmatrix},$$
$$\boldsymbol{R}_{cp} = \begin{pmatrix} \boldsymbol{0}_{M\times L} & \boldsymbol{I}_{M\times M} \end{pmatrix},$$

and $\boldsymbol{F}_{cp}$ and $\boldsymbol{G}_{cp}$ are full rank $M \times M$ matrices. The received block can be written as,

$$\begin{aligned} \hat{\boldsymbol{s}}_{cp} &= \boldsymbol{G}_0\boldsymbol{H}_0\boldsymbol{F}_0\boldsymbol{s} + \boldsymbol{G}_0\boldsymbol{v} \\ &= \boldsymbol{G}_{cp}\boldsymbol{R}_{cp}\boldsymbol{H}_0\boldsymbol{T}_{cp}\boldsymbol{F}_{cp}\boldsymbol{s} + \boldsymbol{G}_{cp}\boldsymbol{R}_{cp}\boldsymbol{v} \\ &= \boldsymbol{G}_{cp}\boldsymbol{H}_{cp}\boldsymbol{F}_{cp}\boldsymbol{s} + \boldsymbol{G}_{cp}\boldsymbol{R}_{cp}\boldsymbol{v}, \end{aligned} \tag{2.10}$$

where $\boldsymbol{H}_{cp} = \boldsymbol{R}_{cp}\boldsymbol{H}_0\boldsymbol{T}_{cp}$ is an $M \times M$ circulant matrix with the following form,

$$\boldsymbol{H}_{cp} = \begin{pmatrix} h(0) & h(L) & \cdots & h(1) \\ h(1) & h(0) & \cdots & h(L) \\ \vdots & \ddots & \ddots & \vdots \\ h(L) & \cdots & \cdots & h(0) \end{pmatrix}. \tag{2.11}$$

If we let $\boldsymbol{v}_{cp} = \boldsymbol{R}_{cp}\boldsymbol{v}$, then $\boldsymbol{v}_{cp}$ is a white Gaussian noise vector because $\boldsymbol{R}_{cp}$ is row

orthogonal. Therefore Eq (2.10) can be written,

$$\hat{\boldsymbol{s}}_{cp} = \boldsymbol{G}_{cp}\boldsymbol{H}_{cp}\boldsymbol{F}_{cp}\boldsymbol{s} + \boldsymbol{G}_{cp}\boldsymbol{v}_{cp} \tag{2.12}$$

Note that $\boldsymbol{H}_{cp}$ is circulant and can be diagonalized by pre and post-multiplication with M-point DFT and IDFT matrices [32],

$$\begin{aligned}\boldsymbol{D}\boldsymbol{H}_{cp}\boldsymbol{D}^{H} &= \boldsymbol{\Delta}_{H} \\ &= diag\Big(\ H\big(e^{j0}\big),\ \ H\big(e^{j2\pi/M}\big),\ \ \cdots\ \ H\big(e^{j2\pi(M-1)/M}\big)\ \Big),\end{aligned} \tag{2.13}$$

where ^{H} denotes the Hermitian conjugate of a matrix, $H(e^{j2\pi f}) = \sum_{n=0}^{L} h(n)\exp(-j2\pi fn)$ corresponds to the channel frequency response for the jth sub-carrier, and $\boldsymbol{D}$ is a DFT matrix with the k,nth element $[\boldsymbol{D}]_{kn} = M^{(-1/2)}\exp(-j2\pi kn/M)$. If linear equalization is used in the cyclic prefix (CP) transmission system, the precoder $\boldsymbol{F}_{cp}$ and receiver $\boldsymbol{G}_{cp}$ have the following forms [32]:

For CP-OFDM,

$$\begin{aligned}\boldsymbol{F}_{cp} &= \alpha_T\boldsymbol{D}^{H} \\ \boldsymbol{G}_{cp} &= \boldsymbol{\Delta}_{R-OFDM}\boldsymbol{D},\end{aligned} \tag{2.14}$$

and for DMT,

$$\begin{aligned}\boldsymbol{F}_{cp} &= \boldsymbol{D}^{H}\boldsymbol{\Delta}_{T} \\ \boldsymbol{G}_{cp} &= \boldsymbol{\Delta}_{R-DMT}\boldsymbol{D},\end{aligned}$$

where $\boldsymbol{\Delta}_{R-OFDM}$ and $\boldsymbol{\Delta}_{R-DMT}$ are diagonal matrices determined by the linear equalization strategy , α_T is a constant satisfying the prescribed transmitting power, $\boldsymbol{\Delta}_T$ is a diagonal matrix governing the power loading on different sub-carriers. The power loading algorithm used in current DMT systems is the water filling algorithm which maximizes the information

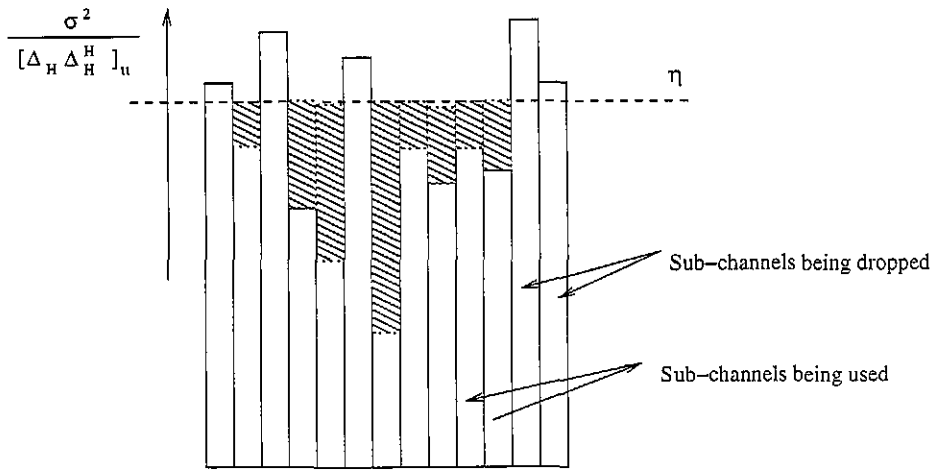

Figure 2.2: Water-filling power loading

rate, the ith diagonal element of $\boldsymbol{\Delta}_T$ is,

$$[\boldsymbol{\Delta}_T]_{ii} = \begin{cases} \sqrt{\eta - \frac{\sigma^2}{[\boldsymbol{\Delta}_H \boldsymbol{\Delta}_H^H]_{ii}}}, & \text{if } \eta > \frac{\sigma^2}{[\boldsymbol{\Delta}_H \boldsymbol{\Delta}_H^H]_{ii}} \\ 0, & \text{otherwise,} \end{cases} \tag{2.15}$$

where $[\boldsymbol{\Delta}_T]_{ii}$ and $[\boldsymbol{\Delta}_H \boldsymbol{\Delta}_H^H]_{ii}$ are the ith diagonal element of $\boldsymbol{\Delta}_T$ and $\boldsymbol{\Delta}_H \boldsymbol{\Delta}_H^H$ respectively, and η is a constant chosen to satisfy the prescribed transmitting power. The diagram is shown in Figure 2.2. If a sub-channel does not satisfy $\eta - \frac{\sigma^2}{[\boldsymbol{\Delta}_H \boldsymbol{\Delta}_H^H]_{ii}} > 0$, it is not allocated power and not used in the transmission. From Eq (2.14), the CP-OFDM system distributes power uniformly to each sub-carrier, the corresponding power loading matrix is simply $\alpha_T \boldsymbol{I}$. The block diagram for the CP-OFDM and DMT transmission scheme are shown in Figure 2.3. The CP-OFDM system can be regarded as a special case of a water-filling DMT system if the channel is an ideal one.

It can be noted that from Eqs (2.7), (2.9), and (2.12), the input/output relationship for zero padding, leading zero, and cyclic prefix share the same structure such that, $\hat{\boldsymbol{s}} = \boldsymbol{GHFs} + \boldsymbol{Gv}$, where the sizes for the precoder $\boldsymbol{F}$, channel $\boldsymbol{H}$ and receiver $\boldsymbol{G}$ matrices are defined appropriately. The general diagram is shown in Figure 2.4. The thesis focuses on the design of the minimum BER precoder for the systems employing zero padding and cyclic

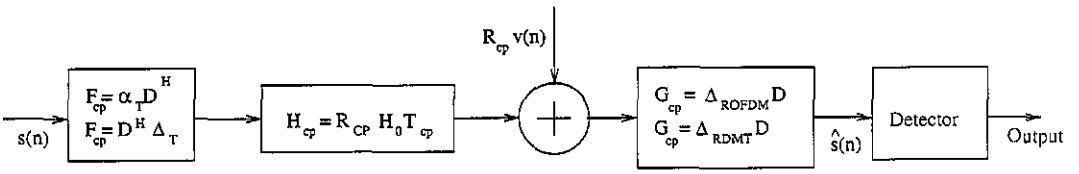

Figure 2.3: CP-ODFM and DMT transmission scheme

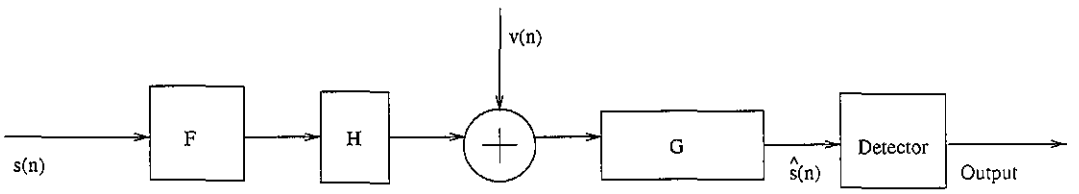

Figure 2.4: General diagram of block transmission

prefix. In both cases the size of the precoder is $M \times M$, and $\boldsymbol{H}$ and $\boldsymbol{G}$ respectively take the forms of $\boldsymbol{H}_{zp}$ and $\boldsymbol{G}_{zp}$ or $\boldsymbol{H}_{cp}$ and $\boldsymbol{G}_{cp}$ according to ZP or CP schemes.

2.3 Assumptions made in the thesis

In the thesis the following assumptions are made in addition to those already made on the model in Section 2.1.

A4) Inter-block interference is eliminated by padding precoder zeros or adding a cyclic prefix. The receiver can estimate the channel exactly, and inter-symbol interference has been eliminated by zero forcing equalization. Therefore, the input/output relation is simplified to,

$$\begin{aligned} \hat{\boldsymbol{s}} &= \boldsymbol{s} + \boldsymbol{G}\boldsymbol{v} \\ &= \boldsymbol{s} + \boldsymbol{F}^{-1}\boldsymbol{H}^{\dagger}\boldsymbol{v} \end{aligned} \tag{2.16}$$

where $\boldsymbol{F}$ is $M \times M$ full-rank matrix, $\boldsymbol{G} = (\boldsymbol{HF})^{\dagger} = \boldsymbol{F}^{-1}\boldsymbol{H}^{\dagger}$, † denotes pseudo-inverse. The conditions for the existence of zero-forcing equalization for ZP schemes are satisfied if Assumptions A1), A2) and A3) are satisfied. An additional requirement that $H(e^{j2\pi k/M}) \neq 0, k \in [0, M-1]$ is needed for CP schemes [28].

A5) The transmitter knows the channel (such as in HDSL/ADSL applications), if it implements the calculation of the MBER precoder.

A6) The transmitting signals are equi-probable binary phase shift keying (BPSK) or quadrature phase shift keying (QPSK), and the covariance matrix of transmitting blocks is $E\{\boldsymbol{ss}^H\} = \boldsymbol{I}$.

A7) The noise is zero-mean white and Gaussian, and in the complex case, its real and imaginary parts are independent with the same covariance, $E\{\boldsymbol{vv}^H\} = \sigma^2\boldsymbol{I}$.

A8) Threshold detection is applied at the equalizer output to form the detected symbols.

Chapter 3

The Design of Minimum BER Precoder

This chapter studies the design of minimum BER precoders. In particular the following problems are considered.

- Block bit error rate and its lower bound
- Analytic solution for MBER precoder and its validity
- The issue of dropping sub-channels and the corresponding MBER precoder
- Relationship between MBER and MMSE precoder
- MMSE power loading for DMT and the relationship between the CP-MBER precoder and the standard DMT precoder
- The extra power needed to transmit the cyclic prefix for precoders of CP-MBER, CP-OFDM and water filling DMT systems

3.1 Block bit error rate

The block bit error rate P_e in this thesis is defined as the average bit error rate over all possible transmitted blocks,

$$P_e = E\{P_{e|s}\}, \tag{3.1}$$

where $P_{e|s}$ is the bit error rate for a given transmitted block s. Taking BPSK signals as an example, to evaluate P_e we let $\mathcal{S}$ be the set of all possible transmitting data vectors and s_j be the jth data vector in the set, $j \in [1, 2^M]$, i.e.,

$$\mathcal{S} = \{s_1, s_2, \cdots, s_{2^M}\} \tag{3.2}$$

where

$$\begin{aligned} s_1 &= [-1, -1, \cdots, -1, -1]^T, \\ s_2 &= [-1, -1, \cdots, -1, +1]^T, \\ &\vdots \\ s_{2^M} &= [+1, +1, \cdots, +1, +1]^T. \end{aligned}$$

The bit error rate $P_{e|s_j}$ is the average of the weighted probabilities of having erroneous bits, given that s_j is the transmitted data vector. Thus,

$$\begin{aligned} P_{e|s_j} &= \frac{1}{M}\Big(P(1 \text{ erroneous bit in } \hat{s}_j) + 2P(2 \text{ erroneous bits in } \hat{s}_j) + \cdots + MP(M \text{ erroneous bits in } \hat{s}_j)\Big) \\ &= \frac{1}{M}\Big(\sum_{i=1}^{M} iP(i \text{ erroneous bits in } \hat{s}_j)\Big), \end{aligned} \tag{3.3}$$

where $\hat{s}_j$ is the received block given that s_j is transmitted. Hence the average block bit error rate for BPSK signals is

$$P_e = \sum_{j=1}^{2^M} P_{e|s_j} P_{s_j}. \tag{3.4}$$

where P_{s_j} is the probability that s_j is transmitted. Since the transmitting signals are assumed to be equi-probable (Section 2.3), therefore $P_{s_j} = \frac{1}{2^M}$. Thus the block bit error rate P_e in Eq (3.4) can be written.

$$P_e = \frac{1}{2^M} \sum_{j=1}^{2^M} P_{e|s_j}. \tag{3.5}$$

It can be shown that under the assumptions made in Section 2.3, the block bit error rate has the following form,

$$P_e = \frac{1}{2M} \sum_{i=1}^{M} \operatorname{erfc}\left(\frac{1}{\sqrt{2\sigma^2 [\boldsymbol{G}\boldsymbol{G}^H]_{ii}}} \right), \tag{3.6}$$

where $\operatorname{erfc}(\cdot)$ is the complementary error function, $\operatorname{erfc}(x) = \frac{2}{\sqrt{\pi}} \int_x^\infty e^{-t^2} dt$, $[\boldsymbol{G}\boldsymbol{G}^H]_{ii}$ is the ith diagonal entry of $\boldsymbol{G}\boldsymbol{G}^H$, M is the block size, and $E\{\boldsymbol{v}\boldsymbol{v}^H\} = \sigma^2 \boldsymbol{I}$. The full mathematical derivation for P_e is given in Appendix A.

In Figure 3.1, the BERs obtained by Eq (3.6) and by simulation respectively are compared. The triple $(M, L, P) = (8, 4, 12)$. The simulation is done over $10,000$ channel realizations with 500 BPSK blocks each. The channel taps are first generated by independent zero mean complex Gaussian variables with unit covariance, and then are normalized by the norm. The plot suggests a good agreement between the theoretical formula of BER and the simulation result. Thus the BERs presented in this thesis are evaluated using the theoretical formula instead of by simulation.

3.2 Convexity of $f(x) = \operatorname{erfc}\left(\frac{1}{\sqrt{2\sigma^2 x}}\right)$ at moderate to high SNR and a lower bound of the BER

The block bit error rate P_e contains a sum of the complementary error function which has the form $f(x) = \operatorname{erfc}\left(\frac{1}{\sqrt{2\sigma^2 x}}\right)$, where x is a continuous variable. We will show that $f(x)$ is convex for small values of x. Since $\operatorname{erfc}(x) = \frac{2}{\sqrt{\pi}} \int_x^\infty e^{-t^2} dt$, we have $\frac{d\operatorname{erfc}(x)}{dx} = -\frac{2}{\sqrt{\pi}} e^{-x^2}$. Therefore

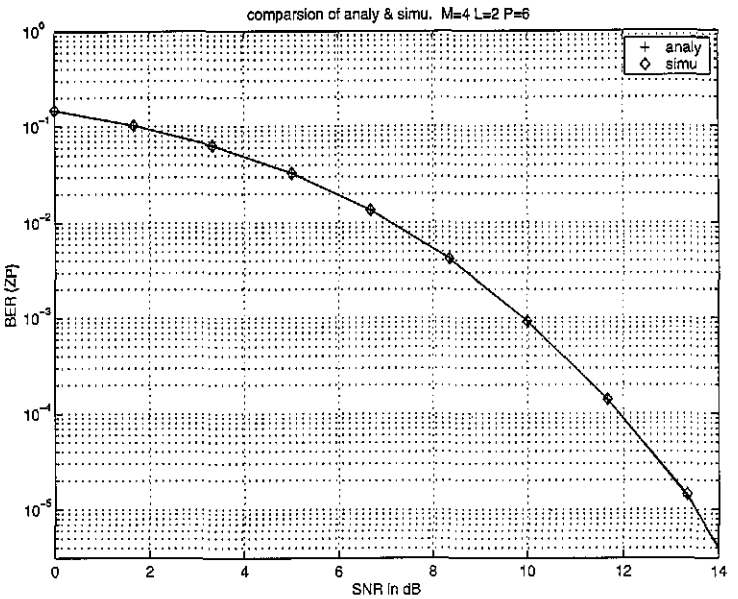

Figure 3.1: BERs by analytic evaluations and simulation

for $f(x) = \text{erfc}\left(\frac{1}{\sqrt{2\sigma^2 x}}\right)$, we have $\frac{df(x)}{dx} = \frac{1}{\sqrt{\pi}}(2\sigma^2)^{-\frac{1}{2}}x^{-\frac{3}{2}}\exp\left(-(2\sigma^2)^{-1}x^{-1}\right)$, hence,

$$\frac{d^2 f(x)}{dx^2} = \frac{1}{\sqrt{\pi}}(2\sigma^2)^{-\frac{1}{2}}\exp\left(-(2\sigma^2)^{-1}x^{-1}\right)\left(-\frac{3}{2}+(2\sigma^2)^{-1}x^{-1}\right)x^{-\frac{5}{2}}. \tag{3.7}$$

From Eq (3.7), if $x < \frac{1}{3\sigma^2}$, then $\frac{\partial^2 f(x)}{\partial x^2} > 0$. Therefore $f(x) = \text{erfc}\left(\frac{1}{\sqrt{2\sigma^2 x}}\right)$ is a convex function for small values of x. In our application this condition actually corresponds to moderate-to-high received SNR, as will be shown in Section 3.4. The property of convexity is very desirable because any local optimum is also a global optimum. This observation provides us with a direction to find a lower bound of the BER and develop a scheme for the optimum design of the precoder under the criterion of minimum BER.

Since $f(x) = \text{erfc}\left(\frac{1}{\sqrt{2\sigma^2 x}}\right)$ is convex for $x < \frac{1}{3\sigma^2}$, a lower bound for the BER can be found by applying Jensen's inequality in the region where the convexity holds. According to Jensen's inequality [23] we have that

$$\frac{1}{M}\sum_{i=1}^{M}\text{erfc}\left(\frac{1}{\sqrt{2\sigma^2 x_i}}\right) \geq \text{erfc}\left(\frac{1}{\sqrt{\frac{2\sigma^2}{M}\sum_{i=1}^{M}x_i}}\right) \tag{3.8}$$

and that equality in (3.8) holds when all x_i are equal, $\forall i \in [1, M]$. Setting $x_i = [\boldsymbol{G}\boldsymbol{G}^H]_{ii}$ in inequality (3.8), we have that

$$\begin{aligned} P_e &= \frac{1}{2M}\sum_i \operatorname{erfc}\left(\frac{1}{\sqrt{2\sigma^2[\boldsymbol{G}\boldsymbol{G}^H]_{ii}}}\right) \\ &\geq \frac{1}{2}\operatorname{erfc}\left(\frac{1}{\sqrt{\frac{2\sigma^2}{M}\sum_{i=1}^{M}[\boldsymbol{G}\boldsymbol{G}^H]_{ii}}}\right) \qquad (3.9) \\ &= \frac{1}{2}\operatorname{erfc}\left(\frac{1}{\sqrt{2\sigma^2\left(\frac{tr(\boldsymbol{G}\boldsymbol{G}^H)}{M}\right)}}\right) \qquad (3.10) \\ &\triangleq \underline{P_e} \qquad (3.11) \end{aligned}$$

and that equality in (3.9) holds if $[\boldsymbol{G}\boldsymbol{G}^H]_{ii}$ are equal, $\forall i \in [1, M]$, and $\underline{P_e}$ in (3.11) is a lower bound on P_e.

3.3 Design scheme for MBER precoders

In practical communication schemes, the transmitting power cannot be arbitrarily large, and this imposes a constraint on the optimal precoder design. The transmitting power is given by $\operatorname{tr}\left(E\{\boldsymbol{F}_0\boldsymbol{s}(\boldsymbol{F}_0\boldsymbol{s})^H\}\right) = \operatorname{tr}\left(\boldsymbol{F}_0E\{\boldsymbol{s}\boldsymbol{s}^H\}\boldsymbol{F}_0^H\right) = \operatorname{tr}(\boldsymbol{F}_0\boldsymbol{F}_0^H)$, where we have used the fact that the covariance matrix of the transmitted data $\boldsymbol{R}_{ss} = E\{\boldsymbol{s}\boldsymbol{s}^H\} = \boldsymbol{I}$ by Assumption A6). For ZP systems $\boldsymbol{F}_0 = \binom{\boldsymbol{I}}{\boldsymbol{0}}\boldsymbol{F}$, thus $\operatorname{tr}(\boldsymbol{F}_0\boldsymbol{F}_0^H) = \operatorname{tr}(\boldsymbol{F}\boldsymbol{F}^H)$. The transmitting power in ZP systems equals the power needed in transmitting the data blocks. For CP systems, $\boldsymbol{F}_0 = \begin{pmatrix} \boldsymbol{0}_{L\times(M-L)} & \boldsymbol{I}_{L\times L} \\ \boldsymbol{I}_{M\times M} & \end{pmatrix}\boldsymbol{F}$, thus $\operatorname{tr}(\boldsymbol{F}_0\boldsymbol{F}_0^H) = \operatorname{tr}(\boldsymbol{F}\boldsymbol{F}^H) + \sum_{i=M-L+1}^{M}\boldsymbol{f}_i\boldsymbol{f}_i^H$, where $\boldsymbol{f}_i$ is the ith row in $\boldsymbol{F}$. The transmitting power in CP systems equals the sum of the power needed to transmit the data and the cyclic prefix. It is standard practice to define the transmitting power as only the power required to transmit the data in the CP system [6], [15], and [32], without regard to the power needed to transmit the cyclic prefix. Therefore the transmitting power constraint for both ZP and CP systems has the same form, $\operatorname{tr}(\boldsymbol{F}\boldsymbol{F}^H) \leq p_0$ (see Section 3.5 for further discussion), where p_0 is the maximum possible transmission power.

The MBER precoder design problem can therefore be formulated as,

$$\begin{aligned} &\min_{\boldsymbol{F}} P_e \\ \text{subject to} \quad &tr(\boldsymbol{F}\boldsymbol{F}^H) \leq p_0. \end{aligned}$$

Since $\underline{P_e}$ is a lower bound on P_e, minimum BER precoders can be designed by the following two stages.

- **Stage 1**

  Minimize the lower bound $\underline{P_e}$ subject to bound on the transmitting power and the constraint that convexity is valid, i.e.,

$$\begin{aligned} &\min_{\boldsymbol{F}} \underline{P_e} \\ \text{subject to} \quad &tr(\boldsymbol{F}\boldsymbol{F}^H) \leq p_0 \\ &[\boldsymbol{G}\boldsymbol{G}^H]_{ii} < \frac{1}{3\sigma^2}, \forall i \in [1, M] \end{aligned}$$

- **Stage 2**

  Show that a particular element from the solution set to **Stage 1** achieves the minimized lower bound for the BER.

These two steps are described in greater details below:

3.3.1 Stage 1: Minimizing the lower bound

Since the complementary error function erfc$(\cdot)$ is a monotonically decreasing function, one can minimize the lower bound $\underline{P_e} = \frac{1}{2}\text{erfc}\left(\frac{1}{\sqrt{2\sigma^2\left(\frac{tr(\boldsymbol{G}\boldsymbol{G}^H)}{M}\right)}}\right)$ by maximizing $\left(tr(\boldsymbol{G}\boldsymbol{G}^H)\right)^{-\frac{1}{2}}$, or, equivalently, minimizing $tr(\boldsymbol{G}\boldsymbol{G}^H)$. Recall Assumption A4) that ZF equalization is used, i.e., $\boldsymbol{G} = \boldsymbol{F}^{-1}\boldsymbol{H}^{\dagger}$, therefore **Stage 1** can be formulated as:

$$\min_{\boldsymbol{F}} tr\left(\boldsymbol{F}^{-1}(\boldsymbol{H}^H\boldsymbol{H})^{-1}\boldsymbol{F}^{-H}\right)$$

$$\begin{aligned} \text{subject to} \quad & tr(\boldsymbol{F}\boldsymbol{F}^H) \leq p_0 \\ & [\boldsymbol{F}^{-1}(\boldsymbol{H}^H\boldsymbol{H})^{-1}\boldsymbol{F}^{-H}]_{ii} < \frac{1}{3\sigma^2}, \forall i \in [1, M] \end{aligned} \tag{3.12}$$

where we have used the fact that $\boldsymbol{G}\boldsymbol{G}^H = \boldsymbol{F}^{-1}(\boldsymbol{H}^H\boldsymbol{H})^{-1}\boldsymbol{F}^{-H}$.

Problem (3.12) appears to be difficult to solve because it is not convex in $\boldsymbol{F}$ and includes two constraints. We seek a reformulation which is easier to solve. If we reparameterize $\boldsymbol{F}$ as $\boldsymbol{F} = \boldsymbol{A}\boldsymbol{V}$, where $\boldsymbol{V}$ is unitary, then **Stage 1** is equivalent to solve the following optimization problem, which we will call **Stage 1'**,

$$\min_{\boldsymbol{A},\boldsymbol{V}} tr(\boldsymbol{A}^{-1}\boldsymbol{Q}\boldsymbol{A}^{-H}) \tag{3.13}$$

$$\text{subject to} \quad tr(\boldsymbol{A}\boldsymbol{A}^H) \leq p_0 \tag{3.14}$$

$$[\boldsymbol{V}^H\boldsymbol{A}^{-1}\boldsymbol{Q}\boldsymbol{A}^{-H}\boldsymbol{V}]_{ii} < \frac{1}{3\sigma^2}, \forall i \in [1, M] \tag{3.15}$$

where $\boldsymbol{Q} = (\boldsymbol{H}^H\boldsymbol{H})^{-1} = \boldsymbol{W}\boldsymbol{\Lambda}\boldsymbol{W}^H$. The optimal solution to $\boldsymbol{F}$ in **Stage 1** can be obtained from the optimal solution to **Stage 1'** by $\boldsymbol{F}_{\text{stage1}} = \boldsymbol{A}_{\text{opt}}\boldsymbol{V}_{\text{opt}}$. In **Stage 1'**, $\boldsymbol{A}^{-1}\boldsymbol{Q}\boldsymbol{A}^{-H}$ in (3.13) and power constraint in (3.14) does not depend on $\boldsymbol{V}$, therefore the solutions to **Stage 1'** can be developed by the following two steps.

- Step 1: Solve the following problem for $\boldsymbol{A}_{\text{opt}}$

$$\begin{aligned} & \min_{\boldsymbol{A}} tr(\boldsymbol{A}^{-1}\boldsymbol{Q}\boldsymbol{A}^{-H}) \\ \text{subject to} \quad & tr(\boldsymbol{A}\boldsymbol{A}^H) \leq p_0. \end{aligned} \tag{3.16}$$

- Step 2: Resolve $\boldsymbol{V}$ from constraint (3.15).

The design criterion in (3.16) in Step 1 is actually the mean square error (MSE) at the receiver, and the set of precoders which minimize the MSE has been obtained in [28] (Proof is also included in Appendix D). The set of optimal matrices $\boldsymbol{A}$ is

$$\boldsymbol{A}_{\text{opt}} = \sqrt{\frac{p_0}{tr(\boldsymbol{\Lambda}^{\frac{1}{2}})}}\,\boldsymbol{W}\boldsymbol{\Lambda}^{\frac{1}{4}}\boldsymbol{U}, \tag{3.17}$$

where $\boldsymbol{U}$ is an arbitrary unitary matrix, and $\boldsymbol{W}\boldsymbol{\Lambda}\boldsymbol{W}^H = (\boldsymbol{H}^H\boldsymbol{H})^{-1}$. For convenience, $\boldsymbol{W}$ is chosen such that $\boldsymbol{\Lambda}$ is ordered in descending order.

To solve Step 2, we employ the following lemma:

Lemma 3.1. *Given* $\boldsymbol{S} = \boldsymbol{N}\boldsymbol{\Gamma}\boldsymbol{N}^H \geq 0, \boldsymbol{S} \in \mathcal{C}^{M\times M}, \boldsymbol{N}\boldsymbol{N}^H = \boldsymbol{I}_M$, *then*

$tr(\boldsymbol{S}) \leq M\tau, \Longleftrightarrow \exists \boldsymbol{R} \in \mathcal{C}^{M\times M}$, $\boldsymbol{R}\boldsymbol{R}^H = \boldsymbol{I}_M$, *such that* $[\boldsymbol{R}^H\boldsymbol{S}\boldsymbol{R}]_{ii} \leq \tau$.

Proof. The sufficiency part is straight forward due to the fact that the trace function is invariant under the linear transformation by a unitary matrix. To show the necessity part, we construct a candidate $\boldsymbol{R}$. Let $\boldsymbol{R} = \boldsymbol{N}\boldsymbol{D}$, then,

$$\boldsymbol{R}^H\boldsymbol{S}\boldsymbol{R} = \boldsymbol{D}^H\boldsymbol{\Gamma}\boldsymbol{D}.$$

Let d_{ij} denote the i,jth element of $\boldsymbol{D}$ and let γ_i denote the ith diagonal element of $\boldsymbol{\Gamma}$. Then

$$\begin{aligned}[\boldsymbol{R}^H\boldsymbol{S}\boldsymbol{R}]_{ii} &= [\boldsymbol{D}^H\boldsymbol{\Gamma}\boldsymbol{D}]_{ii} \\ &= \sum_j \gamma_j |d_{ij}|^2. \end{aligned} \tag{3.18}$$

If all diagonal elements in $\boldsymbol{\Gamma}$ are equal, any unitary matrix can be a candidate of $\boldsymbol{D}$ to satisfy the necessity. On the other hand, if not all the diagonal elements of $\boldsymbol{\Gamma}$ are equal, then $\boldsymbol{D}$ can be chosen as a normalized DFT, IDFT matrix or a normalized Hadamard matrix (if the block size is power of 2). In that case $|d_{i,j}|^2 = \frac{1}{M}$. Therefore

$$\begin{aligned}[\boldsymbol{R}^H\boldsymbol{S}\boldsymbol{R}]_{ii} &= \sum_j \gamma_j \frac{1}{M} \\ &= \frac{tr(\boldsymbol{S})}{M} \leq \tau, \end{aligned}$$

and hence $\boldsymbol{R} = \boldsymbol{N}\boldsymbol{D}$ satisfies the necessary condition. □

(Note that there may exist other choices for $\boldsymbol{R}$ satisfying the necessary condition.)

Now we can use Lemma 3.1 to resolve $\boldsymbol{V}$. Matrices $\boldsymbol{A}^{-1}\boldsymbol{Q}\boldsymbol{A}^{-H}$ and $\boldsymbol{V}$ in constraint (3.15) correspond to $\boldsymbol{S}$ and $\boldsymbol{R}$ in Lemma 3.1 respectively. Substituting $\boldsymbol{A}_{\text{opt}}$ into $\boldsymbol{A}^{-1}\boldsymbol{Q}\boldsymbol{A}^{-H}$, we

have,

$$\boldsymbol{A}_{\text{opt}}^{-1}\boldsymbol{Q}\boldsymbol{A}_{\text{opt}}^{-H} = \frac{tr(\boldsymbol{\Lambda}^{\frac{1}{2}})}{p_0}\boldsymbol{U}^H\boldsymbol{\Lambda}^{\frac{1}{2}}\boldsymbol{U} \tag{3.19}$$

$$\Longrightarrow tr(\boldsymbol{A}_{\text{opt}}^{-1}\boldsymbol{Q}\boldsymbol{A}_{\text{opt}}^{-H}) = \frac{\left(tr(\boldsymbol{\Lambda}^{\frac{1}{2}})\right)^2}{p_0}$$

$$\triangleq \beta.$$

Depending on the values of β we have the following results:

- If $\beta > \frac{M}{3\sigma^2}$

  There is no solution for $\boldsymbol{V}$ from Lemma 3.1, hence no solution for **Stage 1'** or **Stage 1**.

- If $\beta \leq \frac{M}{3\sigma^2}$

  There exist solutions for $\boldsymbol{V}$ from Lemma 3.1, and one of them is $\boldsymbol{V} = \boldsymbol{U}^H\boldsymbol{D}$. Recall that $\boldsymbol{F} = \boldsymbol{A}\boldsymbol{V}$, therefore one precoder $\boldsymbol{F}$ which minimizes the lower bound $\underline{P_e}$ in **Stage 1** is:

$$\begin{aligned}\boldsymbol{F}_{\text{stage1}} &= \boldsymbol{A}_{\text{opt}}\boldsymbol{V} \\ &= \sqrt{\frac{p_0}{tr(\boldsymbol{\Lambda}^{\frac{1}{2}})}}\boldsymbol{W}\boldsymbol{\Lambda}^{\frac{1}{4}}\boldsymbol{U}\boldsymbol{V} \\ &= \sqrt{\frac{p_0}{tr(\boldsymbol{\Lambda}^{\frac{1}{2}})}}\boldsymbol{W}\boldsymbol{\Lambda}^{\frac{1}{4}}\boldsymbol{D}.\end{aligned} \tag{3.20}$$

  By comparing the values $\beta = \frac{\left(tr(\boldsymbol{\Lambda}^{\frac{1}{2}})\right)^2}{p_0}$ to $\frac{M}{3\sigma^2}$ for a given channel and noise variance, we can have an explicit test for the validity of **Stage 1**.

3.3.2 Stage 2: Reaching the minimized lower bound for the BER

We have had a solution for precoder $\boldsymbol{F}$ which minimizes the lower bound of BER $\underline{P_e}$ when **Stage 1** is valid. In that case, we go to **Stage 2** to find a precoder which makes that $P_e = \underline{P_e}$, i.e., which reaches the minimized lower bound for the BER.

From Jensen's inequality, $P_e = \underline{P_e}$ holds if $[\boldsymbol{G}\boldsymbol{G}^H]_{ii}$ are equal, $\forall i \in [1, M]$. Plugging $\boldsymbol{F}_{\text{stage1}} = \sqrt{\frac{p_0}{tr(\boldsymbol{\Lambda}^{\frac{1}{2}})}}\boldsymbol{W}\boldsymbol{\Lambda}^{\frac{1}{4}}\boldsymbol{D}$ into $\boldsymbol{G}\boldsymbol{G}^H$, we get,

$$\begin{aligned}\boldsymbol{G}\boldsymbol{G}^H &= \boldsymbol{F}^{-1}(\boldsymbol{H}^H\boldsymbol{H})^{-1}\boldsymbol{F}^{-H} \\ &= \frac{tr(\boldsymbol{\Lambda}^{\frac{1}{2}})}{p_0}\boldsymbol{D}^H\boldsymbol{\Lambda}^{\frac{1}{2}}\boldsymbol{D}, \\ \Longrightarrow \quad [\boldsymbol{G}\boldsymbol{G}^H]_{ii} &= \frac{tr(\boldsymbol{\Lambda}^{\frac{1}{2}})}{p_0}[\boldsymbol{D}^H\boldsymbol{\Lambda}^{\frac{1}{2}}\boldsymbol{D}]_{ii}, \end{aligned} \tag{3.21}$$

where $[\boldsymbol{D}^H\boldsymbol{\Lambda}^{\frac{1}{2}}\boldsymbol{D}]_{ii}$ is given by,

$$\begin{aligned}[\boldsymbol{D}^H\boldsymbol{\Lambda}^{\frac{1}{2}}\boldsymbol{D}]_{ii} &= \sum_{j=1}^{M}\lambda_j^{\frac{1}{2}}|d_{ij}|^2 \\ &= \frac{1}{M}\sum_{j=1}^{M}\lambda_j^{\frac{1}{2}} \qquad (3.22) \\ &= \frac{tr(\boldsymbol{\Lambda}^{\frac{1}{2}})}{M}, \qquad (3.23)\end{aligned}$$

and d_{ij} denotes the i,jth element in $\boldsymbol{D}, i, j \in [1, M]$, and λ_j is the jth diagonal element in $\boldsymbol{\Lambda}$. Eq (3.23) indicates the diagonal elements in $\boldsymbol{G}\boldsymbol{G}^H$ are equal, hence $P_e = \underline{P_e}$, i.e., the minimized lower bound for the BER has been achieved.

Now we are ready to conclude that $\boldsymbol{F}_{\text{stage1}}$ given in Eq (3.20) is indeed a MBER precoder. The optimal precoder and the minimized lower bound of BER are as follows,

$$\boldsymbol{F}_{\text{opt}} = \sqrt{\frac{p_0}{tr(\boldsymbol{\Lambda}^{\frac{1}{2}})}}\boldsymbol{W}\boldsymbol{\Lambda}^{\frac{1}{4}}\boldsymbol{D} \tag{3.24}$$

$$P_{e,min} = \frac{1}{2}\,\text{erfc}\left(\frac{\sqrt{Mp_0}}{\sqrt{2}\sigma tr(\boldsymbol{\Lambda}^{\frac{1}{2}})}\right). \tag{3.25}$$

For frequency selective channels, the matrix $\boldsymbol{D}$ can be chosen as a normalized DFT matrix or a normalized Hadamard matrix (if the block size is power of 2). For an ideal channel it can be any unitary matrix.

3.4 Remarks

3.4.1 Validity of the MBER precoder

From Section 3.3.1, the analytic solution for the MBER precoder is valid iff

$$\frac{\left(tr(\mathbf{\Lambda}^{\frac{1}{2}})\right)^2}{p_0} \leq \frac{M}{3\sigma^2}. \tag{3.26}$$

We define the received SNR as the ratio of transmitting power and noise power. Since the noise at receiver is P-dimensional, each dimension has power of σ^2, then the noise power is $P\sigma^2$. Therefore SNR can be expressed as:

$$SNR \triangleq \frac{p_0}{P\sigma^2}. \tag{3.27}$$

This definition of SNR is referred as standard SNR. A modified SNR will be defined later in Section 3.5. Re-writing the inequality in (3.26), we have,

$$SNR \geq \frac{3\left(tr(\mathbf{\Lambda}^{\frac{1}{2}})\right)^2}{PM} \triangleq SNR_0. \tag{3.28}$$

The inequality in (3.28) indicates that the condition for the validity of the analytic solution for the MBER precoder corresponds to moderate-to-high SNR. This condition can be ensured by either increasing transmitting power to raise SNR or dropping sub-channels corresponding to the largest values in $\mathbf{\Lambda}$ to lower the value of SNR_0. Dropping sub-channels corresponds to avoiding transmission on the 'low-gain' sub-channels, and re-allocating transmission power among the surviving ones. As a result, dropping sub-channels decreases the block size M. Although the denominator on the right side of (3.28) is also decreased, the numerator decreases more rapidly, and therefore the value of SNR_0 diminishes. The process of dropping channels stops when $SNR > SNR_0 = \frac{3tr(\bar{\mathbf{\Lambda}}^{\frac{1}{2}})^2}{P\bar{M}}$ is satisfied, where $\bar{\mathbf{\Lambda}}$ contains the remaining eigen-values of $(\boldsymbol{H}^H\boldsymbol{H})^{-1}$, and $\bar{M}$ is the new block size. The benefit of dropping sub-channels is that the minimum BER precoder is guaranteed without violating the transmission power budget, but the block size becomes smaller, thus transmission rate is lower (Assumption A6)

that the bit loading is uniform). The sub-channel dropping scheme and the corresponding MBER precoder design can be implemented by the following steps.

- Suppose that $\mathbf{\Lambda}$ is ordered in descending order of the magnitudes of the eigen-values, and let $\bar{M} = M$, $\bar{\mathbf{\Lambda}} = \mathbf{\Lambda}$.
- First determine the new block size $\bar{M}$:
  While $SNR < \frac{3\left(tr(\bar{\mathbf{\Lambda}}^{\frac{1}{2}})\right)^2}{M_1} - \kappa$, set $\bar{M} = \bar{M} - 1$, and set the largest element in $\bar{\mathbf{\Lambda}}$ to zero. Since $\mathbf{\Lambda}$ is ordered, the largest element of $\bar{\mathbf{\Lambda}}$ will be the first non-zero one.
- Then calculate the MBER precoder $\boldsymbol{F}_{\text{MBER-DROP}}$ after dropping sub-channels:
  Form $\bar{\boldsymbol{F}}_{\text{DROP}}$ by removing the first $M - \bar{M}$ columns in matrix $\bar{\boldsymbol{F}}_{\text{predrop}} = \sqrt{\frac{p_0}{tr(\bar{\mathbf{\Lambda}}^{\frac{1}{2}})}}\boldsymbol{W}\bar{\mathbf{\Lambda}}^{\frac{1}{4}}$, then calculate the MBER precoder after dropping sub-channels by $\boldsymbol{F}_{\text{MBER-DROP}} = \bar{\boldsymbol{F}}_{\text{DROP}}\bar{\boldsymbol{D}}$, where $\bar{\boldsymbol{D}}$ is a DFT matrix of size $\bar{M}$.

After dropping sub-channels, the optimal precoder $\boldsymbol{F}_{\text{MBER-DROP}}$ is of size of $M \times \bar{M}$, a tall matrix, implying that of the M sub-channels, $M - \bar{M} + 1$ sub-channels are dropped. The value of SNR_0 determines when the dropping of sub-channels starts, thus it determines how much of a trade-off is made between the bit error rate and transmission rate. If a certain amount of SNR margin is desired, SNR_0 can be chosen as $SNR_0 = \frac{3\left(tr(\mathbf{\Lambda}^{\frac{1}{2}})\right)^2}{PM} - \kappa$, where $\kappa \geq 0$ is the SNR margin. If $\kappa = 0, SNR_0$ becomes, $SNR_0 = \frac{3\left(tr(\mathbf{\Lambda}^{\frac{1}{2}})\right)^2}{PM}$ corresponding to Eq (3.28).

3.4.2 Relationship between MBER precoder and MMSE precoder

In the solution set for the MMSE precoders indicated in Eq (3.17), there is a unitary matrix which can be chosen arbitrarily. Any unitary matrix such as a DCT matrix or an identity matrix produces the same (minimum) MSE, but only those which satisfy the condition in Lemma 3.1 provide minimum BER. Therefore, the MBER precoder is a special MMSE precoder with a carefully chosen degree of freedom for it. In other words, the MBER precoder is a MMSE precoder, however the reverse is not necessarily true.

3.4.3 MBER precoders for ZP and CP

The MBER precoder design scheme in Section 3.3 is applicable to both ZP and CP transmission schemes in which the precoder is a $M \times M$ full rank matrix. Both the ZP-MBER and CP-MBER precoder have the same general formula $\boldsymbol{F}_{\text{MBER}} = \sqrt{\frac{p_0}{tr(\Lambda^{\frac{1}{2}})}}\boldsymbol{W}\Lambda^{\frac{1}{4}}\boldsymbol{D}$. For ZP systems the channel matrix $\boldsymbol{H} = \boldsymbol{H}_{zp}$ is a $P \times M$ tall Toeplitz matrix as indicated in Eq (2.6). For CP systems the channel matrix $\boldsymbol{H} = \boldsymbol{H}_{cp}$ is a $M \times M$ circulant matrix as in Eq (2.11). Recall that $\boldsymbol{H}_{cp}$ can be diagonalized by pre and post multiplication by DFT and IDFT matrices respectively, i.e., $\boldsymbol{D}\boldsymbol{H}_{cp}\boldsymbol{D}^H = \boldsymbol{\Delta}_H$, where $\boldsymbol{\Delta}_H$ is the channel frequency response, i.e., $\boldsymbol{\Delta}_H = diag\left(H(e^{j0}),\ H(e^{j2\pi/M}),\ \cdots\ H(e^{j2\pi(M-1)/M}) \right)$. Therefore one form of the eigen-decomposition for $(\boldsymbol{H}_{cp}^H\boldsymbol{H}_{cp})^{-1}$ is

$$(\boldsymbol{H}_{cp}^H\boldsymbol{H}_{cp})^{-1} = \boldsymbol{D}^H(\boldsymbol{\Delta}_H^H\boldsymbol{\Delta}_H)^{-1}\boldsymbol{D}, \tag{3.29}$$

the diagonal matrix $(\boldsymbol{\Delta}_H^H\boldsymbol{\Delta}_H)^{-1}$ contains the eigen-values of $(\boldsymbol{H}_{cp}^H\boldsymbol{H}_{cp})^{-1}$. Of course we can choose a permutation matrix $\boldsymbol{P}$ such that $\boldsymbol{P}(\boldsymbol{\Delta}_H^H\boldsymbol{\Delta}_H)^{-1}\boldsymbol{P}^H$ is ordered for the convenience of dropping channels, thus the MBER precoder for CP systems can be written,

$$\boldsymbol{F}_{\text{CP-MBER}} = \sqrt{\frac{p_0}{tr\left((\boldsymbol{\Delta}_H^{-1}\boldsymbol{\Delta}_H^{-H})^{\frac{1}{2}}\right)}}\,\boldsymbol{D}^H\boldsymbol{P}(\boldsymbol{\Delta}_H^{-1}\boldsymbol{\Delta}_H^{-H})^{\frac{1}{4}}\boldsymbol{P}^H\boldsymbol{D}, \tag{3.30}$$

where $\boldsymbol{P}$ is a permutation matrix such that $\boldsymbol{P}(\boldsymbol{\Delta}_H^H\boldsymbol{\Delta}_H)^{-1}\boldsymbol{P}^H$ is ordered in descending order of the inverse of the squared magnitudes of the channel frequency response.

From Eq (3.17), the set of MMSE precoders for CP systems can be expressed as,

$$\boldsymbol{F}_{\text{CP-MMSE}} = \sqrt{\frac{p_0}{tr\left((\boldsymbol{\Delta}_H^{-1}\boldsymbol{\Delta}_H^{-H})^{\frac{1}{2}}\right)}}\,\boldsymbol{D}^H\left(\boldsymbol{P}(\boldsymbol{\Delta}_H^{-1}\boldsymbol{\Delta}_H^{-H})^{\frac{1}{4}}\boldsymbol{P}^H\right)\boldsymbol{U}, \tag{3.31}$$

where $\boldsymbol{U}$ is an arbitrary unitary matrix. If we choose $\boldsymbol{U} = \boldsymbol{I}$, the CP-MMSE precoder becomes

$$\boldsymbol{F}_{\text{CP-MMSE-I}} = \boldsymbol{D}^H\boldsymbol{\Delta}_{\text{MMSE}}, \tag{3.32}$$

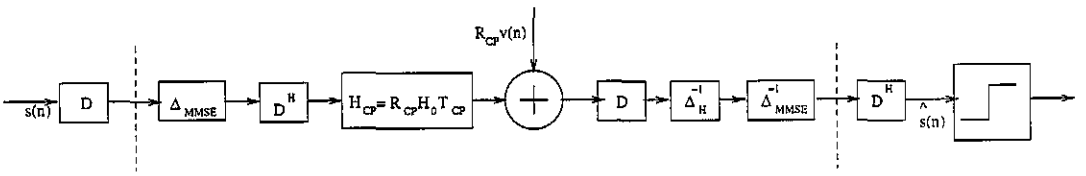

Figure 3.2: MBER precoder for CP transmission scheme

where

$$\boldsymbol{\Delta}_{\text{MMSE}} = \sqrt{\frac{p_0}{tr\big((\boldsymbol{\Delta}_H^{-1}\boldsymbol{\Delta}_H^{-H})^{\frac{1}{2}}\big)}}\,\boldsymbol{P}(\boldsymbol{\Delta}_H^{-1}\boldsymbol{\Delta}_H^{-H})^{\frac{1}{4}}\boldsymbol{P}^H, \tag{3.33}$$

is a diagonal matrix and is the MMSE power loading matrix. Comparing Eqs (3.33) and (3.30), the CP-MBER precoder can be written as

$$\boldsymbol{F}_{\text{CP-MBER}} = \boldsymbol{D}^H\boldsymbol{\Delta}_{\text{MMSE}}\boldsymbol{D}, \tag{3.34}$$

which indicates that the CP-MBER precoder is related to standard DMT in that the diagonal power loading matrix in standard DMT is replaced by a full matrix which consists of a diagonal MMSE power loading matrix post-multiplied by a DFT matrix. The MMSE power loading is less computational demanding and easier to implement than the water filling algorithm. The former is a linear function while the later is a non-linear function which may need recursive trials to fit the limit of the transmitting power. The diagram of a CP transmission system with MBER precoder is shown in Figure 3.2 where the receiver is determined by zero-forcing equalization by Assumption A4), $\boldsymbol{G}_{cp} = (\boldsymbol{H}_{cp}\boldsymbol{F}_{cp})^{-1} = \boldsymbol{D}^H\boldsymbol{\Delta}_{\text{MMSE}}^{-1}\boldsymbol{\Delta}_H^{-1}\boldsymbol{D}$. The scheme between the two vertical dashed lines can be regarded as a DMT system with MMSE power loading.

3.5 Analytic evaluations and analyses

In this section, we evaluate the BER performance of various ZP and CP precoders through an ill-conditioned channel, a well-conditioned channel, and a set of randomly generated channels. The transmitted power is normalized, i.e., $p_0 = 1$. The BERs are plotted versus the standard SNR and modified SNR defined in Eqs (3.27) and (3.46) respectively.

For ZP precoders, comparisons are given among the precoders designed by the criteria of MBER, MMSE, and maximum SNR [28], and the precoders corresponding to popular transmission schemes such as (zero-padded) TDMA and (zero-padded) OFDM in which the precoders are scaled identity and DFT matrix. As mentioned in Section 3.4, any unitary matrix in the solution set for MMSE precoder provides the same minimum mean square error, but not necessarily the same BERs. To illustrate that we choose the unitary matrix to be an identity matrix and a DCT matrix. The precoders are expressed respectively as following,

$$\boldsymbol{F}_{\text{ZP-MBER}} = \sqrt{\frac{p_0}{tr(\boldsymbol{\Lambda}^{\frac{1}{2}})}}\boldsymbol{W}\boldsymbol{\Lambda}^{\frac{1}{4}}\boldsymbol{D}, \tag{3.35}$$

$$\boldsymbol{F}_{\text{ZP-MMSE-I}} = \sqrt{\frac{p_0}{tr(\boldsymbol{\Lambda}^{\frac{1}{2}})}}\boldsymbol{W}\boldsymbol{\Lambda}^{\frac{1}{4}}, \tag{3.36}$$

$$\boldsymbol{F}_{\text{ZP-MMSE-DCT}} = \sqrt{\frac{p_0}{tr(\boldsymbol{\Lambda}^{\frac{1}{2}})}}\boldsymbol{W}\boldsymbol{\Lambda}^{\frac{1}{4}}\boldsymbol{U}_{DCT}, \tag{3.37}$$

$$\boldsymbol{F}_{\text{ZP-TDMA}} = \sqrt{\frac{p_0}{M}}\boldsymbol{I}, \tag{3.38}$$

$$\boldsymbol{F}_{\text{ZP-OFDM}} = \sqrt{\frac{p_0}{M}}\boldsymbol{D}, \tag{3.39}$$

$$\boldsymbol{F}_{\text{ZP-SNR}} = \sqrt{\frac{p_0}{tr(\boldsymbol{\Lambda})}}\boldsymbol{W}\boldsymbol{\Lambda}^{\frac{1}{2}}, \tag{3.40}$$

where $\boldsymbol{W}\boldsymbol{\Lambda}\boldsymbol{W}^H = (\boldsymbol{H}^H\boldsymbol{H})^{-1}$, $\boldsymbol{H}$ is the tall Toeplitz matrix shown in Eq (2.6), $\boldsymbol{D}$ is the DFT matrix, $\boldsymbol{U}_{DCT}$ is a DCT matrix with the i,jth element $[\boldsymbol{U}_{DCT}]_{i,j} = \sqrt{\frac{2}{M}}\cos(\frac{\pi(2i-1)(2j-1)}{4M}), i,j \in [1,M]$.

For CP transmission schemes, we examine the following precoders: MBER, MMSE, OFDM, and water filling DMT. The unitary matrix in the MMSE design is chosen as an

identity matrix. The precoders have the following forms.

$$\boldsymbol{F}_{\text{CP-MBER}} = \sqrt{\frac{p_0}{tr\left((\boldsymbol{\Delta}_H^{-1}\boldsymbol{\Delta}_H^{-H})^{\frac{1}{2}}\right)}}\boldsymbol{D}^H\boldsymbol{P}(\boldsymbol{\Delta}_H^{-1}\boldsymbol{\Delta}_H^{-H})^{\frac{1}{4}}\boldsymbol{P}^H\boldsymbol{D}, \tag{3.41}$$

$$\boldsymbol{F}_{\text{CP-OFDM}} = \sqrt{\frac{p_0}{M}}\boldsymbol{D}^H, \tag{3.42}$$

$$\boldsymbol{F}_{\text{WF-DMT}} = \boldsymbol{D}^H\boldsymbol{\Delta}_T, \tag{3.43}$$

$$\boldsymbol{F}_{\text{CP-MMSE-I}} = \boldsymbol{D}^H\boldsymbol{\Delta}_{\text{MMSE}}, \tag{3.44}$$

where $\boldsymbol{\Delta}_H$ is the channel frequency response indicated in Eq (2.13), $\boldsymbol{D}$ is the DFT matrix, $\boldsymbol{\Delta}_{\text{MMSE}}$ is the MMSE power loading matrix shown in Eq (3.33), $\boldsymbol{\Delta}_T$ is the water filling power loading matrix to maximize information rate, the ith diagonal element is shown in Eq (2.15). We display it again:

$$[\boldsymbol{\Delta}_T]_{ii} = \begin{cases} \sqrt{\eta - \frac{\sigma^2}{[\boldsymbol{\Delta}_H\boldsymbol{\Delta}_H^H]_{ii}}}, & \text{if } \eta > \frac{\sigma^2}{[\boldsymbol{\Delta}_H\boldsymbol{\Delta}_H^H]_{ii}} \\ 0, & \text{otherwise,} \end{cases} \tag{3.45}$$

where $[\boldsymbol{\Delta}_T]_{ii}$ and $[\boldsymbol{\Delta}_H\boldsymbol{\Delta}_H^H]_{ii}$ are the ith diagonal element of $\boldsymbol{\Delta}_T$ and $\boldsymbol{\Delta}_H\boldsymbol{\Delta}_H^H$ respectively, and η is a constant to satisfy the prescribed power $tr(\boldsymbol{\Delta}_T\boldsymbol{\Delta}_T^H) = p_0$. If a subchannel does not satisfy $\eta - \frac{\sigma^2}{[\boldsymbol{\Delta}_H\boldsymbol{\Delta}_H^H]_{ii}} > 0$, it is dropped and the block size is decreased. From Eq (3.45), sub-channel dropping happens when the noise is strong or the magnitude of the frequency response of the channel is small. For the fairness of comparison, the BER performances are also evaluated for the MBER precoders (including ZP and CP) with the same block sizes as water filling DMT. The MBER precoder after dropping sub-channels is obtained by the design scheme described in Section 3.4 except that the first step is omitted by choosing $\bar{M} = M_{DMT}$, where M_{DMT} is the block size according to water filling DMT.

In Section 3.3 we have mentioned that extra power is required in transmitting cyclic prefix in the CP systems. The extra power is $p_{\text{extra}} = \sum_{i=M-L+1}^{M} \boldsymbol{f}_i\boldsymbol{f}_i^H$, where $\boldsymbol{f}_i$ is the ith row in $\boldsymbol{F}$. It has been shown in Appendix C that the extra power for CP-OFDM, CP-MBER, and water-filling DMT precoders is the same. The value is $p_{\text{extra}} = \frac{Lp_0}{M}$, which depends on the ratio of the length of cyclic prefix L and the block size M and the power transmitting

the data block p_0. To take into account of the extra power spent on the cyclic prefix, we define a modified SNR as the total transmitting power, the power needed to transmit the data block, p_0, plus the power needed to transmit the cyclic prefix, p_{extra}, divided by the noise power,

$$SNR_{\text{modified}} \triangleq \frac{p_0 + p_{\text{extra}}}{P\sigma^2} = \frac{p_0 + \sum_{i=M-L+1}^{M} \boldsymbol{f}_i \boldsymbol{f}_i^H}{P\sigma^2}. \tag{3.46}$$

Because the ZP scheme does not spend any extra power, the SNR gain of the ZP-MBER precoder over the CP-MBER precoder is $10\log_{10}\frac{p_0(1+L)}{M}$ dB. The longer the delay of the channel, the greater the SNR gain. Comparisons are given between ZP-MBER and CP-MBER precoders with and without dropping sub-channels based on standard SNR and modified SNR will be used to demonstrate the SNR gain.

3.5.1 Example 1 — ill conditioned channel

In this example we consider a 3rd order channel with zeros at 0.7, $0.5\exp(j2\pi 0.256)$, $0.3\exp(j2\pi 0.141)$. The tap coefficients are $0.6121, -0.5331-0.4481j, 0.369j, 0.0513-0.0388j$. The triple $(M, L, P) = (32, 3, 35)$. Figure 3.3 shows the amplitudes of the channel impulse response and the magnitude of the frequency response of each sub-carrier (elements in $\boldsymbol{\Delta}_H$). Although there are no nulls at the sub-carriers, weak frequency responses do occur at several of the frequencies.

Figure 3.4 demonstrates the BER performance of the set of ZP precoders. The critical point is $SNR_0 = 11.13$ dB in this example. From this figure we can see that when $SNR \geq SNR_0$, the ZP-MBER precoder performs better than all other ZP precoders. As discussed in Section 3.4, at low SNR when $SNR \leq SNR_0$, we can use the technique of dropping sub-channels to guarantee the minimum BER performance. Figure 3.5 shows the block sizes of ZP-MBER at different SNR if the sub-channel dropping technique is used. Figure 3.6 shows the BER performances of ZP-MBER precoder with and without sub-channel dropping.

At lower SNR the version of sub-channel dropping scheme performs better than the non-dropping scheme, but it has a smaller block size and hence a lower data rate. At moderate-to-high SNR, when $SNR \geq SNR_0$, the process of dropping sub-channels stops, thus the BER performance of the dropping sub-channels version is the same as that of the non-dropping version.

To further analyze the BER performance, we examine the mean square errors at the receiver, i.e., $tr(\boldsymbol{G}\boldsymbol{G}^H)$, and the diagonal elements of $\boldsymbol{G}\boldsymbol{G}^H$ for the precoders. For fairness of comparison, we consider the SNR region in which all the precoders have the same block size, i.e., the moderate-to-high SNR where the process of dropping sub-channels is not required. The ZP-MBER, ZP-MMSE-I and ZP-MMSE-DCT precoders provide the same mean square error which is minimum, as shown in Eq (3.47). The ZP-OFDM, ZP-TDMA and ZP-SNR precoders produce the same mean square error which is not minimum as indicated in Eq (3.48):

$$tr(\boldsymbol{G}\boldsymbol{G}^H)_{\text{ZP-MBER}} = tr(\boldsymbol{G}\boldsymbol{G}^H)_{\text{ZP-MMSE-I}} = tr(\boldsymbol{G}\boldsymbol{G}^H)_{\text{ZP-MMSE-DCT}} = \frac{\left(tr(\boldsymbol{\Lambda}^{\frac{1}{2}})\right)^2}{p_0} \tag{3.47}$$

$$tr(\boldsymbol{G}\boldsymbol{G}^H)_{\text{ZP-OFDM}} = tr(\boldsymbol{G}\boldsymbol{G}^H)_{\text{ZP-TDMA}} = tr(\boldsymbol{G}\boldsymbol{G}^H)_{\text{ZP-SNR}} = \frac{Mtr(\boldsymbol{\Lambda})}{p_0} \tag{3.48}$$

The diagonal elements in $\boldsymbol{G}\boldsymbol{G}^H$ of the first group, the ZP-MBER, ZP-MMSE-I and ZP-MMSE-DCT precoders are shown in Figure 3.7, with the greatest fluctuations being observed for the ZP-MMSE-I precoder. A little fluctuation is observed for the ZP-MMSE-DCT precoder and no fluctuation is observed for the ZP-MBER precoder (as expected). In the first group, the ZP-MBER precoder performs best, and ZP-MMSE-DCT precoder better than ZP-MMSE-I precoder. The diagonal elements of $\boldsymbol{G}\boldsymbol{G}^H$ of the second group, the ZP-OFDM, ZP-TDMA and ZP-SNR precoders, are shown in Figure 3.8, with the greatest fluctuation being observed for the ZP-OFDM precoder, a little fluctuation is observed for the ZP-TDMA precoder and no fluctuation is observed for the ZP-SNR precoder. So in the second group, the ZP-SNR precoder gives better performance than both ZP-TDMA and ZP-OFDM precoder, and ZP-TDMA precoder better than ZP-OFDM precoder. Since the fluctuations of the diagonal elements in $\boldsymbol{G}\boldsymbol{G}^H$ of ZP-TDMA precoder is not very large, its BER performance

is close to that of ZP-SNR precoder. Both the ZP-MBER and ZP-SNR precoder have zero fluctuations of the diagonal elements in $\boldsymbol{GG}^H$, but ZP-MBER precoder performs better than ZP-SNR precoder because the former has smaller mean square error. As predicted by the theory the smaller the mean square error at the receiver and the smaller the fluctuations of the diagonal elements of the auto-correlation receiver matrix, the better the BER performance. The MBER precoder has the minimum mean square error and zero fluctuations, so it is the optimal precoder and produces minimum BER. It is also interesting to notice that in this example ZP-TDMA and ZP–SNR precoder perform better than ZP-MMSE-I at high SNR although the former two do not have minimum mean square error. The reason is that the diagonal elements on $\boldsymbol{GG}^H$ for the ZP-MMSE-I precoder vary substantially. This is further testimony to the fact that minimum mean square error does not guarantee minimum bit error rate.

We now examine the BER performance for the set of CP precoders. The block size adjusted according to water filling algorithm at different SNR is plotted in Figure 3.11. Figure 3.12 shows the performance of the various CP precoders. It can be observed that the CP-MBER precoder offers the best BER performance not only at moderate-to-high SNR, but also at lower SNR if the technique of dropping sub-channels is used. The MMSE power loading DMT performs better than both water filling DMT and CP-OFDM. Water filling DMT does not perform better than CP-OFDM unless the bad sub-channels are dropped. It is noted that the ith diagonal element for the power loading matrix is $\sqrt{\eta - \frac{\sigma^2}{[\boldsymbol{\Delta}_H \boldsymbol{\Delta}_H^H]_{ii}}}$ for water filling DMT. On the other hand, for the CP-OFDM, each of the sub-channel is allocated equal power, i.e., the ith diagonal element of the power loading matrix are all equal to $\sqrt{\frac{p_0}{M}}$. From the MMSE precoder design in Eq (3.33), the ith diagonal element should be proportional to $\left(\frac{1}{[\boldsymbol{\Delta}_H \boldsymbol{\Delta}_H^H]_{ii}}\right)^{\frac{1}{4}}$. Thus, it can be concluded that neither the water-filling DMT nor the OFDM satisfies the MMSE criterion. The negative sign before the $\frac{\sigma^2}{[\boldsymbol{\Delta}_H \boldsymbol{\Delta}_H^H]_{ii}}$ term in $\sqrt{\eta - \frac{\sigma^2}{[\boldsymbol{\Delta}_H \boldsymbol{\Delta}_H^H]_{ii}}}$ means that the direction of the channel dependence of water-filling DMT is opposite to that for the MMSE design, whereas the OFDM design is independent of the channel. It is therefore surmised that the OFDM design will have a lower mean square error than water-filling DMT. This can be observed from Figure 3.9 which shows the mean square errors produced by the CP-MBER-DROP and CP-OFDM precoders, and the DMT

schemes with water filling and MMSE power loading. Compared with CP-OFDM, water filling DMT has smaller mean square error at lower SNR due to dropping subchannels, but larger MSE at moderate high SNR when sub-channel dropping is no longer required. The mean square error provided by the CP-MBER-DROP precoder remains the minimum for the whole range of SNR. Figure 3.10 shows the distributions of the diagonal elements of $\boldsymbol{G}\boldsymbol{G}^H$ for the CP-MBER, CP-OFDM, MMSE power loaded DMT precoders (the $\boldsymbol{G}\boldsymbol{G}^H$ matrix for these precoders is SNR independent). Figure 3.10 also shows the distributions of the diagonal elements of $\boldsymbol{G}\boldsymbol{G}^H$ for the water-filling DMT precoder at $SNR = 25$ dB (in the region of moderate-to-high SNR). The fluctuations of the diagonal elements of $\boldsymbol{G}\boldsymbol{G}^H$ for the CP-OFDM and water filling DMT precoders are almost the same at moderate-to-high SNR. However, as mentioned above, the CP-OFDM precoder has lower mean square error than water filling DMT precoder, and therefore the CP-OFDM scheme provides better BER performance than water filling DMT at moderate-to-high SNR.

The comparison between ZP-MBER and CP-MBER precoders with and without dropping sub-channels, and water-filling DMT, based on the standard SNR defined in Eq (3.27) and the modified SNR in Eq (3.46) are shown in Figures 3.13 and 3.14, respectively. The SNR gain of the ZP-MBER precoder over the CP-MBER precoder is $10\log_{10}(p_0 + L/M) = 0.4$ dB in this example. Because of the different sub-channel dropping criteria for the precoders of ZP-MBER, CP-MBER and water-filling DMT, their block sizes are different at the different levels of SNR. For fair comparison, the BER performances of the ZP-MBER-DROP and CP-MBER-DROP in the two figures are evaluated using the same block size as water-filling DMT. The two figures show that the ZP-MBER/ZP-MBER-DROP precoders outperform the CP-MBER/CP-MBER-DROP precoders, especially when the extra power used in the CP transmission schemes is considered. This can explained by the CP transmission scheme in which the signal is transmitted on the sub-carriers of the channel. If a sub-carrier has poor frequency response or happens to be at a null of the channel frequency response, the signal transmitted at that sub-carrier turns out to be very small or zero at the receiver, making it very difficult to recover the original transmitted signal. The ZP scheme avoids the problem by making the channel matrix a tall Toeplitz one. However it needs to calculate the eigen-vectors of $(\boldsymbol{H}_{zp}^H \boldsymbol{H}_{zp})^{-1}$ for each different channel, while for the CP precoder the

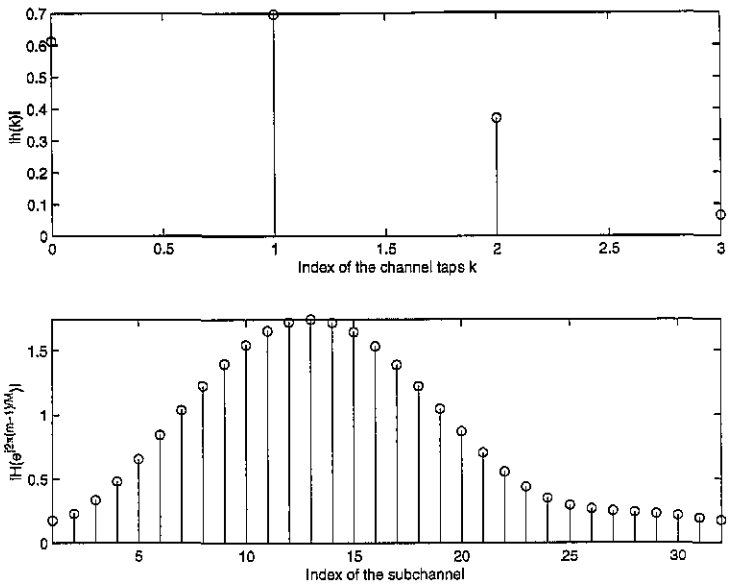

Figure 3.3: Impulse and frequency responses — ill-conditioned channel

eigen-vectors of $(\boldsymbol{H}_{cp}^H \boldsymbol{H}_{cp})^{-1}$ are merely the columns of an IDFT matrix, irrespective of the channel.

3.5.2 Example 2 — well conditioned channel

In this example we consider a 4th order channel which is better conditioned than that in Example 1. The tap coefficients are $\{0.3038+0.2554i, 0.5056+0.5587i, 0.2855+0.0035i, 0.2834+0.1843i, 0.2793+0.0305i\}$. The triple $(M, L, P) = (32, 4, 36)$. The amplitudes of the channel impulse response and the magnitude of the frequency response of the sub-carriers are shown in Figure 3.15. There are no nulls or near nulls at the sub-carriers, and hence fewer subchannels are dropped by water-filling DMT than in Example 1. The block sizes in the water-filling scheme are shown in Figure 3.17.

The BER performances of ZP and CP precoders are illustrated in Figures 3.16 to 3.19. Similar observations to those in Example 1 are obtained, except that a smaller critical value of SNR_0 (7.46 dB for ZP-MBER precoder) is achieved in this example. The BER improvement of the MBER precoders over other designs is still considerable, but it is not as significant as that in Example 1. The SNR gain of the ZP-MBER precoder over the CP-MBER precoder

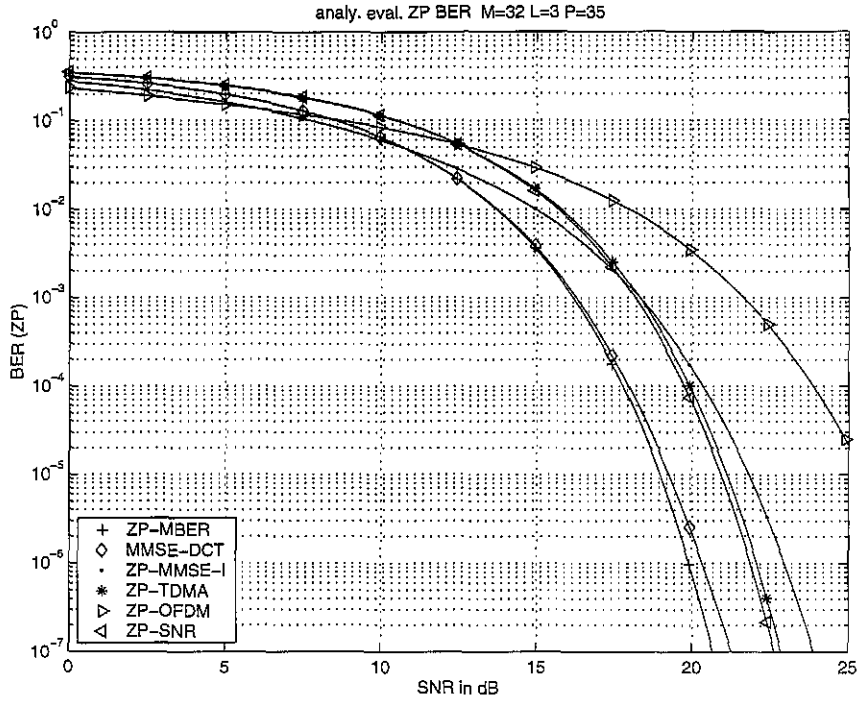

Figure 3.4: ZP precoders — ill-conditioned channel

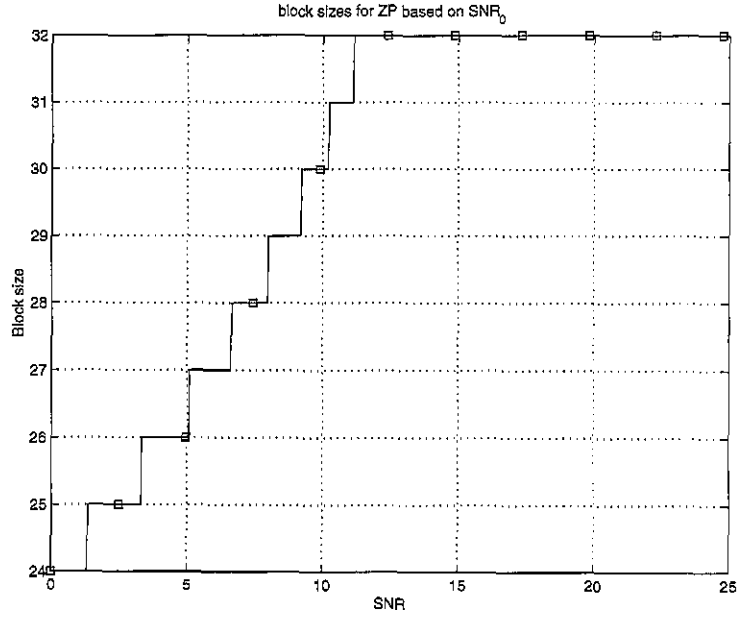

Figure 3.5: The block sizes of ZPMBER precoder by SNR_0 — ill-conditioned channel

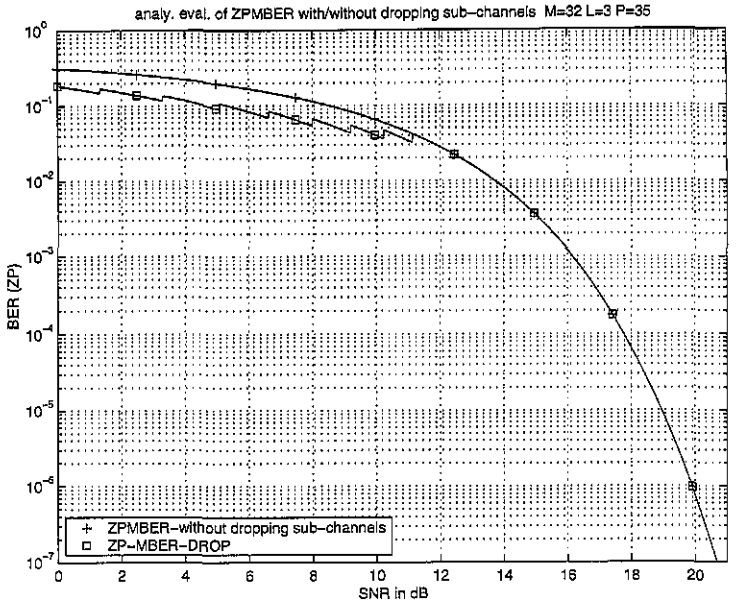

Figure 3.6: ZP-MBER precoders with and without dropping sub-channels — ill-conditioned channel

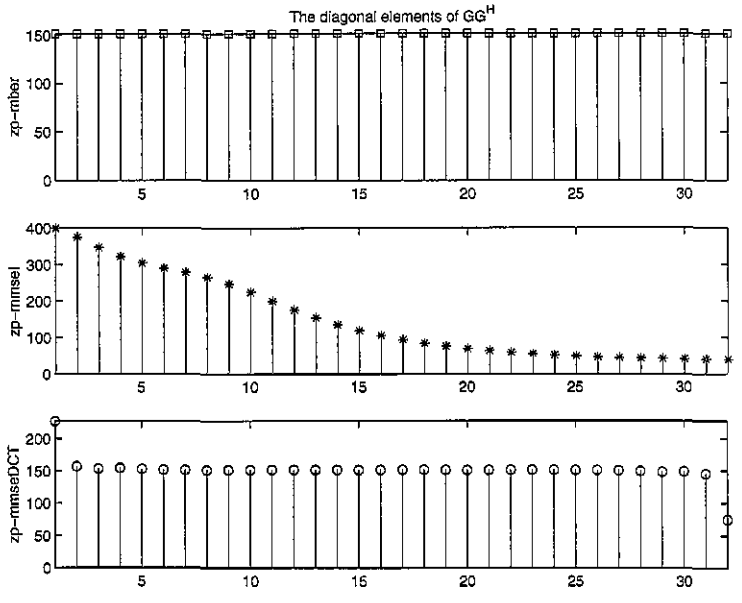

Figure 3.7: Diagonal elements of $\boldsymbol{GG}^H$ for ZP-MBER, ZP-MMSE-I and ZP-MMSE-DCT precoders — ill-conditioned channel

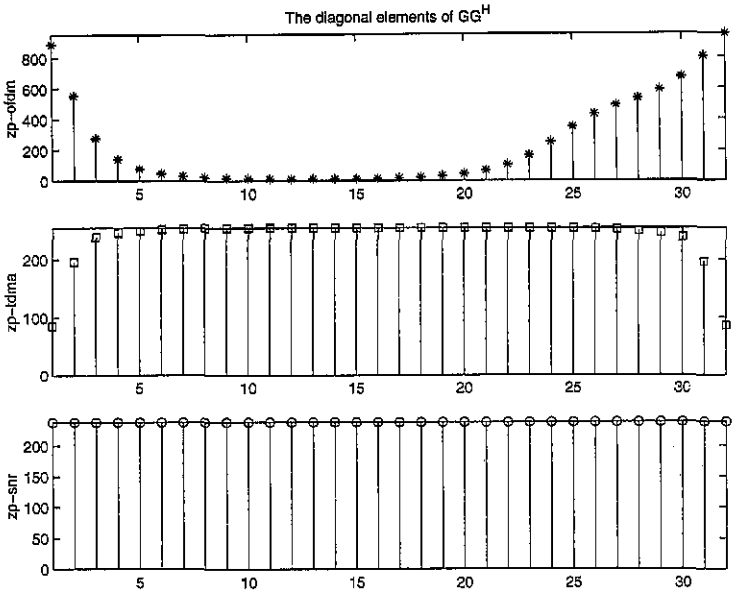

Figure 3.8: Diagonal elements of $\boldsymbol{GG}^H$ for ZP-OFDM, ZP-TDMA and ZP-SNR precoders — ill-conditioned channel

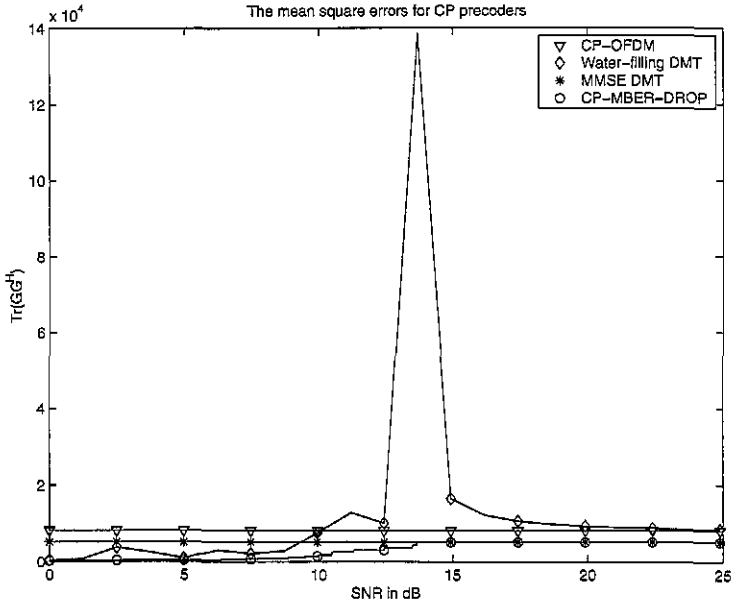

Figure 3.9: $tr(\boldsymbol{GG}^H)$ of CP precoders — ill-conditioned channel

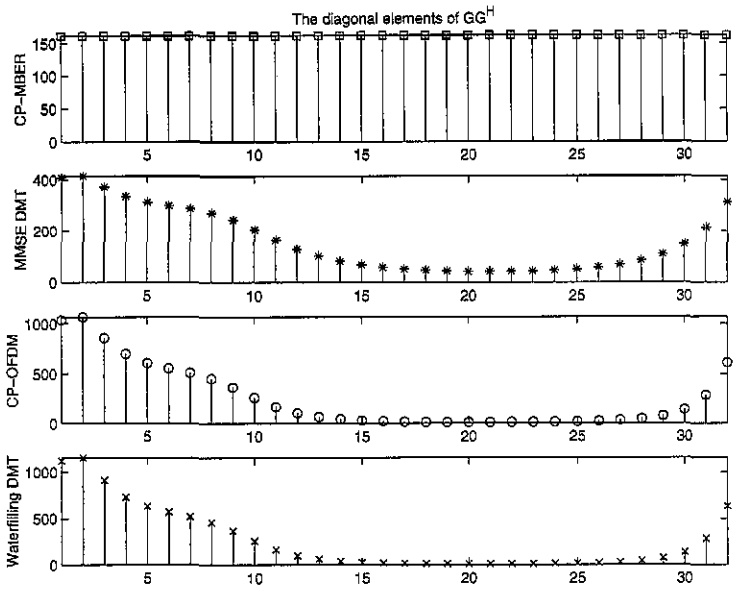

Figure 3.10: Diagonal elements of $\boldsymbol{GG}^{\boldsymbol{H}}$ for CP-MBER,CP-OFDM, MMSE-DMT and water filling DMT precoders — ill-conditioned channel

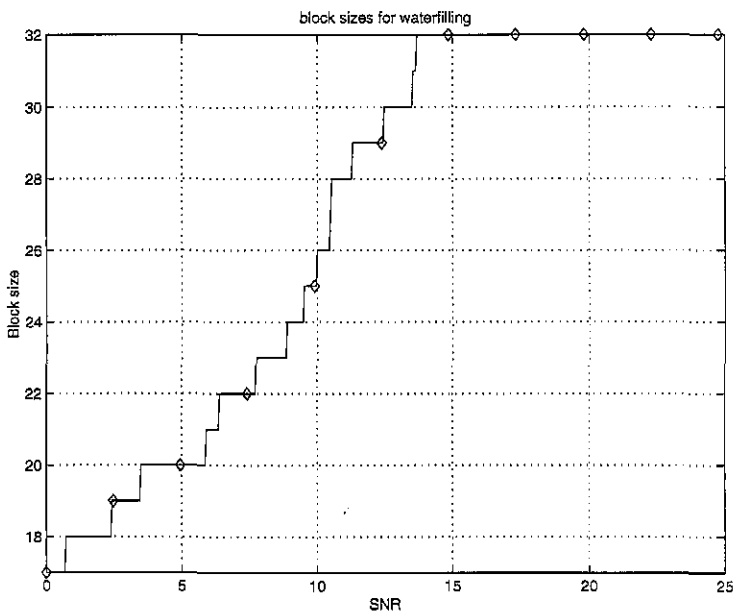

Figure 3.11: Block sizes of water filling DMT — ill-conditioned channel

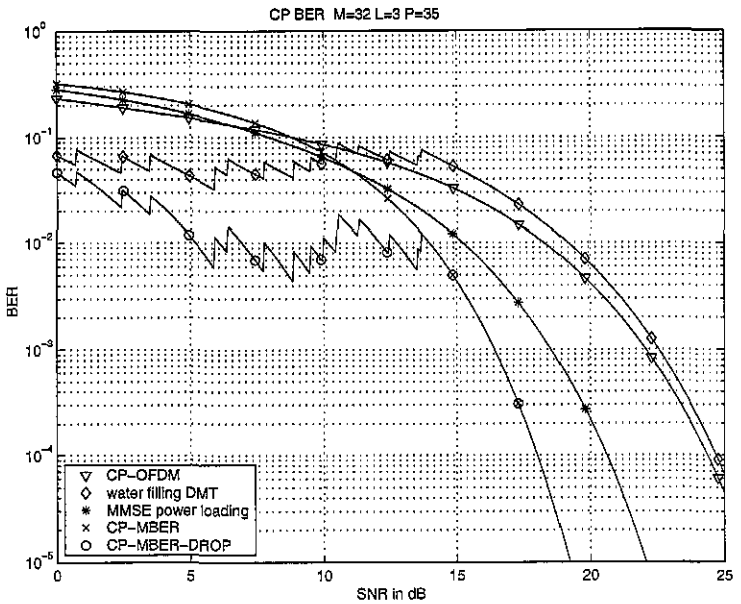

Figure 3.12: CP precoders — ill-conditioned channel

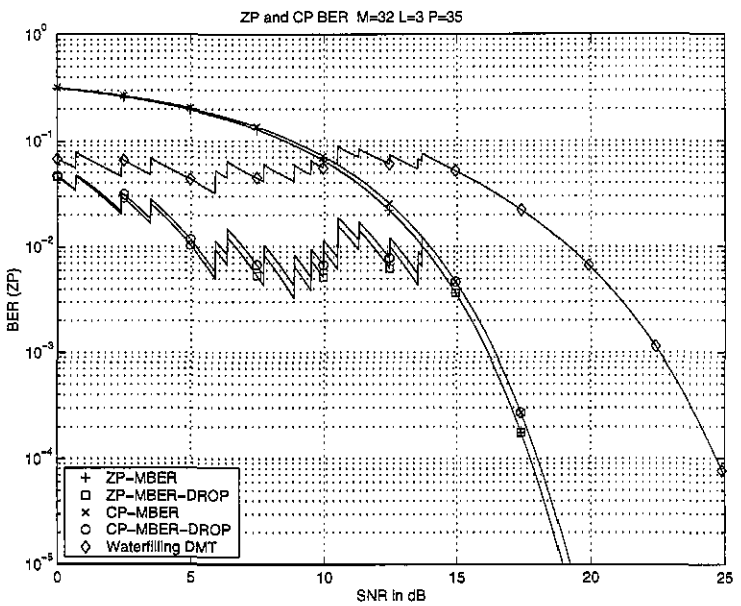

Figure 3.13: Comparisons of CP and ZP precoders — ill-conditioned channel

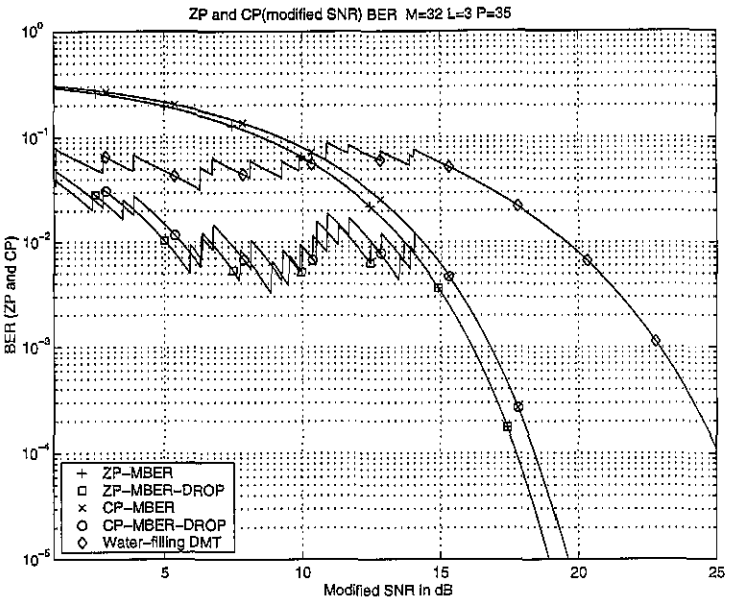

Figure 3.14: Comparisons of CP (modified SNR) and ZP precoders — ill-conditioned channel

is $10\log_{10}(p_0 + L/M) = 0.51$ dB, a little larger than in Example 1 because of the higher channel order, which means that more power has to be allocated to the cyclic-prefix portion in the CP scheme compared to Example 1.

3.5.3 Example 3 — BER average over channels

Examples 1 and 2 reveal that the MBER precoder provides different BER improvements for different channels. The more ill-conditioned the channel, the greater the BER improvement. In real communication systems such as in wireless communications, good channels and bad channels occur randomly, so we would like to investigate the average BERs over a number of random channels. This example demonstrates the BER performance of the two sets of precoders averaged over 500 random frequency-selective channels. The channel taps are generated in the same way described in Section 3.1, i.e., they are first generated by independent zero mean complex Gaussian variables with unit covariance, and then normalized by the norm. The triple $(M, L, P) = (16, 4, 20)$. The plots are shown in Figures 3.21 to 3.23. It is observed that the average BER improvement offered by MBER precoder with or without

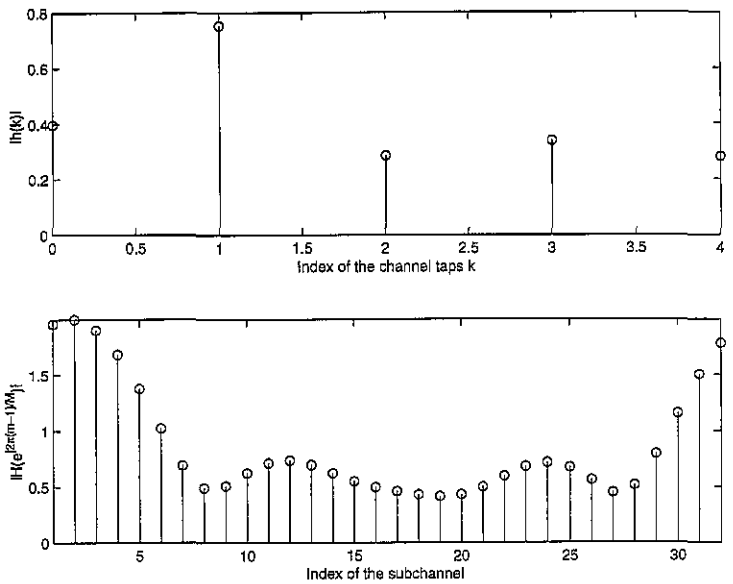

Figure 3.15: Impulse and frequency responses — well conditioned channel

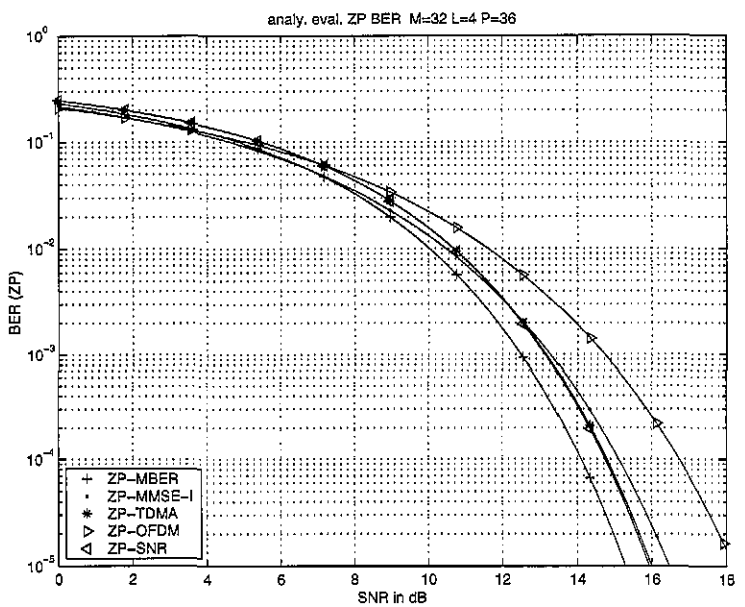

Figure 3.16: ZP precoders — well conditioned channel

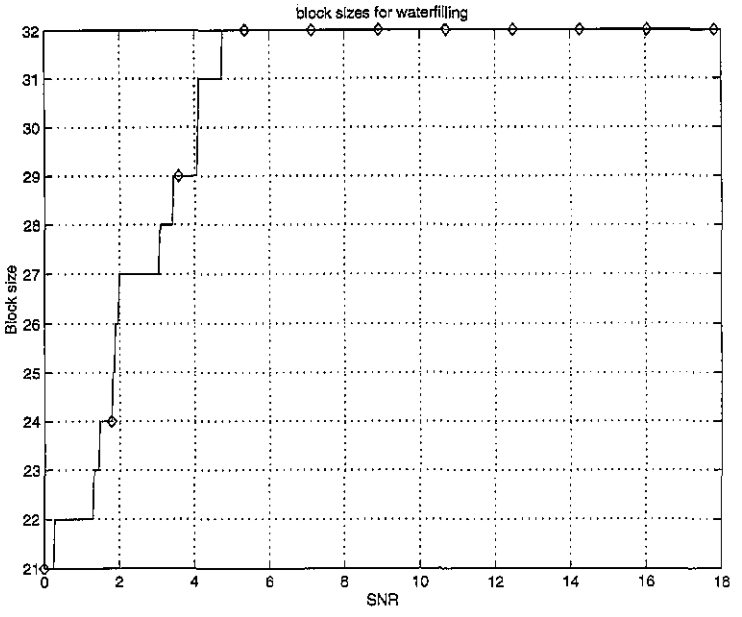

Figure 3.17: Block size of water filling DMT — well conditioned channel

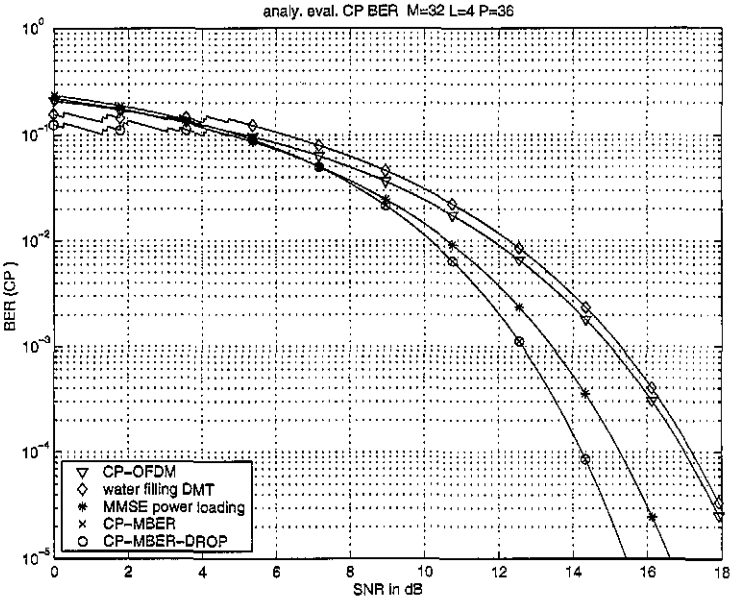

Figure 3.18: CP precoders — well conditioned channel

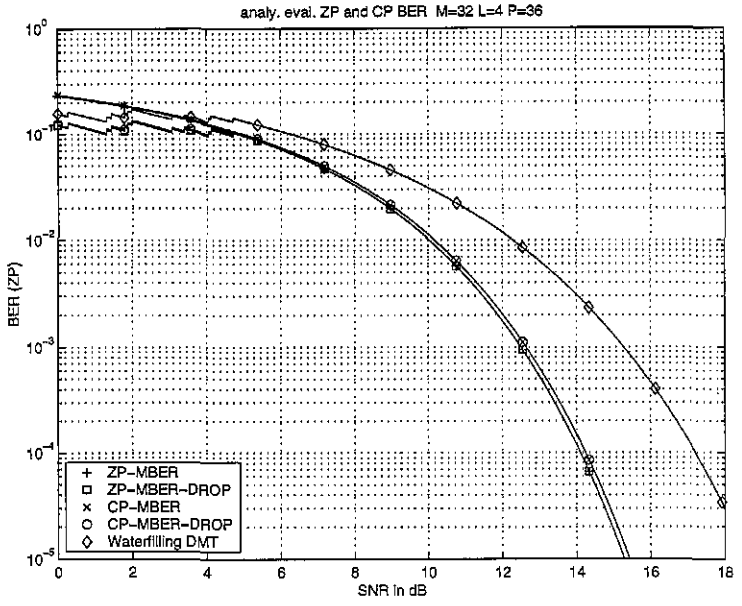

Figure 3.19: Comparisons of CP and ZP precoders — well conditioned channel

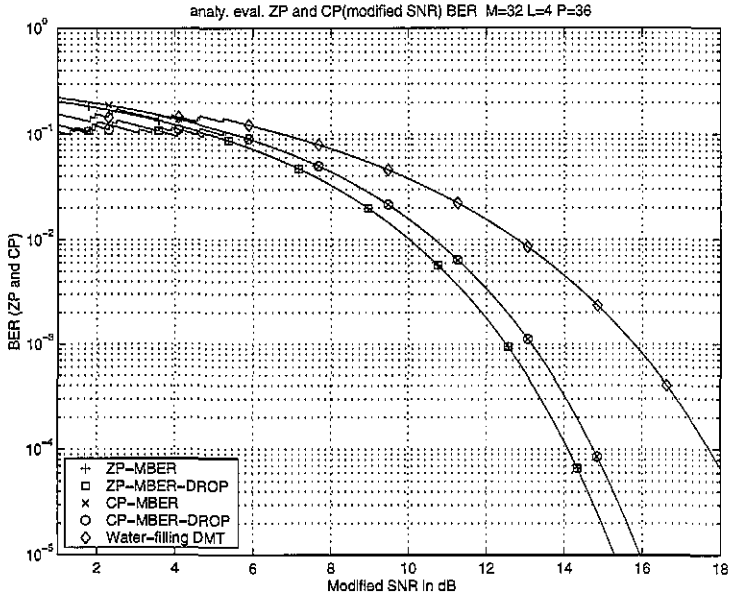

Figure 3.20: Comparisons of CP (modified SNR) and ZP precoders — well conditioned channel

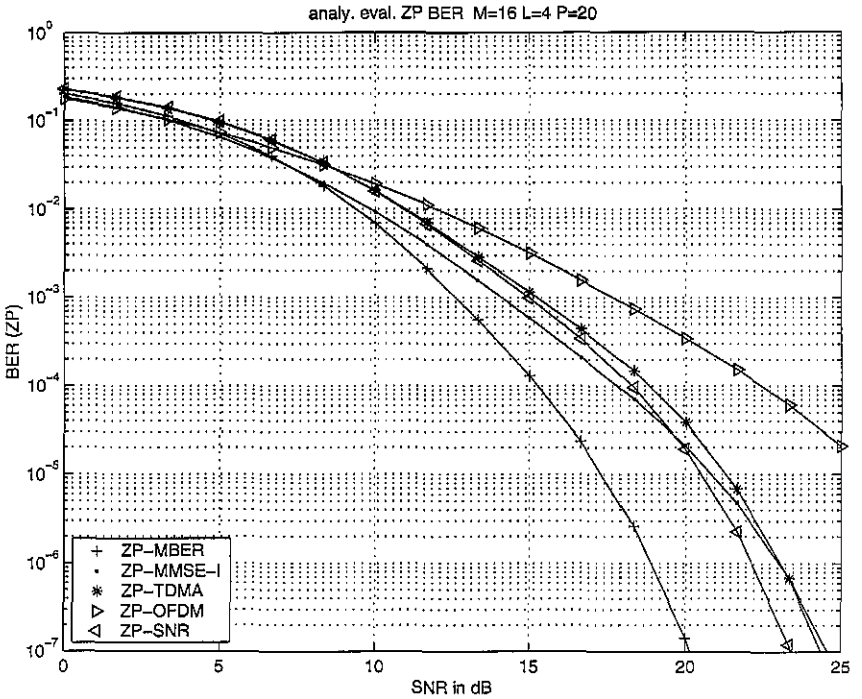

Figure 3.21: ZP precoders — average over 500 random channels

sub-channel dropping is quite significant.

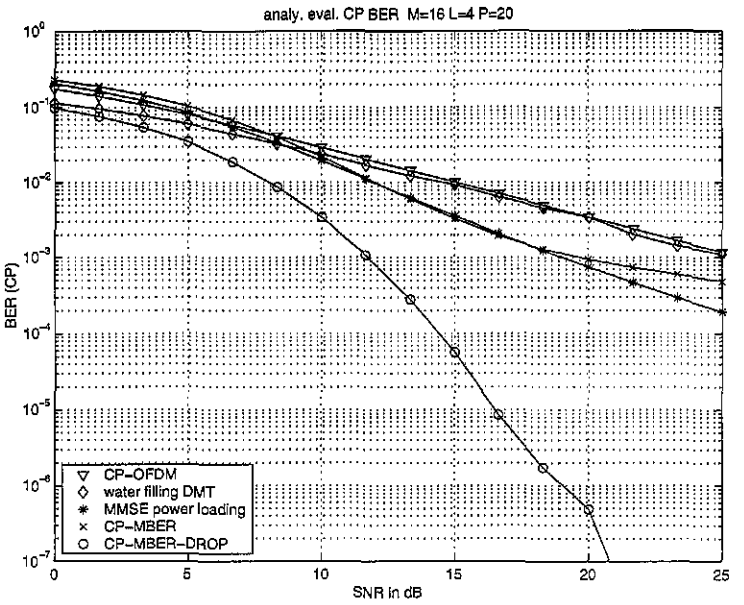

Figure 3.22: CP precoders — average over 500 random channels

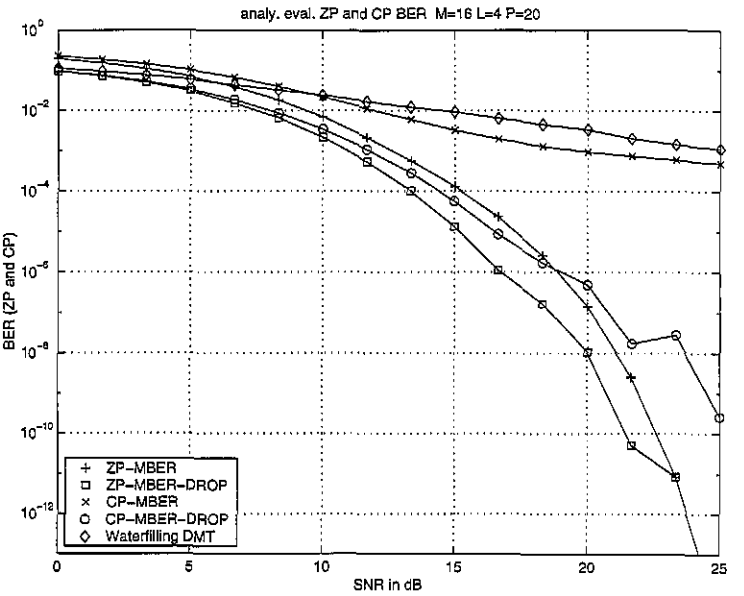

Figure 3.23: ZP and CP precoders — average over 500 random channels

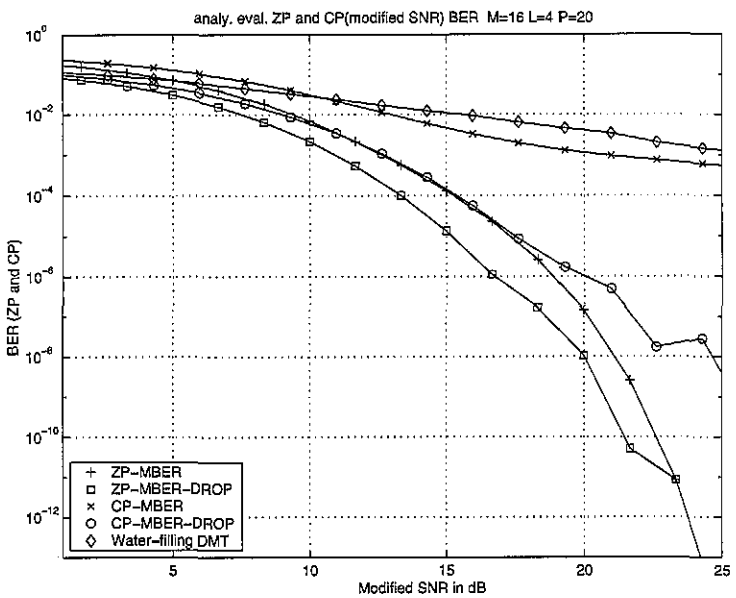

Figure 3.24: Comparisons of CP (modified SNR) and ZP precoders — average over 500 random channels

Chapter 4

Optimal Unitary Matrix for Some Classes of Precoder

In the solution set of some classes of precoder, there is a degree of freedom consisting of a unitary matrix. Examples include the set of optimal precoder maximizing information rate proposed in [28]. The solution set (derivation is also included in Appendix D) is $\boldsymbol{F}_{\text{info}} = \boldsymbol{W}\boldsymbol{\Phi}\boldsymbol{U}$ under the assumption of the thesis in Section 2.3, where $\boldsymbol{U}$ is an arbitrary unitary matrix, $\boldsymbol{W}\boldsymbol{\Lambda}\boldsymbol{W}^H = (\boldsymbol{H}^H\boldsymbol{H})^{-1}$, and $\boldsymbol{\Phi}$ is a diagonal matrix. Although different unitary matrices provide the same maximized information rate, they provide different BERs when ZF equalization and threshold detection are used at receiver. Inspired by the fact obtained in Chapter 3 that a carefully chosen unitary matrix in the MMSE precoder would make it a MBER precoder, we may ask if it is possible to choose the degree of freedom for the class of precoder described above, such that it has one more optimality, the minimum BER, on the basis of the one it originally designed for such as maximum information rate. The answer is positive. This chapter presents a design scheme for choosing the unitary matrix to minimize BER.

4.1 Design objective formulation

We consider a set of precoders which have a general form of

$$\boldsymbol{F} = \boldsymbol{A}\boldsymbol{U}, \tag{4.1}$$

where $\boldsymbol{U}$ is an arbitrary unitary matrix, and $\boldsymbol{A}$ has been determined by some other performance criteria. Our goal is to find the optimal choice for $\boldsymbol{U}$ such that bit error rate is minimized for ZF equalization and threshold detection.

Inserting $\boldsymbol{F} = \boldsymbol{A}\boldsymbol{U}$ into the formula for bit error rate in Eq (3.6), we have that

$$P_e = \frac{1}{2M}\sum_i \operatorname{erfc}\left(\frac{1}{\sqrt{2\sigma^2[\boldsymbol{F}^{-1}(\boldsymbol{H}^H\boldsymbol{H})^{-1}\boldsymbol{F}^{-H}]_{ii}}}\right) \tag{4.2}$$

$$= \frac{1}{2M}\sum_i \operatorname{erfc}\left(\frac{1}{\sqrt{2\sigma^2[\boldsymbol{U}^H\boldsymbol{A}^{-1}(\boldsymbol{H}^H\boldsymbol{H})^{-1}\boldsymbol{A}^{-H}\boldsymbol{U}]_{ii}}}\right) \tag{4.3}$$

$$= \frac{1}{2M}\sum_i \operatorname{erfc}\left(\frac{1}{\sqrt{2\sigma^2[\boldsymbol{U}^H\boldsymbol{S}\boldsymbol{\Gamma}\boldsymbol{S}^H\boldsymbol{U}]_{ii}}}\right)$$

$$= \frac{1}{2M}\sum_i \operatorname{erfc}\left(\frac{1}{\sqrt{2\sigma^2[\boldsymbol{R}^H\boldsymbol{\Gamma}\boldsymbol{R}]_{ii}}}\right), \tag{4.4}$$

where

$$\boldsymbol{S}\boldsymbol{\Gamma}\boldsymbol{S}^H = \boldsymbol{A}^{-1}(\boldsymbol{H}^H\boldsymbol{H})^{-1}\boldsymbol{A}^{-H}, \tag{4.5}$$

and $\boldsymbol{R} = \boldsymbol{S}^H\boldsymbol{U}$ is a unitary matrix. From Eq (4.4), the bit error rate P_e can be formulated as a function of a unitary matrix $\boldsymbol{R}$. The optimal $\boldsymbol{U}$ can be obtained from optimal $\boldsymbol{R}$ by

$$\boldsymbol{U}_{opt} = \boldsymbol{S}\boldsymbol{R}_{opt}. \tag{4.6}$$

From Eq (4.4), if $\boldsymbol{\Gamma}$ has the same entries, i.e. $\boldsymbol{\Gamma} = \gamma\boldsymbol{I}$, where γ is a constant, the solution for $\boldsymbol{R}$ is just an arbitrary unitary matrix. The solution for $\boldsymbol{U}$ is $\boldsymbol{U} = \boldsymbol{S}$, which is also an arbitrary unitary matrix due to the non-uniqueness of the eigen-decomposition of

$\boldsymbol{A}^{-1}(\boldsymbol{H}^H\boldsymbol{H})^{-1}\boldsymbol{A}^{-H} = \boldsymbol{S}\gamma\boldsymbol{I}\boldsymbol{S}^H = \gamma\boldsymbol{I}$. Here we consider a more general case where $\Gamma \neq \gamma\boldsymbol{I}$, i.e., it does not have the same entries. We study the design problem according to the convex and non-convex regions of the BER function respectively.

4.2 The optimal unitary matrix in the convex region of BER

Following the design scheme in Chapter 3, we apply Jensen's inequality in the region where the BER function is convex, i.e. $[\boldsymbol{R}^H\boldsymbol{\Gamma}\boldsymbol{R}]_{ii} < \frac{1}{3\sigma^2}$,

$$P_e \geq \frac{1}{2}\operatorname{erfc}\left(\frac{1}{\sqrt{2\sigma^2\left(\frac{tr(\boldsymbol{R}^H\boldsymbol{\Gamma}\boldsymbol{R})}{M}\right)}}\right) \tag{4.7}$$

$$= \frac{1}{2}\operatorname{erfc}\left(\frac{1}{\sqrt{2\sigma^2\left(\frac{tr(\boldsymbol{\Gamma})}{M}\right)}}\right) \tag{4.8}$$

$$\triangleq \underline{P_e}. \tag{4.9}$$

Equality in (4.7) holds if and only if $[\boldsymbol{R}^H\boldsymbol{\Gamma}\boldsymbol{R}]_{ii}$ are equal, $\forall i \in [i, M]$. Here $\underline{P_e}$ is a lower bound of P_e. From the discussion in Section 3.3, the validity of the solution for $\boldsymbol{R}$ depends on the value of $tr(\boldsymbol{\Gamma})$ which is a known value given a precoder class and the channel. According to Lemma 1 in Section 3.3, if $tr(\boldsymbol{\Gamma}) < \frac{M}{3\sigma^2}$, one solution for $\boldsymbol{R}$ to reach the lower bound is $\boldsymbol{R} = \boldsymbol{D}$, where $\boldsymbol{D}$ is a DFT, IDFT matrix, or a normalized Hadamard matrix if the block size M is of power of 2. Therefore, if

$$tr(\boldsymbol{\Gamma}) < \frac{M}{3\sigma^2}, \tag{4.10}$$

an optimal $\boldsymbol{U}$ is given by

$$\boldsymbol{U}_{opt} = \boldsymbol{S}\boldsymbol{R} = \boldsymbol{S}\boldsymbol{D}. \tag{4.11}$$

4.3 The optimal unitary matrix in the non-convex region of BER

In the region in which the bit error rate function is not convex, Jensen's inequality cannot be applied. We now use the Lagrange multiplier technique to find the optimal unitary matrix. We are going to construct the Lagrangian function, find the stationary points and pick up the one that provides the global minima. Our design objective can be formulated as the following constrained optimization problem,

$$\min_{\boldsymbol{R}} P_e$$
$$\text{subject to } \boldsymbol{R}^H\boldsymbol{R} = \boldsymbol{I}. \tag{4.12}$$

We omit the factor $\frac{1}{2M}$ in P_e, so minimizing P_e is equivalent to minimizing $\sum_i \text{erfc}\left(\frac{1}{\sqrt{2\sigma^2[\boldsymbol{R}^H\boldsymbol{\Gamma}\boldsymbol{R}]_{ii}}}\right)$. The constraint in Eq (4.12) is $(\boldsymbol{R}^H\boldsymbol{R}-\boldsymbol{I}) = \boldsymbol{0}$. Since $(\boldsymbol{R}^H\boldsymbol{R}-\boldsymbol{I})$ is Hermitian, the Lagrangian function [18] is as follows:

$$\begin{aligned} J &= \sum_i \text{erfc}\left(\frac{1}{\sqrt{2\sigma^2[\boldsymbol{R}^H\boldsymbol{\Gamma}\boldsymbol{R}]_{ii}}}\right) + tr\big(\boldsymbol{L}(\boldsymbol{R}^H\boldsymbol{R}-\boldsymbol{I})\big) \\ &= \sum_i \text{erfc}\left(\frac{1}{\sqrt{2\sigma^2[\boldsymbol{R}^H\boldsymbol{\Gamma}\boldsymbol{R}]_{ii}}}\right) + tr\big((\boldsymbol{R}^H\boldsymbol{R}-\boldsymbol{I})\boldsymbol{L}\big) \end{aligned} \tag{4.13}$$

where $\boldsymbol{L}$, an $M \times M$ Hermitian matrix, is the Lagrange multiplier [18].

4.3.1 The stationary points

A necessary condition for optimality in Eq (4.12) is that the precoder is at a stationary point for the Lagrangian function in Eq (4.13). The optimal solution for the optimization problem can be found among the stationary points of (4.13). In this section we are going to find these stationary points by taking the first derivative of the Lagrangian function according to $\boldsymbol{R}$. We reformulate $[\boldsymbol{R}^H\boldsymbol{\Gamma}\boldsymbol{R}]_{ii}$ as the trace function of some matrix product by introducing matrix $\boldsymbol{E}_i$, a matrix with zeros everywhere except for the iith element which is equal to 1.

Hence $[\boldsymbol{R}^H\boldsymbol{\Gamma}\boldsymbol{R}]_{ii}$ can be written as,

$$\begin{aligned}[\boldsymbol{R}^H\boldsymbol{\Gamma}\boldsymbol{R}]_{ii} &= \boldsymbol{e}_i^T\boldsymbol{R}^H\boldsymbol{\Gamma}\boldsymbol{R}\boldsymbol{e}_i \\ &= tr(\boldsymbol{R}^H\boldsymbol{\Gamma}\boldsymbol{R}\boldsymbol{E}_i),\end{aligned} \tag{4.14}$$

where $\boldsymbol{E}_i = \boldsymbol{e}_i\boldsymbol{e}_i^T$, $\boldsymbol{e}_i$ is the ith column of identity matrix. From Appendix B, we have $\frac{\partial tr(\boldsymbol{R}^H\boldsymbol{\Gamma}\boldsymbol{R}\boldsymbol{E}_i)}{\partial \boldsymbol{R}} = \boldsymbol{\Gamma}\boldsymbol{R}^*\boldsymbol{E}_i$, where $\boldsymbol{R}$ is complex, $\boldsymbol{\Gamma}$ and $\boldsymbol{E}_i$ are symmetric, * represents complex conjugate. Therefore, the first derivative of the Lagrangian function with respect to $\boldsymbol{R}$ has the following form,

$$\begin{aligned}\frac{\partial J}{\partial \boldsymbol{R}} &= \sum_i -\exp\{-\sigma^{-2}\big(tr(\boldsymbol{R}^H\boldsymbol{\Gamma}\boldsymbol{R}\boldsymbol{E}_i)\big)^{-1}\}(-\frac{1}{2\sigma})[tr(\boldsymbol{R}^H\boldsymbol{\Gamma}\boldsymbol{R}\boldsymbol{E}_i)]^{-\frac{3}{2}}\boldsymbol{\Gamma}\boldsymbol{R}^*\boldsymbol{E}_i + \boldsymbol{R}^*\boldsymbol{L} \\ &= \sum_i k_i\boldsymbol{\Gamma}\boldsymbol{R}^*\boldsymbol{E}_i + \boldsymbol{R}^*\boldsymbol{L},\end{aligned}$$

where

$$k_i = \frac{1}{\sqrt{2\pi}\sigma}\exp\Big(-\big(2\sigma^2 tr(\boldsymbol{R}^H\boldsymbol{\Gamma}\boldsymbol{R}\boldsymbol{E}_i)\big)^{-1}\Big)\Big(tr(\boldsymbol{R}^H\boldsymbol{\Gamma}\boldsymbol{R}\boldsymbol{E}_i)\Big)^{-\frac{3}{2}}, \tag{4.15}$$

and k_i is real. By setting $\frac{\partial J}{\partial \boldsymbol{R}} = \boldsymbol{0}$, we have that

$$\begin{aligned}&\sum_i k_i\boldsymbol{\Gamma}\boldsymbol{R}^*\boldsymbol{E}_i + \boldsymbol{R}^*\boldsymbol{L} = 0 \\ \Longrightarrow\quad &\sum_i k_i\boldsymbol{\Gamma}\boldsymbol{R}\boldsymbol{E}_i + \boldsymbol{R}\boldsymbol{L}^* = 0 \\ \Longrightarrow\quad &\boldsymbol{\Gamma}\boldsymbol{R}\boldsymbol{K} + \boldsymbol{R}\boldsymbol{L}^* = 0 \\ \Longrightarrow\quad &\boldsymbol{L}^* = -\boldsymbol{R}^H\boldsymbol{\Gamma}\boldsymbol{R}\boldsymbol{K},\end{aligned} \tag{4.16}$$

where $\boldsymbol{K}$ is a real diagonal matrix with the ith diagonal element equal to k_i. Suppose that $\boldsymbol{R}$ can be written as,

$$\begin{aligned}\boldsymbol{R} &= \begin{pmatrix} r_{11} & r_{12} & \cdots & r_{1m} \\ r_{21} & r_{22} & \cdots & r_{2m} \\ \vdots & \vdots & \cdots & \vdots \\ r_{m1} & r_{m2} & \cdots & r_{mm} \end{pmatrix} \\ &= \begin{pmatrix} \boldsymbol{r}_1 & \boldsymbol{r}_2 & \cdots & \boldsymbol{r}_m \end{pmatrix}\end{aligned}$$

where $\boldsymbol{r}_i, i = 1, 2, \cdots, m$ denotes the ith column in $\boldsymbol{R}$. Expanding the right side of Eq (4.16), we get,

$$\boldsymbol{L}^* = - \begin{pmatrix} k_1 \boldsymbol{r}_1^H \boldsymbol{\Gamma} \boldsymbol{r}_1 & k_1 \boldsymbol{r}_1^H \boldsymbol{\Gamma} \boldsymbol{r}_2 & \cdots & k_1 \boldsymbol{r}_1^H \boldsymbol{\Gamma} \boldsymbol{r}_m \\ k_2 \boldsymbol{r}_2^H \boldsymbol{\Gamma} \boldsymbol{r}_1 & k_2 \boldsymbol{r}_2^H \boldsymbol{\Gamma} \boldsymbol{r}_2 & \cdots & k_2 \boldsymbol{r}_2^H \boldsymbol{\Gamma} \boldsymbol{r}_m \\ \vdots & \vdots & \cdots & \\ k_m \boldsymbol{r}_m^H \boldsymbol{\Gamma} \boldsymbol{r}_1 & k_m \boldsymbol{r}_m^H \boldsymbol{\Gamma} \boldsymbol{r}_2 & \cdots & k_m \boldsymbol{r}_m^H \boldsymbol{\Gamma} \boldsymbol{r}_m \end{pmatrix}.$$

Recalling that $\boldsymbol{L}$ is Hermitian, and k_i is real, $\forall i \in [1, M]$, we have

$$k_i \boldsymbol{r}_i^H \boldsymbol{\Gamma} \boldsymbol{r}_j = (k_j \boldsymbol{r}_j^H \boldsymbol{\Gamma} \boldsymbol{r}_i)^*, \quad i \neq j. \tag{4.17}$$

Since $\boldsymbol{r}_i^H \boldsymbol{\Gamma} \boldsymbol{r}_j = (\boldsymbol{r}_j^H \boldsymbol{\Gamma} \boldsymbol{r}_i)^*$, thus Eq (4.17) becomes $(k_i - k_j) \boldsymbol{r}_i^H \boldsymbol{\Gamma} \boldsymbol{r}_j = 0$, which is equivalent to,

$$k_i = k_j, \quad i \neq j \quad \text{or} \tag{4.18}$$

$$\boldsymbol{r}_i^H \boldsymbol{\Gamma} \boldsymbol{r}_j = 0. \tag{4.19}$$

From Eqs (4.14) and (4.15), k_i is the function of $[\boldsymbol{R}^H \boldsymbol{\Gamma} \boldsymbol{R}]_{ii}$. One solution to Eq (4.18) is that all $[\boldsymbol{R}^H \boldsymbol{\Gamma} \boldsymbol{R}]_{ii}$ are equal, $i \in [1, M]$. As discussed in Section 3.3, for all the diagonal elements of $\boldsymbol{R}^H \boldsymbol{\Gamma} \boldsymbol{R}$ to be equal, possible choices for $\boldsymbol{R}$ include the DFT and IDFT matrices, and the normalized Hadamard matrix if the block size is of power of 2. To satisfy Eq (4.19), we need

$\boldsymbol{R}^H\boldsymbol{\Gamma}\boldsymbol{R}$ to be a diagonal matrix. Since $\boldsymbol{\Gamma}$ is diagonal, $\boldsymbol{R}$ can be a permutation matrix. So the two solution sets for $\boldsymbol{R}$ are,

$$\boldsymbol{R} \quad \text{is a DFT, IDFT or normalized Hadamard matrix ,} \tag{4.20}$$

$$\boldsymbol{R} \quad \text{is a permutation matrix .} \tag{4.21}$$

The first solution set is actually the one obtained in Section 4.2, which is the optimal solution in the convex region of the BER function.

From the solutions for $\boldsymbol{R}$, we can get the solutions for the unitary matrix $\boldsymbol{U}$ in $\boldsymbol{F} = \boldsymbol{A}\boldsymbol{U}$ by Eq (4.6), i.e., $\boldsymbol{U} = \boldsymbol{S}\boldsymbol{R}$, where $\boldsymbol{S}$ is determined by Eq (4.5). Since the solutions for $\boldsymbol{R}$ in (4.20) and (4.21) are proposed based on a general form of the class of precoder, we need to examine a specific precoder in order to evaluate the performance of the solutions. Let's consider the precoder which maximizes information rate mentioned at the beginning at the chapter. Its solution is re-displayed as follows:

$$\boldsymbol{F}_{\text{info}} = \boldsymbol{W}\boldsymbol{\Phi}\boldsymbol{U}, \tag{4.22}$$

where $\boldsymbol{U}$ is an arbitrary unitary matrix, $\boldsymbol{W}\boldsymbol{\Lambda}\boldsymbol{W}^H = (\boldsymbol{H}^H\boldsymbol{H})^{-1}$, $\boldsymbol{\Phi}$ is a diagonal matrix with the ith diagonal entry,

$$\phi_{ii} = \sqrt{\max\left(\frac{p_0 + \sigma^2 tr(\boldsymbol{\Lambda})}{M} - \sigma^2\lambda_{ii}, 0\right)}, \tag{4.23}$$

and λ_{ii} is the ith diagonal entry of $\boldsymbol{\Lambda}$. Comparing (4.22) with the general form of the precoders in Eq (4.1), we have $\boldsymbol{A} = \boldsymbol{W}\boldsymbol{\Phi}$ in this example. Inserting $\boldsymbol{A}$ into Eq (4.5), we have,

$$\begin{aligned}\boldsymbol{S}\boldsymbol{\Gamma}\boldsymbol{S}^H &= \boldsymbol{A}^{-1}(\boldsymbol{H}^H\boldsymbol{H})^{-1}\boldsymbol{A}^{-H} \\ &= \boldsymbol{\Phi}^{-1}\boldsymbol{W}^H\boldsymbol{W}\boldsymbol{\Lambda}\boldsymbol{W}^H\boldsymbol{W}\boldsymbol{\Phi}^{-1} \\ &= \boldsymbol{\Phi}^{-2}\boldsymbol{\Lambda}.\end{aligned} \tag{4.24}$$

Eq (4.24) indicates that the matrix $\boldsymbol{A}^{-1}(\boldsymbol{H}^H\boldsymbol{H})^{-1}\boldsymbol{A}^{-H}$ is diagonal. Therefore one possible form for its eigen-vectors is $\boldsymbol{S} = \boldsymbol{I}$. The choice for $\boldsymbol{U}$ becomes:

$$\boldsymbol{U} = \boldsymbol{S}\boldsymbol{R} = \boldsymbol{R} \tag{4.25}$$

for the precoder to maximize information rate.

The BER performances are evaluated by,

$$P_e = \frac{1}{2M}\sum_{i=1}^{M} \text{erfc}\left(\frac{1}{\sqrt{2\sigma^2[\boldsymbol{F}_{\text{info}}^{-1}(\boldsymbol{H}^H\boldsymbol{H})^{-1}\boldsymbol{F}_{\text{info}}^{-H}]_{ii}}}\right),$$

where the unitary matrix $\boldsymbol{U}$ in $\boldsymbol{F}_{\text{info}}$ is chosen as: a DFT matrix, an identity matrix $\boldsymbol{I}$ which is a special permutation matrix, and the 90^0 rotation matrix of identity matrix which is another permutation matrix. We consider the same two channels in Chapter 3, an ill-conditioned channel and a well-conditioned channel. The plots are illustrated in Figure 4.1 and 4.2 respectively. It can be observed that choosing $\boldsymbol{U}$ to be a DFT matrix is the optimal choice at moderate-to-high SNR, while choosing $\boldsymbol{U}$ to be a permutation matrix is optimal at low SNR. Further more, different permutation matrices produce the same BER. This is expected if we examine the BER function in Eq (4.4) — the permutation matrix just permutes the positions of the terms under the summation sign, but the sum remains the same no matter how the terms are permutated. Again, the conditioning of the channel affects the amount of BER improvement obtained by the optimal unitary matrix. The BER performance improvement for an ill-conditioned channel is more significant than the improvement for a well-conditioned channel.

4.4 Applications

Although the optimal design for the unitary matrix is proposed for systems which employ zero-forcing equalization and have channel knowledge available, it can also be applied to systems where MMSE equalization is used and the exact channel knowledge is not available.

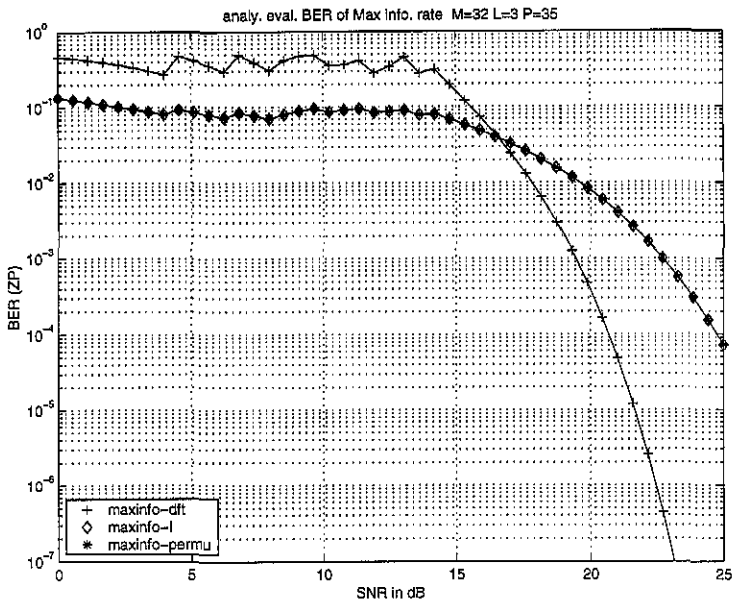

Figure 4.1: BER performance by the unitary matrices in precoder to maximize information rate — ill-conditioned channel

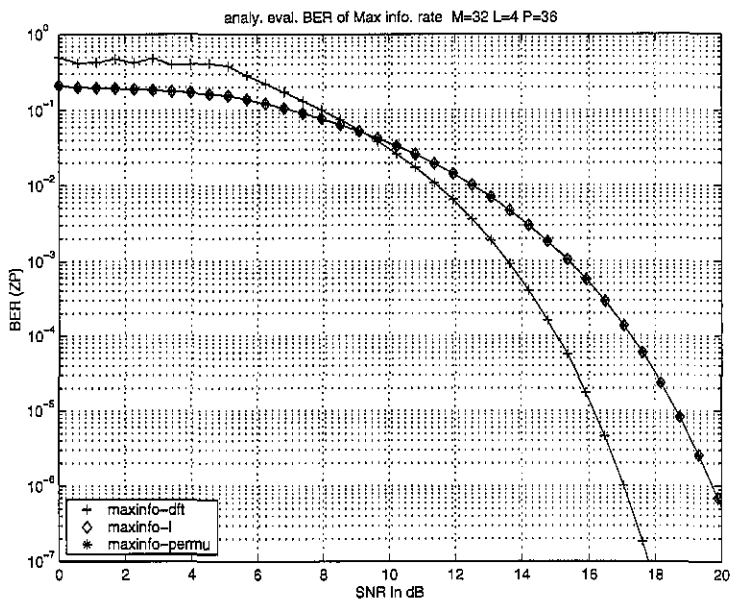

Figure 4.2: BER performance by the unitary matrices in precoder to maximize information rate — well-conditioned channel

4.4.1 Precoder for unknown channel

In [19] an MMSE precoder based on zero-forcing equalization is designed under the assumption that the exact channel information is not available but that the second order statistics are known. The optimal precoder has the form $\boldsymbol{F}_{\text{MMSE}} = \sqrt{\frac{p_0}{tr(\boldsymbol{\Lambda}^{\frac{1}{2}})}}\boldsymbol{W}\boldsymbol{\Lambda}^{\frac{1}{4}}\boldsymbol{U}$, where $E\{(\boldsymbol{H}^H\boldsymbol{H})^{-1}\} = \boldsymbol{W}\boldsymbol{\Lambda}\boldsymbol{W}^H$ [19]. In such circumstances the optimal solutions for $\boldsymbol{U}$ discussed in previous section are still applicable with the minor modification of replacing $(\boldsymbol{H}^H\boldsymbol{H})^{-1}$ with $E\{(\boldsymbol{H}^H\boldsymbol{H})^{-1}\}$. The optimal choice of $\boldsymbol{U}$ is $\boldsymbol{U}_{opt} = \boldsymbol{S}\boldsymbol{R}_{opt}$; the same formula as in previous discussion with $\boldsymbol{S}\boldsymbol{\Gamma}\boldsymbol{S}^H = \boldsymbol{A}^{-1}\big(E\{(\boldsymbol{H}^H\boldsymbol{H})^{-1}\}\big)\boldsymbol{A}^{-H} = \boldsymbol{\Lambda}^{\frac{1}{2}}$. Because $\boldsymbol{\Lambda}^{\frac{1}{2}}$ is diagonal, $\boldsymbol{S}$ can be an identity matrix. Therefore, the solution for $\boldsymbol{U}$ in this case is $\boldsymbol{U} = \boldsymbol{R}$, as for the precoder that maximized information rate. Simulation results are shown in Figure 4.3 and 4.4 where the triple $(M, L, P) = (8, 4, 12)$, $\boldsymbol{U}$ is chosen as a DFT matrix and an identity matrix respectively. The second order statistics of the channel are obtained by averaging over $900,000$ random channels. The channel taps are generated in the same way as in Section 3.1. The BERs are obtained by $20,000$ channel realizations with 500 blocks each. It is observed that choosing the unitary matrix $\boldsymbol{U}$ to be a DFT matrix is optimal at high SNR, while the choice of identity matrix (a permutation matrix) is optimal at low SNR.

4.4.2 Precoder for MMSE equalizer

Optimal MMSE precoders based on MMSE equalization are studied in [28]. Under the assumptions of the thesis, the optimal precoder is $\boldsymbol{F} = \boldsymbol{W}\boldsymbol{\Phi}\boldsymbol{U}$, where $\boldsymbol{U}$ is an arbitrary unitary matrix, $\boldsymbol{\Phi}$ is diagonal with the ith element determined by $[\boldsymbol{\Phi}]_{ii} = \sqrt{\frac{p_0+\sigma^2 tr(\boldsymbol{\Lambda})}{tr(\boldsymbol{\Lambda}^{\frac{1}{2}})}\sqrt{\lambda_{ii}} - \sigma^2\lambda_{ii}}$. Figure 4.5 shows the BER performance for two choices of $\boldsymbol{U}$ — a DFT and an identity matrix. The simulation results are obtained for $10,000$ channel realizations with 500 blocks each. Again, the channels are generated the same way as in Section 3.1. The triple $(M, L, P) = (8, 4, 12)$. The plot indicates that the DFT matrix offers BER improvement at high SNR, as in the case that ZF equalization (ZFE) is used. This can be explained as MMSE equalization approximates to ZFE at high SNR, so the optimal unitary matrix design based on ZEF may improve the BER for MMSE equalization in high SNR region. It is also observed that the two different choices of $\boldsymbol{U}$ provide almost the same performance at low

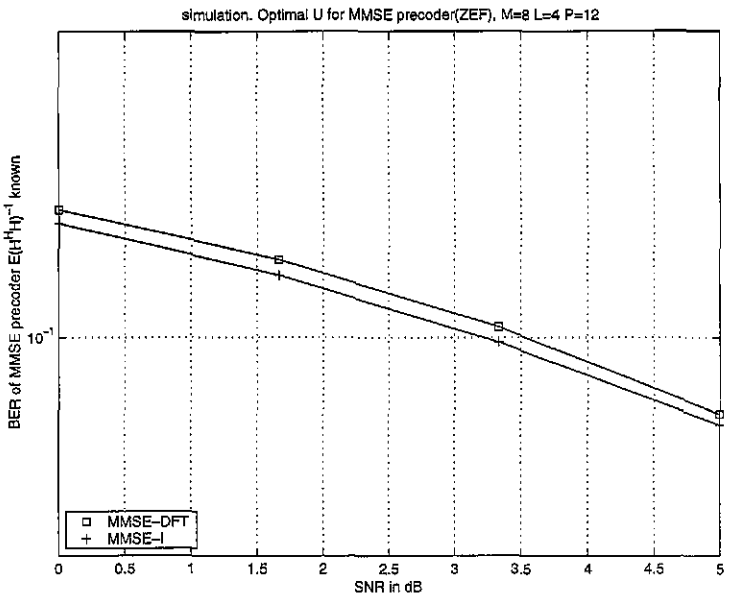

Figure 4.3: Simulation (low SNR) for the optimal unitary matrix for the MMSE precoder in which only $E\{(\boldsymbol{H}^H\boldsymbol{H})^{-1}\}$ is known

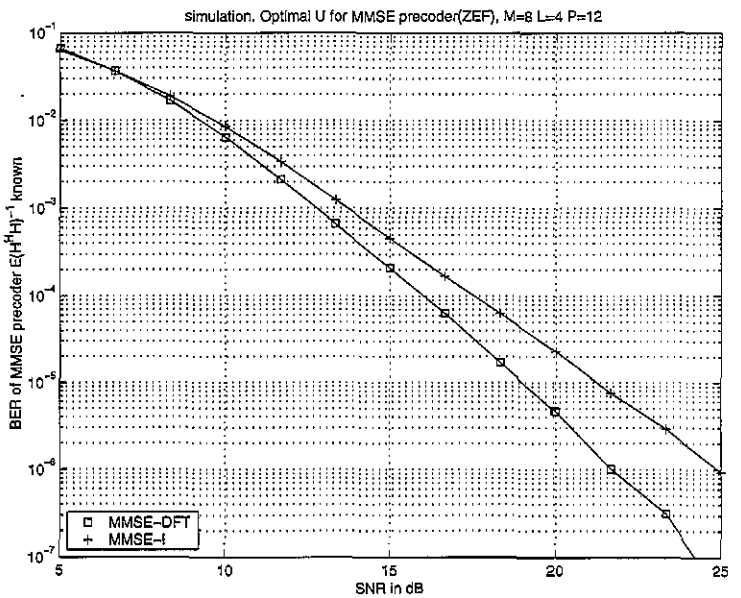

Figure 4.4: Simulation (high SNR) about the optimal unitary matrix for MMSE precoder in which only $E\{(\boldsymbol{H}^H\boldsymbol{H})^{-1}\}$ is known

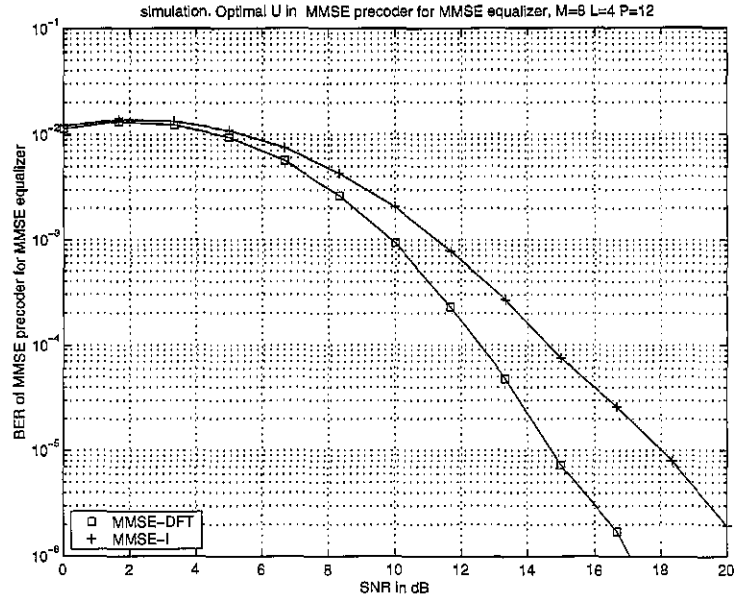

Figure 4.5: Simulation about the optimal unitary matrix for MMSE equalization

SNR, this indicates that the design proposed for ZF equalization is not necessarily optimal for MMSE equalization at low SNR. This is also expected since the MMSE equalization can not be approximated as ZF equalization at low SNR.

Chapter 5

Conclusions and Future Work

5.1 Conclusions

In this thesis the precoder which minimizes the BER of a block transmission system is derived. We assume that zero-forcing equalization and threshold detection are employed, the channel is slowly-varying frequency-selective corrupted by additive Gaussian noise, and the channel information is available at the transmitter. The transmitting signals are white. Redundancy is introduced at the precoder to eliminate IBI by zero padding (ZP) or cyclic prefix (CP) which are used in current OFDM and DMT systems.

An analytic solutions for the optimal precoder is derived in the region where the bit error function is convex. The solutions are obtained by a two-stage design scheme: First, find a lower bound on the BER is obtained by applying Jensen's inequality, then a certain parameter in the precoder is chosen so that the minimized lower bound is achieved. The condition for the validity of the analytic solution corresponds to moderate-to-high SNR in the applications defined in the thesis. When the SNR is not sufficiently large we can either increase the transmitting power or drop some bad sub-channels. A flexible scheme for dropping channels based on the received SNR is suggested, and its implementation and the corresponding MBER precoder design scheme are described. The optimal precoders are discussed for both ZP and CP systems. The the CP transmission scheme with the MBER precoder can be implemented as an extension of standard DMT with MMSE power loading

plus pre multiplication by a DFT matrix at the transmitter and post multiplication by an IDFT matrix at the receiver. The MMSE power loading scheme suggested in the thesis is less computationally demanding than the water filling scheme used in standard DMT.

Evaluations and analyses of the BER performance justify the optimality of the optimal designs. The BER improvement provided by the optimal precoders depends on the conditions of the channel. The more ill-conditioned the channel, the greater the observed improvement. This is promising since in practical transmission systems, such as wireless systems, good channels are not always guaranteed. It is shown that the ZP-MBER precoder outperforms the CP-MBER precoder especially when the extra power spent on transmitting the cyclic prefix is considered. However, the ZP-MBER precoder demands more computational cost on the eigen-decomposition of inverse of the auto-correlation of channel matrix than CP-MBER precoder. Despite the relative inferiority of the CP-MBER precoder to ZP-MBER precoder, the CP-MBER precoder is superior to water filling DMT and standard CP-OFDM precoders, and it does not spend more transmitting power on the cyclic prefix than the CP-OFDM precoder.

The design scheme for the MBER precoder reveals that the MBER precoder is an MMSE precoder with a carefully chosen unitary matrix. Therefore, it can be concluded that minimum mean square error does not guarantee minimum BER. Analyses of the BER performance indicate that the BERs depends on the level of the mean square error at receiver and the spread of the diagonal elements in the auto-correlation matrix of the receiver. The smaller the mean square error and the smaller the fluctuations of the diagonal elements, the better the BER performance. The MBER precoder manages to reach the lowest mean square error and has no fluctuations in the values of the diagonal elements. Hence, it offers minimum BER.

From the fact that the MBER precoder is a MMSE precoder with a special choice of the unitary matrix, the optimal unitary matrix which minimizes BER is designed for precoders whose solution sets are characterized by a unitary matrix degree of freedom. The optimal solutions for the unitary matrix are proposed according to the convex and non-convex region of the BER function respectively. It is shown that the BER improvement obtained by choosing the optimal unitary matrix depends on the condition of the channel — more significant

improvement is found in ill-conditioned channels than in good channels. The optimal design can be applied to precoders for scenarios in which only the second-order statistics of the channel are known and the scenarios of based on MMSE equalization (at high SNR only). In the case of MMSE equalization some approximation is incorporated.

5.2 Future work

The criterion of optimal design studied in the thesis is minimum BER which is highly desired in real communication systems. Based on the results obtained in the thesis, future work on this topic might consider the following aspects.

5.2.1 The MBER precoder design in non-convex region of BER function

The non-convex region of the BER function corresponds to lower SNR according to the discussion in Section 3.4. We have proposed a way to design the MBER precoder at low SNR — dropping enough bad sub-channels. The tradeoff incurred in this method is a smaller block size and thus a lower transmission rate if the bit loading is constant. If the sub-channel dropping technique is not preferred, one can use the standard Lagrange multiplier method for MBER precoder design. Further study of this problem can be considered in future work.

5.2.2 Other equalization techniques

The MBER precoder in the thesis is designed for zero-forcing equalization and threshold detection which offers a simple receiver structure. In real communication systems other equalization methods such as MMSE, decision feedback, or maximum likelihood detection may be used. Therefore it is desired to explore MBER precoder design for these equalization techniques.

Maximum likelihood (ML) detection for block transmission can be expressed as

$$\min_{\boldsymbol{s}\in\mathcal{S}} ||\hat{\boldsymbol{s}} - \boldsymbol{H}\boldsymbol{F}\boldsymbol{s}|| \tag{5.1}$$

where $\mathcal{S}$ is the set contains the whole transmitting blocks, $\mathcal{S} = \{\boldsymbol{s}_1, \boldsymbol{s}_2, \cdots, \boldsymbol{s}_{2^M}\}$, and $\boldsymbol{s}_1, \boldsymbol{s}_2, \cdots, \boldsymbol{s}_{2^M}$ are expressed by,

$$\begin{aligned}
\boldsymbol{s}_1 &= [-1, -1, \cdots, -1, -1]^T \\
\boldsymbol{s}_2 &= [-1, -1, \cdots, -1, +1]^T \\
&\vdots \\
\boldsymbol{s}_{2^M} &= [+1, +1, \cdots, +1, +1]^T
\end{aligned}$$

Figure 5.1 shows the BERs of the ZP-MBER precoder if ZF equalization (ZFE) plus threshold detection and maximum likelihood detection is used at the receiver respectively. The triple is chosen $(M, L, P) = (4, 2, 6)$, and the simulation is done for BPSK signals over $10,000$ channel realizations with 500 blocks each. The simulation shows that the BER of the ZP-MBER precoder can be improved by employing Maximum likelihood (ML) detection (as expected). This observation suggests another interesting question: Is the MBER precoder designed in the thesis also the optimal one for maximum likelihood detection? If not what is the optimal precoder for ML detection? Figure 5.2 shows the simulation of BERs using ZP-MMSE-I, ZP-MBER and ZP-TDMA precoders and maximum likelihood detection. The simulation environment is the same as in Figure 5.1. The plots indicate that different precoders do provide different BERs if ML detection is used, and that the ZP-TDMA precoder performs even better than the MBER precoder derived in the thesis. Determining which precoder minimizes the BER for ML detection is an interesting area of research which could be explored in the future.

For MMSE equalization, the inter-symbol interference is not canceled completely, therefore the evaluations of the block bit error may not be as simple as in the case of zero-forcing equalization. Some approximation technique might be used to obtain the block bit error function, then the MBER precoder design could be implemented by following the design schemes proposed in the thesis. This research work is being considered by another graduate student in the Advanced Signal Processing for Communications Group in the Department of Electrical & Computer Engineering at McMaster University.

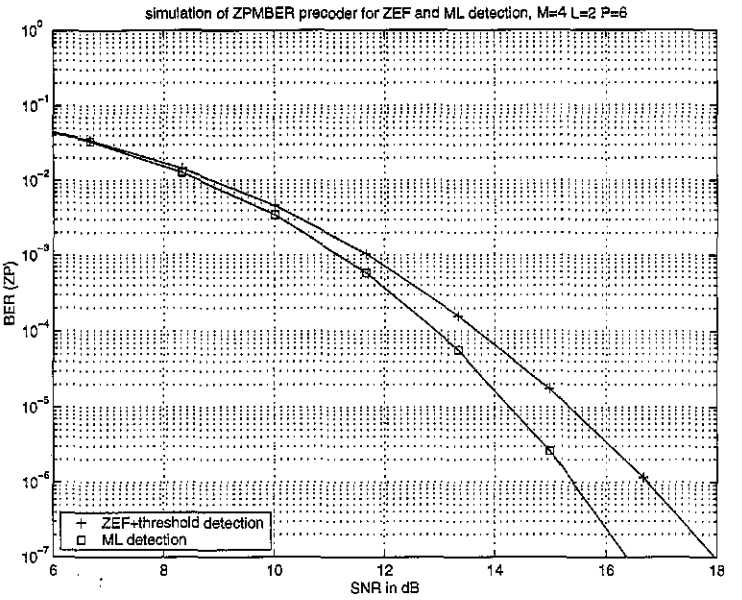

Figure 5.1: BER simulations of ZFE + threshold detection and ML detection for ZP-MBER precoder

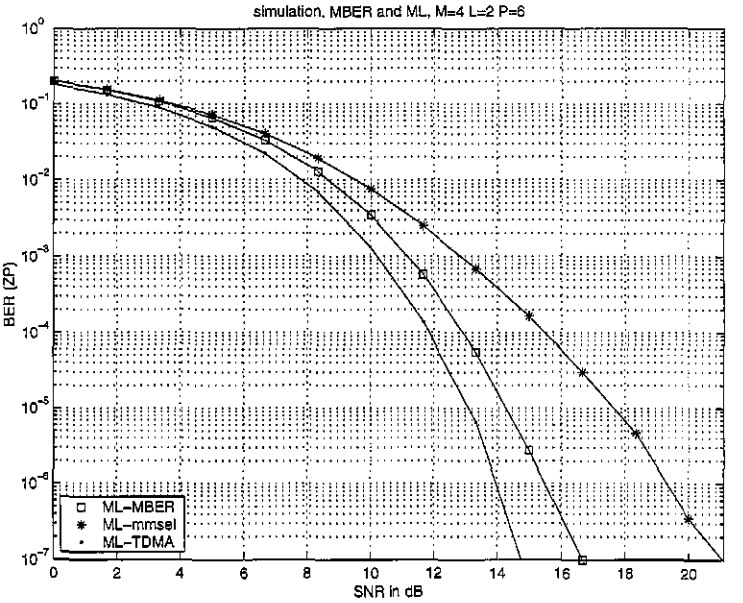

Figure 5.2: BER simulations of different precoders for ML detection

5.2.3 Unknown channel

In some practical communication systems, the channel information may not be available at transmitter. What is the MBER precoder under such circumstances? One possible criteria might be to minimize $E\{P_e\}$ instead of P_e, and a sub-optimal design scheme can be described as follows.

By applying Jensen's inequalities in the region where the BER function is convex, we have,

$$E[P_e] = \frac{1}{2M}\sum_i E\left\{ \operatorname{erfc}\left(\frac{1}{\sqrt{2\sigma^2[\boldsymbol{F}^{-1}(\boldsymbol{H}^H\boldsymbol{H})^{-1}\boldsymbol{F}^{-H}]_{ii}}}\right)\right\}$$

$$\geq \frac{1}{2M}\sum_i \operatorname{erfc}\left(\frac{1}{\sqrt{2\sigma^2\left[\boldsymbol{F}^{-1}E\{(\boldsymbol{H}^H\boldsymbol{H})^{-1}\}\boldsymbol{F}^{-H}\right]_{ii}}}\right) \tag{5.2}$$

$$\geq \frac{1}{2}\operatorname{erfc}\left(\frac{1}{\sqrt{\frac{2\sigma^2}{M}tr\left(\boldsymbol{F}^{-1}E\{(\boldsymbol{H}^H\boldsymbol{H})^{-1}\}\boldsymbol{F}^{-H}\right)}}\right) \tag{5.3}$$

From Jensen's inequalities, equality in (5.2) holds when $(\boldsymbol{H}^H\boldsymbol{H})^{-1}$ becomes deterministic, equality in (5.3) holds when the diagonal elements in $\boldsymbol{F}^{-1}E\{(\boldsymbol{H}^H\boldsymbol{H})^{-1}\}\boldsymbol{F}^{-H}$ are equal. The channel is random by assumption, and therefore the first equality is unlikely to hold. Thus the lower bound may not be reachable in such design scheme, and the solution for the precoder $\boldsymbol{F}$ will be sub-optimal. Are there any other methods to find the truly optimal precoders if the channel is not known?

5.2.4 Some other aspects

- Multiuser systems

  The MBER precoder design in the thesis is performed for a single user system. Extensions to multiuser cases can be considered for future work. The optimal transceiver design for multiple access using the MMSE criterion has been studied in [17]. Like in the single user case, the minimum BER may not be guaranteed by minimum MSE. Therefore, minimum BER precoder or transceiver design for multiuser systems would

be another very interesting problem to explore.

- Coded data

  One of the assumptions made for the optimal design in the thesis is that the transmitting blocks are uncorrelated. This may not be true if the data is coded, such as by convolutional coding. To tackle the problem, further study can be done by assuming that $E\{\boldsymbol{s}\boldsymbol{s}^H\} = \boldsymbol{R}_{ss}$, where $\boldsymbol{R}_{ss}$ is a full matrix rather than the identity matrix.

- Space time coding

  The algebraic structure of space time coding is very similar to that of precoding, but the channel matrix $\boldsymbol{H}$ has more general form. One interesting research direction might be to determine what is the space time coding scheme that minimizes BER?

Appendix A

Proof for Block Bit Error Rate

We consider the block transmission system under the assumption made in the thesis (Section 2.3). The equalized block can be expressed as, $\hat{\boldsymbol{s}} = \boldsymbol{s} + \boldsymbol{Gv}$, where $\boldsymbol{s} = [s_1, s_2, \cdots, s_M]^T$, and $\hat{\boldsymbol{s}} = [\hat{s}_1, \hat{s}_2, \cdots, \hat{s}_M]^T$ denote size M transmitted and received signal blocks respectively. Then the following three theorems about block bit error rate are in order.

Theorem A.1. *For a given transmitting block $\boldsymbol{s}$, the bit error rate $P_{e|s}$ can be expressed as,*

$$P_{e|s} = \frac{1}{M} \sum_{i=1}^{M} \int_{-\infty}^{\infty} \cdots \int_{z_{e_i}} \cdots \int_{-\infty}^{\infty} p_{\hat{\boldsymbol{s}}|s} d\hat{\boldsymbol{s}} \tag{A.1}$$

where M is the block size, z_{e_i} is the region in which the ith bit is erroneously decided, $p_{\hat{\boldsymbol{s}}|s}$ is the conditional probability density function of $\hat{\boldsymbol{s}}$ given $\boldsymbol{s}$ is transmitted.

For a simple case the block size is 2, $M = 2$, BPSK signal, $\boldsymbol{s} = [-1, -1]^T$, the theorem states that

$$P_{e|s} = \frac{1}{2}\Big(\int_0^{\infty} \int_{-\infty}^{\infty} p_{\hat{\boldsymbol{s}}|s} d\hat{\boldsymbol{s}} + \int_{-\infty}^{\infty} \int_0^{\infty} p_{\hat{\boldsymbol{s}}|s} d\hat{\boldsymbol{s}} \Big).$$

Theorem A.2. *The bit error rate $P_{e|s}$ for a given transmitting block $\boldsymbol{s}$ is the same for any form of $\boldsymbol{s} = [s_1, s_2, \cdots, s_M]^T$, i.e. it does not depend on the combination of individual bits in the transmitting block.*

Theorem A.3. *The block bit error rate P_e which is defined as as the average bit error rate over all possible forms of the transmitting blocks is given by*

$$P_e = \frac{1}{2M}\sum_{i=1}^{M} \text{erfc}\left(\frac{1}{\sqrt{2\sigma^2[\boldsymbol{G}\boldsymbol{G}^H]_{ii}}}\right), \tag{A.2}$$

where $E\{\boldsymbol{v}\boldsymbol{v}^H\} = \sigma^2 I$, $[\boldsymbol{G}\boldsymbol{G}^H]_{ii}$ is the ith diagonal entry of $\boldsymbol{G}\boldsymbol{G}^H$.

A.1 Proof for Theorem 1

We employ induction for the proof. We observe the following simple fact.

Fact A.1. *For a given transmitting block $\boldsymbol{s}$, the sum of the probabilities of no wrong bit, one wrong bit , ..., and M wrong bits in the received block $\hat{\boldsymbol{s}}$ at the receiver is* 1, *i.e.*

$$\begin{aligned} &P(\text{no wrong bit in } \hat{\boldsymbol{s}}|\boldsymbol{s}) + P(1 \text{ wrong bit in } \hat{\boldsymbol{s}}|\boldsymbol{s}) + P(2 \text{ wrong bits in } \hat{\boldsymbol{s}}|\boldsymbol{s}) + \cdots \\ &\quad + P(M \text{ wrong bits in } \hat{\boldsymbol{s}}|\boldsymbol{s}) = 1 \end{aligned} \tag{A.3}$$

The right side of Eq (A.3) can be expressed as the integral of the probability density function over the whole region.

$$\begin{aligned} &P(\hat{\boldsymbol{s}} = [s_1, \cdots, s_M]^T|\boldsymbol{s}) + \sum_{i_1=1}^{M} P(\hat{\boldsymbol{s}} = [s_1, \cdots, \overline{s}_{i_1}, \cdots, s_M]^T|\boldsymbol{s}) \\ &\quad + \sum_{\substack{i_1=1, i_2=1 \\ i_1 \neq i_2}}^{M} P(\hat{\boldsymbol{s}} = [s_1, \cdots, \overline{s}_{i_1}, \cdots, \overline{s}_{i_2}, \cdots, s_M]^T|\boldsymbol{s}) + \cdots \\ &\quad + \sum_{\substack{i_1, \cdots, i_{M-1}=1 \\ i_j \neq i_k, \forall i,j \in [1, M-1]}}^{M} P(\hat{\boldsymbol{s}} = [\overline{s}_{i_1}, \cdots, \overline{s}_{i_{M-1}}, \cdots, s_M]^T|\boldsymbol{s}) + P(\hat{\boldsymbol{s}} = [\overline{s}_1, \cdots, \overline{s}_M]^T|\boldsymbol{s}) \\ &= \int_{-\infty}^{\infty} \cdots \int_{-\infty}^{\infty} p_{\hat{\boldsymbol{s}}|\boldsymbol{s}} d\hat{\boldsymbol{s}} \end{aligned}$$

where $\overline{s}_k$ is the inverse of s_k, $\overline{s}_k = \pm 1$, if $s_k = \mp 1$, $k = 1, 2, \cdots$.

Proof of Theorem 1. It can be easily shown that Eq (A.1) holds for $M = 2$.

Suppose $\boldsymbol{s} = [s_1, s_2]^T$, where $s_i = +1$ or $-1, i = 1, 2$, then the bit error rate for a given $\boldsymbol{s}$ is,

$$\begin{aligned} P_{e|\boldsymbol{s}} &= \frac{1}{2}\Big(P(\hat{\boldsymbol{s}} = [\overline{s}_1, s_2]^T|\boldsymbol{s}) + P(\hat{\boldsymbol{s}} = [s_1, \overline{s}_2]^T|\boldsymbol{s}) + 2P(\hat{\boldsymbol{s}} = [\overline{s}_1, \overline{s}_2]^T|\boldsymbol{s})\Big) \\ &= \frac{1}{2}\Big(\int_{z_{e_1}}\int_{z_{d_2}} + \int_{z_{d_1}}\int_{z_{e_2}} + 2\int_{z_{e_1}}\int_{z_{e_2}} p_{\hat{\boldsymbol{s}}|\boldsymbol{s}} d\hat{s}_2 d\hat{s}_1\Big) \\ &= \frac{1}{2}\Big((\int_{z_{e_1}}\int_{-\infty}^{\infty} + \int_{-\infty}^{\infty}\int_{z_{e_2}})p_{\hat{\boldsymbol{s}}|\boldsymbol{s}} d\hat{s}_2 d\hat{s}_1\Big) \end{aligned}$$

where z_{d_i} and z_{e_i} are regions in which the ith bit in the block is correctly and erroneously detected respectively, and $z_{d_i} \cup z_{e_i} = (-\infty, \infty)$.

Suppose that Eq (A.1) holds for $M > 2$, i.e.,

$$P_{e|\boldsymbol{s}} = \frac{1}{M}\sum_{i=1}^{M}\int_{-\infty}^{\infty}\cdots\int_{z_{e_i}}\cdots\int_{-\infty}^{\infty} p_{\hat{\boldsymbol{s}}|\boldsymbol{s}} d\hat{\boldsymbol{s}} \tag{A.4}$$

The left side of Eq (A.4) can also be expressed as

$$\begin{aligned} P_{e|\boldsymbol{s}} &= \frac{1}{M}\Big(P(1 \text{ wrong bit } |\boldsymbol{s}) + 2P(2 \text{ wrong bits } |\boldsymbol{s}) + \cdots + MP(M \text{ wrong bits } |\boldsymbol{s})\Big) \\ &= \frac{1}{M}\Big(\sum_{i_1=1}^{M} P(\hat{\boldsymbol{s}} = [s_1, \cdots, \overline{s}_{i_1}, \cdots, s_M]^T|\boldsymbol{s}) + 2\sum_{\substack{i_1,i_2=1 \\ i_1\neq i_2}}^{M} P(\hat{\boldsymbol{s}} = [s_1, \cdots, \overline{s}_{i_1}, \cdots, \overline{s}_{i_2}, \cdots, s_M]^T|\boldsymbol{s}) \\ &\quad + \cdots \\ &\quad + (M-1)\sum_{\substack{i_1,\cdots,i_{M-1}=1 \\ i_j\neq i_k, \forall j,k\in[1,M-1]}}^{M} P(\hat{\boldsymbol{s}} = [\overline{s}_{i_1}, \cdots, \overline{s}_{i_{M-1}}, \cdots, s_M]^T|\boldsymbol{s}) + MP(\hat{\boldsymbol{s}} = [\overline{s}_1, \cdots, \overline{s}_M]^T|\boldsymbol{s})\Big). \end{aligned}$$

For block size of $(M+1)$, $\boldsymbol{s} = [s_1, \cdots, s_M, s_{M+1}]^T = [\boldsymbol{s}_0^T, s_{M+1}]^T$, where $\boldsymbol{s}_0$ is a block of size M containing the first M-bits. The bit error for a block whose size is $(M+1)$ can be written as,

$$P_{e|\boldsymbol{s}} = \frac{1}{M+1}\Big(P(1 \text{ wrong bit in } \hat{\boldsymbol{s}}|\boldsymbol{s}) + 2P(2 \text{ wrong bits in } \hat{\boldsymbol{s}}|\boldsymbol{s}) + \cdots$$

$$
\begin{aligned}
&+ MP(M \text{ wrong bits in } \hat{\boldsymbol{s}}|\boldsymbol{s}) + (M+1)P(M+1 \text{ wrong bits in } \hat{\boldsymbol{s}}|\boldsymbol{s})\Big) \\
&= \frac{1}{M+1}\Big(P(1 \text{ wrong bit in } \hat{\boldsymbol{s}}_0, \hat{s}_{M+1} = s_{M+1}|\boldsymbol{s}) + P(0 \text{ wrong bits in } \hat{\boldsymbol{s}}_0, \hat{s}_{M+1} = \overline{s}_{M+1}|\boldsymbol{s}) \\
&\quad + 2\big(P(2 \text{ wrong bits in } \hat{\boldsymbol{s}}_0, \hat{s}_{M+1} = s_{M+1}|\boldsymbol{s}) + P(1 \text{ wrong bit in } \hat{\boldsymbol{s}}_0, \hat{s}_{M+1} = \overline{s}_{M+1}|\boldsymbol{s})\big) \\
&\quad \vdots \\
&\quad + M[P(M \text{ wrong bits in } \hat{\boldsymbol{s}}_0, \hat{s}_{M+1} = s_{M+1}|\boldsymbol{s}) + P(M-1 \text{ wrong bit in } \hat{\boldsymbol{s}}_0, \hat{s}_{M+1} = \overline{s}_{M+1}|\boldsymbol{s}) \\
&\quad + (M+1)[P(M \text{ wrong bits in } \hat{\boldsymbol{s}}_0, \hat{s}_{M+1} = \overline{s}_{M+1}|\boldsymbol{s})]\Big) \\
&= \frac{1}{M+1}\Big(\{P(1 \text{ wrong bit in } \hat{\boldsymbol{s}}_0, \hat{s}_{M+1} = s_{M+1}|\boldsymbol{s}) + 2P(2 \text{ wrong bits in } \hat{\boldsymbol{s}}_0, \hat{s}_{M+1} = s_{M+1}|\boldsymbol{s}) \\
&\quad \cdots + MP(M \text{ wrong bits in } \hat{\boldsymbol{s}}_0, \hat{s}_{M+1} = s_{M+1}|\boldsymbol{s})\} \\
&\quad + \{P(1 \text{ wrong bit in } \hat{\boldsymbol{s}}_0, \hat{s}_{M+1} = \overline{s}_{M+1}|\boldsymbol{s}) + \cdots \\
&\quad + (M-1)P(M-1 \text{ wrong bit in } \hat{\boldsymbol{s}}_0, \hat{s}_{M+1} = \overline{s}_{M+1}|\boldsymbol{s}) \\
&\quad + MP(M \text{ wrong bits in } \hat{\boldsymbol{s}}_0, \hat{s}_{M+1} = \overline{s}_{M+1}|\boldsymbol{s})\} \\
&\quad + \{P(0 \text{ wrong bits in } \hat{\boldsymbol{s}}_0, \hat{s}_{M+1} = \overline{s}_{M+1}|\boldsymbol{s}) + P(1 \text{ wrong bits in } \hat{\boldsymbol{s}}_0, \hat{s}_{M+1} = \overline{s}_{M+1}|\boldsymbol{s}) \\
&\quad + \cdots + P(M \text{ wrong bits in } \hat{\boldsymbol{s}}_0, \hat{s}_{M+1} = \overline{s}_{M+1}|\boldsymbol{s})\}\Big) \\
&= \frac{1}{M+1}\Big(\sum_{i=1}^{M}\int_{-\infty}^{\infty}\cdots\int_{z_{e_i}}\cdots\int_{-\infty}^{\infty}\int_{z_{d_{M+1}}} p_{\hat{\boldsymbol{s}}|\boldsymbol{s}}d\hat{\boldsymbol{s}} + \sum_{i=1}^{M}\int_{-\infty}^{\infty}\cdots\int_{z_{e_i}}\cdots\int_{-\infty}^{\infty}\int_{z_{e_{M+1}}} p_{\hat{\boldsymbol{s}}|\boldsymbol{s}}d\hat{\boldsymbol{s}} \\
&\quad + \int_{-\infty}^{\infty}\cdots\int_{-\infty}^{\infty}\int_{z_{e_{M+1}}} p_{\hat{\boldsymbol{s}}|\boldsymbol{s}}d\hat{\boldsymbol{s}}\Big) \\
&= \frac{1}{M+1}\Big(\sum_{i=1}^{M}\int_{-\infty}^{\infty}\cdots\int_{z_{e_i}}\cdots\int_{-\infty}^{\infty}\int_{-\infty}^{\infty} p_{\hat{\boldsymbol{s}}|\boldsymbol{s}}d\hat{\boldsymbol{s}} + \int_{-\infty}^{\infty}\cdots\int_{-\infty}^{\infty}\int_{z_{e_{M+1}}} p_{\hat{\boldsymbol{s}}|\boldsymbol{s}}d\hat{\boldsymbol{s}}\Big) \\
&= \frac{1}{M+1}\Big(\sum_{i=1}^{M+1}\int_{-\infty}^{\infty}\cdots\int_{z_{e_i}}\cdots\int_{-\infty}^{\infty}\int_{-\infty}^{\infty} p_{\hat{\boldsymbol{s}}|\boldsymbol{s}}d\hat{\boldsymbol{s}}\Big)
\end{aligned}
$$

Therefore Theorem A.1 holds for any block size.

□

A.2 Proof for Theorem 2

Proof of Theorem 2. For a given the transmitted block $\boldsymbol{s}$, the output block $\hat{\boldsymbol{s}}$ is Gaussian distributed with the conditional probability density function,

$$p_{\hat{\boldsymbol{s}}|\boldsymbol{s}} = (2\pi)^{-\frac{M}{2}}|\boldsymbol{C}|^{-\frac{1}{2}} \exp\big(-\frac{1}{2}(\hat{\boldsymbol{s}}-\boldsymbol{s})^T\boldsymbol{C}^{-1}(\hat{\boldsymbol{s}}-\boldsymbol{s})\big), \tag{A.5}$$

where $\boldsymbol{C}$ is the covariance matrix. For a M-dimension block, the transmitting block $\boldsymbol{s} = [s_1, s_2, \cdots, s_M]^T$ has 2^M different forms. From Theorem A.1 the bit error rate for a given transmitted block $\boldsymbol{s}$ is,

$$\begin{aligned}
P_{e|\boldsymbol{s}} &= \frac{1}{M}\Big(\sum_{i=1}^{M}\int_{-\infty}^{\infty}\cdots\int_{z_{e_i}}\cdots\int_{-\infty}^{\infty} p_{\hat{\boldsymbol{s}}|\boldsymbol{s}}d\hat{\boldsymbol{s}}\Big) \\
&= \frac{1}{M}\Big(\sum_{i=1}^{M}\int_{-\infty}^{\infty}\cdots\int_{z_{e_i}}\cdots\int_{-\infty}^{\infty}(2\pi)^{-\frac{M}{2}}|\boldsymbol{C}|^{-\frac{1}{2}}\exp\big(-\frac{1}{2}(\hat{\boldsymbol{s}}-\boldsymbol{s})^T\boldsymbol{C}^{-1}(\hat{\boldsymbol{s}}-\boldsymbol{s})\big)d\hat{\boldsymbol{s}}\Big) \\
&= \frac{1}{M(2\pi)^{\frac{M}{2}}|\boldsymbol{C}|^{\frac{1}{2}}}\sum_{i=1}^{M}\int_{-\infty}^{\infty}\cdots\int_{z_{e_i}}\cdots\int_{-\infty}^{\infty}\exp\big(-\frac{1}{2}(\hat{\boldsymbol{s}}-\boldsymbol{s})^T\boldsymbol{C}^{-1}(\hat{\boldsymbol{s}}-\boldsymbol{s})\big)d\hat{\boldsymbol{s}} \\
&= \frac{1}{M(2\pi)^{\frac{M}{2}}|\boldsymbol{C}|^{\frac{1}{2}}}\sum_{i=1}^{M}\int_{-\infty}^{\infty}\cdots\int_{z_{y_i}}\cdots\int_{-\infty}^{\infty}\exp(-\frac{1}{2}\boldsymbol{y}^T\boldsymbol{C}^{-1}\boldsymbol{y})d\boldsymbol{y},
\end{aligned} \tag{A.6}$$

where $\boldsymbol{y} = \hat{\boldsymbol{s}} - \boldsymbol{s}$, z_{y_i} is the region corresponding to z_{e_i} via the transformation $y_i = \hat{s}_i - s_i, i \in [1, M]$.

There are two possible values for the ith bit in the block, $s_i = +1$ and $s_i = -1$. Let's examine the integral under the summation sign in Eq (A.6) for these two values of s_i.

For $s_i = -1$,

$$\begin{aligned}
d_{s_i=1} &= \int_{-\infty}^{\infty}\cdots\int_{z_{y_i}}\cdots\int_{-\infty}^{\infty}\exp(-\frac{1}{2}\boldsymbol{y}^T\boldsymbol{C}^{-1}\boldsymbol{y})d\boldsymbol{y} \\
&= \int_{-\infty}^{\infty}\cdots\int_{1}^{\infty}\cdots\int_{-\infty}^{\infty}\exp(-\frac{1}{2}\boldsymbol{y}^T\boldsymbol{C}^{-1}\boldsymbol{y})d\boldsymbol{y}
\end{aligned}$$

For $s_i = 1$,

$$\begin{aligned} d_{s_i=-1} &= \int_{-\infty}^{\infty} \cdots \int_{-\infty}^{-1} \cdots \int_{-\infty}^{\infty} \exp(-\frac{1}{2}\boldsymbol{y}^T \boldsymbol{C}^{-1}\boldsymbol{y}) d\boldsymbol{y} \\ &= \int_{\infty}^{-\infty} \cdots \int_{\infty}^{1} \cdots \int_{\infty}^{-\infty} \exp(-\frac{1}{2}\boldsymbol{z}^T \boldsymbol{C}^{-1}\boldsymbol{z}) d(-\boldsymbol{z}) \\ &= \int_{-\infty}^{\infty} \cdots \int_{-\infty}^{-1} \cdots \int_{-\infty}^{\infty} \exp(-\frac{1}{2}\boldsymbol{z}^T \boldsymbol{C}^{-1}\boldsymbol{z}) d(\boldsymbol{z}) \\ &= d_{s_i=1} \end{aligned}$$

Thus the integral under the summation sign in Eq (A.6) is the same regardless of the value of s_i, so $P_{e|\boldsymbol{s}}$ is the same for any form of $\boldsymbol{s} = [s_1, s_2, \cdots, s_M]^T$. Therefore, Theorem A.2 holds. □

A.3 Proof for Theorem 3

Proof of Theorem 3. The average block bit error rate P_e is the average of bit error rate over all possible transmitting blocks. From Theorem A.2, the bit error rate is the same for any form of $\boldsymbol{s} = [s_1, s_2, \cdots, s_M]^T$, then the block bit error rate P_e is equal to $P_{e|\boldsymbol{s}}$ for an arbitrary $\boldsymbol{s}$, we take $\boldsymbol{s}$ an all -1 block, $\boldsymbol{s} = [-1, -1, \cdots, -1]^T$, for convenience.

$$\begin{aligned} P_e &= \frac{1}{M(2\pi)^{\frac{M}{2}}|\boldsymbol{C}|^{\frac{1}{2}}} \sum_{i=1}^{M} \int_{-\infty}^{\infty} \cdots \int_{z_{y_i}} \cdots \int_{-\infty}^{\infty} \exp(-\frac{1}{2}\boldsymbol{y}^T \boldsymbol{C}^{-1}\boldsymbol{y}) d\boldsymbol{y} \\ &= \frac{1}{M(2\pi)^{\frac{M}{2}}|\boldsymbol{C}|^{\frac{1}{2}}} \Big(\int_{1}^{\infty} \int_{-\infty}^{\infty} \cdots \int_{-\infty}^{\infty} + \int_{-\infty}^{\infty} \int_{1}^{\infty} \cdots \int_{-\infty}^{\infty} + \cdots + \int_{-\infty}^{\infty} \cdots \int_{-\infty}^{\infty} \int_{1}^{\infty} \Big) \\ &\qquad \exp(-\frac{1}{2}\boldsymbol{y}^T \boldsymbol{C}^{-1}\boldsymbol{y}) d\boldsymbol{y} \\ &= \frac{1}{M(2\pi)^{\frac{M}{2}}|\boldsymbol{C}|^{\frac{1}{2}}} \int_{1}^{\infty} \int_{-\infty}^{\infty} \cdots \int_{-\infty}^{\infty} \Big(\exp(-\frac{1}{2}\boldsymbol{y}^T \boldsymbol{C}^{-1}\boldsymbol{y}) + \exp(-\frac{1}{2}\boldsymbol{y}^T \boldsymbol{P}_{2,1}^T \boldsymbol{C}^{-1} \boldsymbol{P}_{2,1}\boldsymbol{y}) \\ &\qquad + \exp(-\frac{1}{2}\boldsymbol{y}^T \boldsymbol{P}_{3,1}^T \boldsymbol{C}^{-1} \boldsymbol{P}_{3,1}\boldsymbol{y}) + \cdots + \exp(-\frac{1}{2}\boldsymbol{y}^T \boldsymbol{P}_{M,1}^T \boldsymbol{C}^{-1} \boldsymbol{P}_{M,1}\boldsymbol{y}) \Big) dy_M \cdots dy_1 \end{aligned} \tag{A.7}$$

$$= \sum_{i=1}^{M} t_i \tag{A.8}$$

where $z_{y_i} \in (1, \infty)$, and

$$t_i = \frac{1}{M(2\pi)^{\frac{M}{2}}|\boldsymbol{C}|^{\frac{1}{2}}} \int_1^{\infty} \int_{-\infty}^{\infty} \cdots \int_{-\infty}^{\infty} \exp(-\frac{1}{2}\boldsymbol{y}^T \boldsymbol{P}_{i,1}^T \boldsymbol{C}^{-1} \boldsymbol{P}_{i,1} \boldsymbol{y}) d\boldsymbol{y}. \tag{A.9}$$

Here $\boldsymbol{P}_{i,1}$ is the permutation matrix with ith column and the first column of identity matrix interchanged,

$$\boldsymbol{P}_{i,1} = [e_i, e_2, \cdots, e_{i-1}, e_1, e_{i+1}, \cdots, e_M]$$

where $\boldsymbol{e}_j$ is the jth column of the $M \times M$ identity matrix, $j \in [1, M]$. Pre-multiplication of $\boldsymbol{P}_{i,1}$ to vector $\boldsymbol{y}$ permutates the positions of y_i and y_1 in $\boldsymbol{y}$.

$$\boldsymbol{P}_{i,1} \begin{pmatrix} y_1 \\ \vdots \\ y_i \\ \vdots \\ y_M \end{pmatrix} = \begin{pmatrix} y_i \\ \vdots \\ y_1 \\ \vdots \\ y_M \end{pmatrix}.$$

Suppose $\boldsymbol{C}^{-1}$ is expressed by another matrix $\boldsymbol{R}$,

$$\boldsymbol{R} = \boldsymbol{C}^{-1} = \begin{pmatrix} r_{11} & r_{12} & \cdots & r_{1M} \\ r_{21} & r_{22} & \cdots & r_{2M} \\ \vdots & & \ddots & \\ r_{M1} & r_{M2} & \cdots & r_{MM} \end{pmatrix}.$$

Therefore $\boldsymbol{y}^T \boldsymbol{C}^{-1} \boldsymbol{y} = \boldsymbol{y}^T \boldsymbol{R} \boldsymbol{y}$. We expand the right side of the equation,

$$\begin{pmatrix} y_1 & y_2 & \cdots & y_M \end{pmatrix} \begin{pmatrix} r_{11} & r_{12} & \cdots & r_{1M} \\ r_{21} & r_{22} & \cdots & r_{2M} \\ \vdots & & \ddots & \\ r_{1M} & r_{2M} & \cdots & r_{MM} \end{pmatrix} \begin{pmatrix} y_1 \\ y_2 \\ \vdots \\ y_M \end{pmatrix}$$

$$
\begin{aligned}
&= \begin{pmatrix} y_1 & \boldsymbol{y}_2^T \end{pmatrix} \begin{pmatrix} r_{11} & \boldsymbol{r}_{12} \\ \boldsymbol{r}_{21} & \boldsymbol{R}_{22} \end{pmatrix} \begin{pmatrix} y_1 \\ \boldsymbol{y}_2 \end{pmatrix} \\
&= y_1(r_{11} - \boldsymbol{r}_{12}\boldsymbol{R}_{22}^{-1}\boldsymbol{r}_{21})y_1 + (\boldsymbol{y}_2 + \boldsymbol{R}_{22}^{-1}\boldsymbol{r}_{21}y_1)^T\boldsymbol{R}_{22}(\boldsymbol{y}_2 + \boldsymbol{R}_{22}^{-1}\boldsymbol{r}_{21}y_1) \\
&= y_1^2(r_{11} - \boldsymbol{r}_{12}\boldsymbol{R}_{22}^{-1}\boldsymbol{r}_{21}) + (\boldsymbol{y}_2 + \boldsymbol{R}_{22}^{-1}\boldsymbol{r}_{21}y_1)^T\boldsymbol{R}_{22}(\boldsymbol{y}_2 + \boldsymbol{R}_{22}^{-1}\boldsymbol{r}_{21}y_1),
\end{aligned}
$$

where $\boldsymbol{y}_2 = [y_2, \cdots, y_M]^T$. Using the following facts [12],

$$
\begin{aligned}
&\int_{-\infty}^{\infty} \cdots \int_{-\infty}^{\infty} \exp\big(-\frac{1}{2}(\boldsymbol{X}-\boldsymbol{D})^T\boldsymbol{B}(\boldsymbol{X}-\boldsymbol{D})\big)d\boldsymbol{X} = (2\pi)^{n/2}|\boldsymbol{B}|^{-\frac{1}{2}}, \\
&|\boldsymbol{R}| = \begin{vmatrix} r_{11} & \boldsymbol{r}_{12} \\ \boldsymbol{r}_{21} & \boldsymbol{R}_{22} \end{vmatrix} = |\boldsymbol{R}_{22}||r_{11} - \boldsymbol{r}_{12}\boldsymbol{R}_{22}^{-1}\boldsymbol{r}_{21}| = |r_{11}^c|(r_{11} - \boldsymbol{r}_{12}\boldsymbol{R}_{22}^{-1}\boldsymbol{r}_{21}),
\end{aligned} \tag{A.10}
$$

where $|r_{11}^c|$ is the cofactor of r_{11} in $\boldsymbol{R}$, and $|r_{11}^c| = |\boldsymbol{R}_{22}|$, the first term in the summation of Eq (A.7) can be evaluated as,

$$
\begin{aligned}
t_1 &= \frac{1}{M(2\pi)^{\frac{M}{2}}|\boldsymbol{C}|^{\frac{1}{2}}} \int_1^{\infty}\int_{-\infty}^{\infty}\cdots\int_{-\infty}^{\infty} \exp(-\frac{1}{2}\boldsymbol{y}^T\boldsymbol{C}^{-1}\boldsymbol{y})d\boldsymbol{y} \\
&= \frac{|\boldsymbol{R}|^{\frac{1}{2}}}{M(2\pi)^{\frac{M}{2}}} \int_1^{\infty}\int_{-\infty}^{\infty}\cdots\int_{-\infty}^{\infty} \\
&\quad \exp\Big(-\frac{1}{2}\big(y_1^2(r_{11} - \boldsymbol{r}_{12}\boldsymbol{R}_{22}^{-1}\boldsymbol{r}_{21}) + (\boldsymbol{y}_2 + \boldsymbol{R}_{22}^{-1}\boldsymbol{r}_{21}y_1)^T\boldsymbol{R}_{22}(\boldsymbol{y}_2 + \boldsymbol{R}_{22}^{-1}\boldsymbol{r}_{21}y_1)\big)\Big)d\boldsymbol{y}_2 dy_1 \\
&= \frac{|\boldsymbol{R}|^{\frac{1}{2}}}{M(2\pi)^{\frac{M}{2}}}(2\pi)^{\frac{M-1}{2}}|\boldsymbol{R}_{22}|^{-\frac{1}{2}} \int_1^{\infty} \exp\big(-\frac{1}{2}y_1^2(r_{11} - \boldsymbol{r}_{12}\boldsymbol{R}_{22}^{-1}\boldsymbol{r}_{21})\big)dy_1 \\
&= \frac{1}{M(2\pi)^{\frac{1}{2}}}(r_{11} - \boldsymbol{r}_{12}\boldsymbol{R}_{22}^{-1}\boldsymbol{r}_{21})^{\frac{1}{2}} \int_1^{\infty} \exp\big(-\frac{1}{2}y_1^2(r_{11} - \boldsymbol{r}_{12}\boldsymbol{R}_{22}^{-1}\boldsymbol{r}_{21})\big)dy_1 \\
&= \frac{1}{2M}\,\mathrm{erfc}\left(\sqrt{\frac{(r_{11} - \boldsymbol{r}_{12}\boldsymbol{R}_{22}^{-1}\boldsymbol{r}_{21})}{2}}\right) \\
&= \frac{1}{2M}\,\mathrm{erfc}\left(\sqrt{\frac{|\boldsymbol{R}|}{2|\boldsymbol{R}_{22}|}}\right) \\
&= \frac{1}{2M}\,\mathrm{erfc}\left(\sqrt{\frac{|\boldsymbol{R}|}{2|r_{11}^c|}}\right),
\end{aligned}
$$

where r_{11}^c is the cofactor of r_{11} in $\boldsymbol{R}$. To evaluate other terms $t_2, \cdots, t_M$ in the right side of Eq (A.7), we examination of $\boldsymbol{P}_{i,1}^T \boldsymbol{C}^{-1} \boldsymbol{P}_{i,1}$ first,

$$
\begin{aligned}
\boldsymbol{P}_{i,1}^T \boldsymbol{C}^{-1} \boldsymbol{P}_{i,1} &= \boldsymbol{P}_{i,1}^T \boldsymbol{R} \boldsymbol{P}_{i,1} \\
&= \begin{pmatrix} r_{i1} & r_{i2} & \cdots & r_{ii} & \cdots & r_{iM} \\ r_{21} & r_{22} & \cdots & r_{2i} & \cdots & r_{iM} \\ \vdots & \vdots & & \vdots & & \\ r_{11} & r_{12} & \cdots & r_{1i} & \cdots & r_{1M} \\ \vdots & & \vdots & & \vdots & \\ r_{M1} & r_{M2} & \cdots & r_{Mi} & \cdots & r_{MM} \end{pmatrix} \boldsymbol{P}_{i1} \\
&= \begin{pmatrix} r_{ii} & r_{i2} & \cdots & r_{i1} & \cdots & r_{iM} \\ r_{2i} & r_{22} & \cdots & r_{i1} & \cdots & r_{iM} \\ \vdots & & \vdots & & \vdots & \\ r_{1i} & r_{12} & \cdots & r_{11} & \cdots & r_{1M} \\ \vdots & & \vdots & & \vdots & \\ r_{Mi} & r_{M2} & \cdots & r_{M1} & \cdots & r_{MM} \end{pmatrix} \\
&= \begin{pmatrix} r_{ii} & \boldsymbol{r}_{12i} \\ \boldsymbol{r}_{21i} & \boldsymbol{R}_{22i} \end{pmatrix}
\end{aligned}
$$

$$
\begin{aligned}
|\boldsymbol{R}_{22i}| &= \det \begin{pmatrix} r_{22} & \cdots & r_{i1} & \cdots & r_{iM} \\ \vdots & & \vdots & & \\ r_{12} & \cdots & r_{11} & \cdots & r_{1M} \\ \vdots & & \vdots & & \\ r_{M2} & \cdots & r_{M1} & \cdots & r_{MM} \end{pmatrix} \\
&= |\boldsymbol{P}_{1,i-1}^T \boldsymbol{P}_{2,i-1}^T \cdots P_{i-2,i-1}^T \boldsymbol{R}_{ii}^c \boldsymbol{P}_{i-2,i-1} \cdots \boldsymbol{P}_{2,i-1} \boldsymbol{P}_{1,i-1}| \\
&= |\boldsymbol{R}_{ii}^c|,
\end{aligned}
$$

where $\boldsymbol{R}_{ii}^c$ is the cofactor of r_{ii} in $\boldsymbol{R}$. Therefore the t_i, $i \geq 2$, is calculated by

$$
t_i = \frac{1}{M(2\pi)^{\frac{M}{2}} |\boldsymbol{C}|^{\frac{1}{2}}} \int_1^\infty \int_{-\infty}^\infty \cdots \int_{-\infty}^\infty \exp(-\frac{1}{2} \boldsymbol{y}^T \boldsymbol{P}_{i,1}^T \boldsymbol{C}^{-1} \boldsymbol{P}_{i,1} \boldsymbol{y}) d\boldsymbol{y}
$$

$$
\begin{aligned}
&= \frac{1}{2M}\operatorname{erfc}\left(\sqrt{\frac{(r_{ii} - \boldsymbol{r}_{12i}\boldsymbol{R}_{22i}^{-1}\boldsymbol{r}_{21i})}{2}}\right) \\
&= \frac{1}{2M}\operatorname{erfc}\left(\sqrt{\frac{|\boldsymbol{R}|}{2|\boldsymbol{R}_{22i}|}}\right) \\
&= \frac{1}{2M}\operatorname{erfc}\left(\sqrt{\frac{|\boldsymbol{R}|}{2|r_{ii}^{c}|}}\right),
\end{aligned}
$$

where r_{ii}^{c} is the cofactor of r_{ii} in $\boldsymbol{R}$. By plugging the $t_i, i \in [1, M]$ into Eq (A.8), we have,

$$
\begin{aligned}
P_e &= \sum_{i=1}^{M} t_i \\
&= \frac{1}{2M}\sum_{i=1}^{M}\operatorname{erfc}\left(\sqrt{\frac{|\boldsymbol{R}|}{2|r_{ii}^{c}|}}\right) \\
&= \frac{1}{2M}\sum_{i}\operatorname{erfc}\left(\sqrt{\frac{1}{2[\boldsymbol{C}]_{ii}}}\right) \qquad \text{(A.11)}
\end{aligned}
$$

where we have used Cramer's Rule. Next let's evaluate the covariance matrix $\boldsymbol{C}$. Suppose the noise, receiver $\boldsymbol{G}$ and received block $\hat{\boldsymbol{s}}$ can be expressed as follows,

$$
\begin{aligned}
\boldsymbol{v} &= \boldsymbol{v}_{re} + j\boldsymbol{v}_{im} \\
\boldsymbol{G} &= \boldsymbol{G}_{re} + j\boldsymbol{G}_{im} \\
\hat{\boldsymbol{s}} &= \hat{\boldsymbol{s}}_{re} + j\hat{\boldsymbol{s}}_{im}
\end{aligned}
$$

where $\hat{\boldsymbol{s}}_{re}$ and $\hat{\boldsymbol{s}}_{im}$ are the real and imaginary parts of the received block, $\boldsymbol{v}_{re}$ and $\boldsymbol{v}_{im}$ are independent zero-mean real Gaussian noises with the same covariance $\sigma^2\boldsymbol{I}$, $\boldsymbol{G}_{re}$ and $\boldsymbol{G}_{im}$ are real matrices. For BPSK signals the detection at receiver is made on the real part of the received block $\hat{\boldsymbol{s}}_{re}$. From $\hat{\boldsymbol{s}}_{re} = \boldsymbol{s} + \boldsymbol{G}_{re}\boldsymbol{v}_{re} - \boldsymbol{G}_{im}\boldsymbol{v}_{im}$, we have $\hat{\boldsymbol{s}}_{re} \sim \mathcal{N}\Big(\boldsymbol{s}, \sigma^2(\boldsymbol{G}_{re}\boldsymbol{G}_{re}^{T} + \boldsymbol{G}_{im}\boldsymbol{G}_{im}^{T})\Big)$. Thus the covariance matrix $\boldsymbol{C}$ for BPSK is:

$$
\begin{aligned}
\boldsymbol{C} &= \sigma^2(\boldsymbol{G}_{re}\boldsymbol{G}_{re}^{T} + \boldsymbol{G}_{im}\boldsymbol{G}_{im}^{T}) \qquad \text{(A.12)} \\
&= \sigma^2(\boldsymbol{G}\boldsymbol{G}^{H}) \qquad \text{(A.13)}
\end{aligned}
$$

For QPSK signals, the transmitting block $\boldsymbol{s}$ can be expressed as $\boldsymbol{s} = \boldsymbol{s}_{re} + j\boldsymbol{s}_{im}$, where the real part $\boldsymbol{s}_{re}$ and imaginary part $\boldsymbol{s}_{im}$ are BPSK signals. The received block is,

$$\hat{\boldsymbol{s}}_{re} = \boldsymbol{s}_{re} + \boldsymbol{G}_{re}\boldsymbol{v}_{re} - \boldsymbol{G}_{im}\boldsymbol{v}_{im} \tag{A.14}$$

$$\hat{\boldsymbol{s}}_{im} = \boldsymbol{s}_{im} + \boldsymbol{G}_{re}\boldsymbol{v}_{im} + \boldsymbol{G}_{im}\boldsymbol{v}_{re} \tag{A.15}$$

The detection of QPSK signals is performed on the real part and imaginary part of the received blocks independently, the block bit error rate for a transmitted block $\boldsymbol{s}$ is calculated by the average over that of real part and imaginary part, i.e. $P_{e|\boldsymbol{s}} = \frac{1}{2}(P_{e|\boldsymbol{s}_{re}} + P_{e|\boldsymbol{s}_{im}})$. From Eqs (A.14) and (A.15), the received real and imaginary parts are both Gaussian distributed, $\hat{\boldsymbol{s}}_{re} \sim \mathcal{N}\Big(\boldsymbol{s}_{re}, (\boldsymbol{G}_{re}\boldsymbol{G}_{re}^T + \boldsymbol{G}_{im}\boldsymbol{G}_{im}^T)\sigma^2\Big)$, and $\hat{\boldsymbol{s}}_{im} \sim \mathcal{N}\Big(\boldsymbol{s}_{im}, (\boldsymbol{G}_{re}\boldsymbol{G}_{re}^T + \boldsymbol{G}_{im}\boldsymbol{G}_{im}^T)\sigma^2\Big)$. They have the same covariance matrix which is also the same as in Eq (A.12) when the transmitting signals are BPSK. Because $\boldsymbol{s}_{re}$ and $\boldsymbol{s}_{im}$ are both BPSK signals, the bit error rate for the real part and imaginary part are the same, $P_{e|\boldsymbol{s}_{re}} = P_{e|\boldsymbol{s}_{im}}$. Therefore the block bit error rate for QPSK becomes $P_e = P_e(\hat{\boldsymbol{s}}_{re}|\boldsymbol{s}_{re}) = P_e(\hat{\boldsymbol{s}}_{im}|\boldsymbol{s}_{im})$. Insetting Eq (A.13) into Eq (A.11), we can concluded that the block bit error rate for BPSK and QPSK obeys the same formula:

$$P_e = \frac{1}{2M}\sum_{i=1}^{M} \operatorname{erfc}\Big(\frac{1}{\sqrt{2\sigma^2[\boldsymbol{G}\boldsymbol{G}^H]_{ii}}}\Big)$$

where $[\boldsymbol{G}\boldsymbol{G}^H]_{ii}$ denotes the ith diagonal entry of $\boldsymbol{G}\boldsymbol{G}^H$. □

Appendix B

Some Derivatives with Respect to a Complex Matrix

In this section, we derive the derivatives of some trace functions with respect to a complex matrix. The formula for the derivatives of trace functions with respect to a real matrix can be found in many references; eg, [3], [11], [12] and [20]. In the derivation, we follow the definition of differentiation with respect to a complex matrix given in [21] which can be expressed as follows:

Suppose $\phi(\boldsymbol{X})$ is a function of complex matrix $\boldsymbol{X}$, and $\boldsymbol{X} = \boldsymbol{X}_1 + j\boldsymbol{X}_2$, where $\boldsymbol{X}_1$ and $\boldsymbol{X}_2$ are real, then $\frac{\partial \phi(\boldsymbol{X})}{\partial \boldsymbol{X}} = \frac{1}{2}(\frac{\partial \phi(\boldsymbol{X})}{\partial \boldsymbol{X}_1} - j\frac{\partial \phi(\boldsymbol{X})}{\partial \boldsymbol{X}_2})$.

We are going to derive $\frac{\partial tr(\boldsymbol{X}^H \boldsymbol{A}\boldsymbol{X}\boldsymbol{B})}{\partial \boldsymbol{X}}$. In this case $\phi(\boldsymbol{X}) = tr(\boldsymbol{X}^H \boldsymbol{A}\boldsymbol{X}\boldsymbol{B})$, and $\boldsymbol{A}$ and $\boldsymbol{B}$ are real matrices, and $\boldsymbol{X}$ is complex. Inserting $\boldsymbol{X} = \boldsymbol{X}_1 + j\boldsymbol{X}_2$ into $\phi(\boldsymbol{X})$, we have

$$\begin{aligned}
\phi(\boldsymbol{X}) &= tr\big((\boldsymbol{X}_1^T - j\boldsymbol{X}_2^T)\boldsymbol{A}(\boldsymbol{X}_1 + j\boldsymbol{X}_2)\boldsymbol{B}\big) \\
&= tr\big(\boldsymbol{X}_1^T\boldsymbol{A}\boldsymbol{X}_1\boldsymbol{B} - j\boldsymbol{X}_2^T\boldsymbol{A}\boldsymbol{X}_1\boldsymbol{B} + \boldsymbol{X}_2^T\boldsymbol{A}\boldsymbol{X}_2\boldsymbol{B} + j\boldsymbol{X}_1^T\boldsymbol{A}\boldsymbol{X}_2\boldsymbol{B}\big) \\
&= tr(\boldsymbol{X}_1^T\boldsymbol{A}\boldsymbol{X}_1\boldsymbol{B} + \boldsymbol{X}_2^T\boldsymbol{A}\boldsymbol{X}_2\boldsymbol{B}) + jtr(\boldsymbol{X}_1^T\boldsymbol{A}\boldsymbol{X}_2\boldsymbol{B} - j\boldsymbol{X}_2^T\boldsymbol{A}\boldsymbol{X}_1\boldsymbol{B}). \qquad \text{(B.1)}
\end{aligned}$$

Since the real part and imaginary part in the right side of Eq (B.1) are the trace function of real matrices, we can use the formula of the derivative of the trace with respect to a real

matrix [3], [11], [12] and [20]. Therefore,

$$\begin{aligned}
\frac{\partial \phi(\boldsymbol{X})}{\partial \boldsymbol{X}_1} &= \boldsymbol{A}\boldsymbol{X}_1\boldsymbol{B} + \boldsymbol{A}^T\boldsymbol{X}_1\boldsymbol{B}^T - j(\boldsymbol{X}_2^T\boldsymbol{A})^T\boldsymbol{B}^T + j\boldsymbol{A}\boldsymbol{X}_2\boldsymbol{B} \\
&= \boldsymbol{A}\boldsymbol{X}_1\boldsymbol{B} + \boldsymbol{A}^T\boldsymbol{X}_1\boldsymbol{B}^T - j\boldsymbol{A}^T\boldsymbol{X}_2\boldsymbol{B}^T + j\boldsymbol{A}\boldsymbol{X}_2\boldsymbol{B}, \\
\frac{\partial \phi(\boldsymbol{X})}{\partial \boldsymbol{X}_2} &= \boldsymbol{A}\boldsymbol{X}_2\boldsymbol{B} + \boldsymbol{A}^T\boldsymbol{X}_2\boldsymbol{B}^T - j\boldsymbol{A}\boldsymbol{X}_1\boldsymbol{B} + j(\boldsymbol{X}_1^T\boldsymbol{A})^T\boldsymbol{B}^T \\
&= \boldsymbol{A}\boldsymbol{X}_2\boldsymbol{B} + \boldsymbol{A}^T\boldsymbol{X}_2\boldsymbol{B}^T - j\boldsymbol{A}\boldsymbol{X}_1\boldsymbol{B} + j\boldsymbol{A}^T\boldsymbol{X}_1\boldsymbol{B}^T,
\end{aligned}$$

Hence,

$$\frac{\partial \phi(\boldsymbol{X})}{\partial \boldsymbol{X}_1} - j\frac{\partial \phi(\boldsymbol{X})}{\partial \boldsymbol{X}_2} = 2\boldsymbol{A}\boldsymbol{X}_1\boldsymbol{B} - 2j\boldsymbol{A}^T\boldsymbol{X}_2\boldsymbol{B}^T,$$

and finally,

$$\frac{\partial tr\left(\boldsymbol{X}^H\boldsymbol{A}\boldsymbol{X}\boldsymbol{B}\right)}{\partial \boldsymbol{X}} = \boldsymbol{A}\boldsymbol{X}_1\boldsymbol{B} - j\boldsymbol{A}^T\boldsymbol{X}_2\boldsymbol{B}^T.$$

Appendix C

The Extra Power for CP System

From the discussion in Section 3.3, the extra power used to transmit the cyclic prefix is $p_{\text{extra}} = \sum_{i=M-L+1}^{M} \boldsymbol{f}_i \boldsymbol{f}_i^H$, where $\boldsymbol{f}_i$ is the ith row in $\boldsymbol{F}$. We will show that the extra power for CP-OFDM, CP-MBER and water-filling DMT precoders are the same, the value is $p_{\text{extra}} = \frac{Lp_0}{M}$; a constant which depends on the ratio of the length of cyclic prefix L and the block size M and the power transmitting the data block p_0.

C.1 The extra power for CP-OFDM precoder

Because the CP-OFDM precoder is a scaled unitary matrix, i.e. $\boldsymbol{F}_{\text{CP-OFDM}} = \sqrt{\frac{p_0}{M}}\boldsymbol{D}^H$, it is easy to see that the extra power for CP-OFDM precoder is $p_{\text{extra-OFDM}} = \frac{Lp_0}{M}$.

C.2 The extra power for CP-MBER precoder

From Eq (3.30), the CP-MBER precoder is

$$\boldsymbol{F}_{\text{CP-MBER}} = \sqrt{\frac{p_0}{tr\big((\boldsymbol{\Delta}_H^{-1}\boldsymbol{\Delta}_H^{-H})^{\frac{1}{2}}\big)}}\boldsymbol{D}^H\boldsymbol{P}(\boldsymbol{\Delta}_H^{-1}\boldsymbol{\Delta}_H^{-H})^{\frac{1}{4}}\boldsymbol{P}^H\boldsymbol{D}.$$

Therefore the ith diagonal element of $\boldsymbol{F}_{\text{CP-MBER}}\boldsymbol{F}_{\text{CP-MBER}}^{H}$ is,

$$\begin{aligned}[\boldsymbol{F}_{\text{CP-MBER}}\boldsymbol{F}_{\text{CP-MBER}}^{H}]_{ii} &= \frac{p_0}{tr\big((\boldsymbol{\Delta}_H^{-1}\boldsymbol{\Delta}_H^{-H})^{\frac{1}{2}}\big)}[\boldsymbol{D}^H\boldsymbol{P}(\boldsymbol{\Delta}_H^{-1}\boldsymbol{\Delta}_H^{-H})^{\frac{1}{4}}\boldsymbol{P}^H\boldsymbol{D}\boldsymbol{D}^H\boldsymbol{P}(\boldsymbol{\Delta}_H^{-1}\boldsymbol{\Delta}_H^{-H})^{\frac{1}{4}}\boldsymbol{P}^H\boldsymbol{D}]_{ii} \\ &= \frac{p_0}{tr\big((\boldsymbol{\Delta}_H^{-1}\boldsymbol{\Delta}_H^{-H})^{\frac{1}{2}}\big)}[\boldsymbol{D}^H\boldsymbol{P}(\boldsymbol{\Delta}_H^{-1}\boldsymbol{\Delta}_H^{-H})^{\frac{1}{2}}\boldsymbol{P}^H\boldsymbol{D}]_{ii} \\ &= \frac{p_0}{tr\big((\boldsymbol{\Delta}_H^{-1}\boldsymbol{\Delta}_H^{-H})^{\frac{1}{2}}\big)}\sum_{j=1}^{M}[\boldsymbol{P}(\boldsymbol{\Delta}_H^{-1}\boldsymbol{\Delta}_H^{-H})^{\frac{1}{2}}\boldsymbol{P}^H]_{jj}|d_{ij}|^2 \qquad \text{(C.1)}\end{aligned}$$

where $[\boldsymbol{P}(\boldsymbol{\Delta}_H^{-1}\boldsymbol{\Delta}_H^{-H})^{\frac{1}{2}}\boldsymbol{P}^H]_{jj}$ is the $j$the diagonal element in $\boldsymbol{P}(\boldsymbol{\Delta}_H^{-1}\boldsymbol{\Delta}_H^{-H})^{\frac{1}{2}}\boldsymbol{P}^H$, and d_{ij} is the i,jth element in $\boldsymbol{D}$. Recall that $|d_{ij}|^2 = \frac{1}{M}$. Therefore, Eq (C.1) becomes

$$\begin{aligned}[\boldsymbol{F}_{\text{CP-MBER}}\boldsymbol{F}_{\text{CP-MBER}}^{H}]_{ii} &= \frac{p_0}{tr\big(\boldsymbol{P}(\boldsymbol{\Delta}_H^{-1}\boldsymbol{\Delta}_H^{-H})^{\frac{1}{2}}\boldsymbol{P}^H\big)}\,\frac{tr\big((\boldsymbol{\Delta}_H^{-1}\boldsymbol{\Delta}_H^{-H})^{\frac{1}{2}}\big)}{M} \\ &= \frac{p_0}{tr\big((\boldsymbol{\Delta}_H^{-1}\boldsymbol{\Delta}_H^{-H})^{\frac{1}{2}}\big)}\,\frac{tr\big((\boldsymbol{\Delta}_H^{-1}\boldsymbol{\Delta}_H^{-H})^{\frac{1}{2}}\big)}{M} \\ &= \frac{p_0}{M}.\end{aligned}$$

Hence, the extra power to transmit cyclic prefix for CP-MBER precoder is

$$\begin{aligned}p_{extra-CPMBER} &= \sum_{i=M-L+1}^{M}[\boldsymbol{F}_{\text{CP-MBER}}\boldsymbol{F}_{\text{CP-MBER}}^{H}]_{ii} \\ &= \frac{Lp_0}{M}. \qquad \text{(C.2)}\end{aligned}$$

That is, the extra power for CP-MBER precoder is $p_{\text{extra-CPMBER}} = \frac{Lp_0}{M}$.

C.3 The extra power for water-filling DMT precoder

From Eq (3.43), the water-filling DMT precoder is

$$\boldsymbol{F}_{\text{WF-DMT}} = \boldsymbol{D}^H\boldsymbol{\Delta}_T$$

where $[\boldsymbol{\Delta}_T]_{ii}$ takes the form in Eq (3.45). The ith diagonal element of $\boldsymbol{F}_{\text{WF-DMT}}\boldsymbol{F}_{\text{WF-DMT}}^H$ is,

$$\begin{aligned}[\boldsymbol{F}_{\text{WF-DMT}}\boldsymbol{F}_{\text{WF-DMT}}^H]_{ii} &= [\boldsymbol{D}^H\boldsymbol{\Delta}_T\boldsymbol{\Delta}_T^H\boldsymbol{D}]_{ii} \\ &= \sum_{j=1}^{M}[\boldsymbol{\Delta}_T\boldsymbol{\Delta}_T^H]_{jj}|d_{ij}|^2 \\ &= \frac{tr(\boldsymbol{\Delta}_T\boldsymbol{\Delta}_T^H)}{M} \\ &= \frac{p_0}{M}\end{aligned}$$

The extra power for water-filling DMT is

$$\begin{aligned}p_{\text{extra-DMT}} &= \sum_{i=M-L+1}^{M}[\boldsymbol{F}_{\text{WF-DMT}}\boldsymbol{F}_{\text{WF-DMT}}^H]_{ii} \\ &= \frac{Lp_0}{M}.\end{aligned} \tag{C.3}$$

Therefore the extra power for water-filling DMT is $p_{\text{extra-DMT}} = \frac{Lp_0}{M}$.

Appendix D

Proof of (3.17) and (4.22)

Eqs (3.17) and (4.22) are the solutions for the precoders based on the criteria of MMSE and maximum information rate respectively. The derivations can be found in [28] and [27]. For the completeness of the thesis, we include the derivations in this appendix.

D.1 Proof of (3.17)

Proof. The constraint optimization problem is:

$$\min_{\boldsymbol{A}} tr(\boldsymbol{A}^{-1}\boldsymbol{Q}\boldsymbol{A}^{-H}) \tag{D.1}$$

$$\text{subject to} \quad tr(\boldsymbol{A}\boldsymbol{A}^{H}) \leq p_0. \tag{D.2}$$

where $\boldsymbol{Q} = (\boldsymbol{H}^{H}\boldsymbol{H})^{-1}$. We construct the Lagrangian function:

$$J = tr(\boldsymbol{A}^{-1}\boldsymbol{Q}\boldsymbol{A}^{-H}) + \mu\big(tr(\boldsymbol{A}\boldsymbol{A}^{H}) - p_0\big), \tag{D.3}$$

$$= tr(\boldsymbol{B}^{-1}\boldsymbol{Q}) + \mu\big(tr(\boldsymbol{B}) - p_0\big), \tag{D.4}$$

where μ is the Lagrangian multiplier, and

$$\boldsymbol{B} = \boldsymbol{A}\boldsymbol{A}^{H}. \tag{D.5}$$

By taking the first derivative of the Lagrangian function with respect to $\boldsymbol{B}$ and μ, we have,

$$\frac{\partial J}{\partial \boldsymbol{B}} = -(\boldsymbol{B}^{-1}\boldsymbol{Q}\boldsymbol{B}^{-1})^T + \mu \boldsymbol{I} \tag{D.6}$$

$$\frac{\partial J}{\partial \mu} = tr(\boldsymbol{B}) - p_0 \tag{D.7}$$

Setting Eqs (D.6) and (D.7) to zero, we have,

$$-(\boldsymbol{B}^{-1}\boldsymbol{Q}\boldsymbol{B}^{-1})^T + \mu \boldsymbol{I} = \boldsymbol{0} \tag{D.8}$$

$$tr(\boldsymbol{B}) - p_0 = 0 \tag{D.9}$$

Recall that $\boldsymbol{Q}$ is Hermitian, its eigen-decomposition has the form $\boldsymbol{Q} = \boldsymbol{W}\boldsymbol{\Lambda}\boldsymbol{W}^H$. Therefore Eq (D.8) becomes,

$$\boldsymbol{W}\boldsymbol{\Lambda}\boldsymbol{W}^H = \mu \boldsymbol{B}^2$$

$$\Longrightarrow \quad \boldsymbol{W}\boldsymbol{\Lambda}^{\frac{1}{2}}\boldsymbol{W}^H = \sqrt{\mu}\boldsymbol{B} \tag{D.10}$$

$$\Longrightarrow \quad tr(\boldsymbol{\Lambda}^{\frac{1}{2}}) = \sqrt{\mu} tr(\boldsymbol{B}) \tag{D.11}$$

From Eq (D.9) and (D.11), we have $\sqrt{\mu} = \frac{tr(\boldsymbol{\Lambda}^{\frac{1}{2}})}{p_0}$. From Eq (D.10), we have $\boldsymbol{B} = \frac{p_0}{tr(\boldsymbol{\Lambda}^{\frac{1}{2}})}\boldsymbol{W}\boldsymbol{\Lambda}^{\frac{1}{2}}\boldsymbol{W}^H$. From Eq (D.5), the solution for $\boldsymbol{A}$ is $\boldsymbol{A} = \boldsymbol{B}^{\frac{1}{2}}\boldsymbol{N}$, where $\boldsymbol{N}$ is an arbitrary unitary matrix. Hence,

$$\begin{aligned}\boldsymbol{A} &= \sqrt{\frac{p_0}{tr(\boldsymbol{\Lambda}^{\frac{1}{2}})}}\boldsymbol{W}\boldsymbol{\Lambda}^{\frac{1}{4}}\boldsymbol{W}^H\boldsymbol{N} \\ &= \sqrt{\frac{p_0}{tr(\boldsymbol{\Lambda}^{\frac{1}{2}})}}\boldsymbol{W}\boldsymbol{\Lambda}^{\frac{1}{4}}\boldsymbol{U}\end{aligned}$$

where $\boldsymbol{U} = \boldsymbol{W}^H\boldsymbol{N}$ is an arbitrary unitary matrix.

(In the derivation we have assumed that the matrices in Eq (D.4) are real, however the same result holds for complex case; the proof is omitted here.) □

D.2 Proof of (4.22)

Proof. Consider a vector model $\hat{\boldsymbol{s}} = \boldsymbol{GHu} + \boldsymbol{Gv}$, the normalized (per input symbol) mutual information, $I(\boldsymbol{u}; \hat{\boldsymbol{s}})$, between any block $\boldsymbol{u}$ of P channel input symbols and the corresponding block $\hat{\boldsymbol{s}}$ of M receiver output symbols is maximized when $\boldsymbol{u}$ is Gaussian, and is given by [27],

$$I(\boldsymbol{u}; \hat{\boldsymbol{s}}) = \frac{1}{P} \log_2 |\big(\boldsymbol{I} + (\boldsymbol{GH})^T (\boldsymbol{G}\boldsymbol{R}_{vv}\boldsymbol{G}^H)^{-1} (\boldsymbol{GH})\big)\boldsymbol{R}_{uu}|. \tag{D.12}$$

In this case $\boldsymbol{u} = \boldsymbol{Fs}$, therefore $\boldsymbol{R}_{uu} = \boldsymbol{F}\boldsymbol{R}_{ss}\boldsymbol{F}^H = \boldsymbol{F}\boldsymbol{F}^H$. From the assumptions of the thesis, we have $\boldsymbol{R}_{vv} = \sigma^2 \boldsymbol{I}$, and $\boldsymbol{GHF} = \boldsymbol{I}$, therefore Eq (D.12) becomes,

$$I(\boldsymbol{u}; \hat{\boldsymbol{s}}) = \frac{1}{P} \log_2 |\boldsymbol{I} + \sigma^{-2} \boldsymbol{H}^H \boldsymbol{H} \boldsymbol{F} \boldsymbol{F}^H|. \tag{D.13}$$

Suppose the singular decomposition of $\boldsymbol{F}$ can be written $\boldsymbol{F} = \boldsymbol{M}\boldsymbol{\Phi}\boldsymbol{N}^H$, where $\boldsymbol{M}, \boldsymbol{N}$ are unitary, $\boldsymbol{\Phi}$ is diagonal. From $\boldsymbol{Q} = (\boldsymbol{H}^H\boldsymbol{H})^{-1} = \boldsymbol{W}\boldsymbol{\Lambda}\boldsymbol{W}^H$, we have $\boldsymbol{H}^H\boldsymbol{H} = \boldsymbol{W}\boldsymbol{\Lambda}^{-1}\boldsymbol{W}^H$. Inserting $\boldsymbol{H}^H\boldsymbol{H}$ and $\boldsymbol{F}$ into Eq (D.13), we have,

$$I(\boldsymbol{u}; \hat{\boldsymbol{s}}) = \frac{1}{P} \log_2 |\boldsymbol{I} + \sigma^{-2} \boldsymbol{W}\boldsymbol{\Lambda}^{-1}\boldsymbol{W}^H \boldsymbol{M}\boldsymbol{\Phi}\boldsymbol{\Phi}^H\boldsymbol{M}^H|. \tag{D.14}$$

The matrix product $\boldsymbol{W}^H\boldsymbol{M}$ is another unitary matrix, we denote it as $\boldsymbol{P}$, i.e., $\boldsymbol{W}^H\boldsymbol{M} = \boldsymbol{P}$. Hence Eq (D.14) can be further written as,

$$\begin{aligned} I(\boldsymbol{u}; \hat{\boldsymbol{s}}) &= \frac{1}{P} \log_2 |\boldsymbol{I} + \sigma^{-2} \boldsymbol{M}\boldsymbol{P}^H\boldsymbol{\Lambda}^{-1}\boldsymbol{P}\boldsymbol{\Phi}\boldsymbol{\Phi}^H\boldsymbol{M}^H| \\ &= \frac{1}{P} \log_2 |\boldsymbol{I} + \sigma^{-2} \boldsymbol{P}^H\boldsymbol{\Lambda}^{-1}\boldsymbol{P}\boldsymbol{\Phi}\boldsymbol{\Phi}^H|. \end{aligned} \tag{D.15}$$

According to Hadamard's inequality, to maximize the determinant in the right side of Eq (D.15), matrix $\boldsymbol{P}^H\boldsymbol{\Lambda}^{-1}\boldsymbol{P}\boldsymbol{\Phi}\boldsymbol{\Phi}^H$ must be diagonal. Since $\boldsymbol{\Lambda}^{-1}$ and $\boldsymbol{\Phi}\boldsymbol{\Phi}^H$ are both diagonal, $\boldsymbol{P}$ must be a permutation matrix. For simplicity, we choose $\boldsymbol{P} = \boldsymbol{I}$, therefore

$$\boldsymbol{M} = \boldsymbol{W}^H. \tag{D.16}$$

Then Eq (D.15) becomes,

$$I(\boldsymbol{u};\hat{\boldsymbol{s}}) = \frac{1}{P}\log_2|\boldsymbol{I} + \sigma^{-2}\boldsymbol{\Lambda}^{-1}\boldsymbol{\Phi}\boldsymbol{\Phi}^H|.$$

Considering the power constraint $tr(\boldsymbol{F}\boldsymbol{F}^H) = tr(\boldsymbol{\Phi}\boldsymbol{\Phi}^H) \leq p_0$, the optimization problem is,

$$\max_{\boldsymbol{F}} \frac{1}{P}\log_2|\boldsymbol{I} + \sigma^{-2}\boldsymbol{\Lambda}^{-1}\boldsymbol{\Phi}\boldsymbol{\Phi}^H|$$
$$\text{subject to} \quad tr(\boldsymbol{\Phi}\boldsymbol{\Phi}^H) \leq p_0.$$

We construct the Lagrangian function as follows:

$$\begin{aligned} J &= \frac{1}{P}\log_2|\boldsymbol{I} + \sigma^{-2}\boldsymbol{\Lambda}^{-1}\boldsymbol{\Phi}\boldsymbol{\Phi}^H| - \mu\big(tr(\boldsymbol{\Phi}\boldsymbol{\Phi}^H) - p_0\big) \\ &= \frac{1}{P}\sum_{i=1}^{M}\log_2\big(1 + \frac{|\phi|_{ii}^2}{\sigma^2\lambda_{ii}}\big) - \mu\Big(\sum_{i=1}^{M}|\phi|_{ii}^2 - p_0\Big), \end{aligned} \tag{D.17}$$

where μ is the Lagrangian multiplier. Taking the partial derivatives of the Lagrangian with respect to $|\phi|_{ii}^2$, we get,

$$\frac{\partial J}{\partial|\phi|_{ii}^2} = \frac{\log_2(e)}{P\big(1 + \frac{|\phi|_{ii}^2}{\sigma^2\lambda_{ii}}\big)}\frac{1}{\sigma^2\lambda_{ii}} - \mu \tag{D.18}$$

By setting Eq (D.18) to zero, we get,

$$|\phi|_{ii}^2 = \frac{\log_2(e)}{P\mu} - \sigma^2\lambda_{ii}. \tag{D.19}$$

By the constraint of the power, $\sum_{i=1}^{M}|\phi|_{ii}^2 = p_0$, and Eq (D.19), we obtain,

$$\frac{\log_2(e)}{P\mu} = \frac{p_0 + \sigma^2 tr(\boldsymbol{\Lambda})}{M} \tag{D.20}$$

From Eqs (D.19) and (D.20), we have

$$|\phi|_{ii}^2 = \frac{p_0 + \sigma^2 tr(\boldsymbol{\Lambda})}{M} - \sigma^2\lambda_{ii} \tag{D.21}$$

$$\Longrightarrow \quad \phi_{ii} = \sqrt{\max\{\frac{p_0 + \sigma^2 tr(\boldsymbol{\Lambda})}{M} - \sigma^2 \lambda_{ii}, 0\}} \tag{D.22}$$

From Eq (D.16), we have $\boldsymbol{F} = \boldsymbol{W}\boldsymbol{\Phi}\boldsymbol{N}^H$, where the unitary matrix $\boldsymbol{N}^H$ is a degree of freedom; any unitary matrix satisfies the condition of maximum mutual information $I(\boldsymbol{u}; \hat{\boldsymbol{s}})$ in Eq (D.13). Denote $\boldsymbol{N}^H$ as $\boldsymbol{U}$, where $\boldsymbol{U}$ is an arbitrary unitary matrix, therefore the solution for $\boldsymbol{F}$ is,

$$\boldsymbol{F} = \boldsymbol{W}\boldsymbol{\Phi}\boldsymbol{U} \tag{D.23}$$

where the ith diagonal element of $\boldsymbol{\Phi}$ is determined by Eq (D.22). □

Bibliography

[1] A. R. S. Bahai and B. R. Saltzberg, *Multi-Carrier Digital Communications — Theory and Applications of OFDM.* Kluwer Academic/Plenmum Publishers, New York, 1999.

[2] S. Barnett, *Matrices — Methods and Applications.* Clarendon Press, Oxford, 1990.

[3] J. W. Brewer, "Kronecker products and matrix calculus in system theory," *IEEE Transactions on Circuits and Systems*, vol. CAS–25, pp. 772–781, Sep. 1978.

[4] P. S. Chow, J. M. Cioffi and J. A. C. Bingham, "A practical discrete multitone transceiver loading algorithm for data transmission over spectrally shaped channels," *IEEE Transactions on Communications*, vol. 43, pp. 773–775, Feb/Mar/Apr. 1995.

[5] J. S. Chow, J. C. Tu and J. M. Cioffi, "Performance evaluation of a multichannel transceiver system for ADSL and VHDSL receivers," *IEEE Journal on Selected area in Communications*, vol 9, pp. 909–919, Aug. 1991.

[6] J. S. Chow, J. C. Tu and J. M. Cioffi, "A discrete multitone transceiver system for HDSL applications," *IEEE Journal on Selected Areas in Communications*, vol. 9, pp. 895–908, Aug. 1991.

[7] T. M. Cover and J. A. Thomas, *Elements of Information Theory.* John Wiley & Sons, New York, 1991.

[8] C. N. Dorny, *A Vector Space Approach to Models and Optimization.* John Wiley & Sons New York, 1983.

[9] N. J. Fliege, "Orthogonal multiple carrier data transmission," *European Transactions on Telecommunications*, vol. 3, pp. 255–264, May 1992.

[10] G. D. Forney and M. V. Eyuboğlu, "Combined equalization and coding using precoding," *IEEE Communication Magazine*, pp. 25–34, Dec. 1991.

[11] A. Graham, *Kronecker Products and Matrix Calculus with Applications.* Ellis Horwood Limited, 1981.

[12] F. A. Graybill, *Matrices with Applications in Statistics.* 2nd Edition, Wadsworth International, Belmont, California, 1983.

[13] H. Harashima and H. Miyakawa, "Matched-transmission technique for channel with intersymbol interference," *IEEE Transactions on Communications*, vol. COM-20, pp. 774–780, Aug. 1972.

[14] S. Haykin, *Communication Systems.* 3rd edition, John Wiley & Sons, New York, 1994.

[15] B. S. Krongold, K. Ramchandran, and D. L. Jones, "Computationally efficient optimal power allocation algorithms for multicarrier communication systems," *IEEE Transactions on Communications*, vol. 48, pp. 23–27, Jan. 2000.

[16] J. W. Lechleider, "High bit rate digital subscriber lines: A review of HDSL progress," *IEEE Journal on Selected Areas in Communications*, vol. 9, pp. 769–784, Aug. 1991.

[17] Z-Q. Luo, T. N. Davidson, G. B. Giannakis and K. M. Wong, "Transceiver optimization for multiple acces through ISI channel," submitted, June 2001.

[18] J. R. Magnus and H. Neudecker, *Matrix Differential Calculus with Application in Statistics and Economics.* John Wiley & Sons, New York, 1988.

[19] J. P. Milanović, T. N. Davidson, Z-Q Luo, and K. M. Wong, "Design of robust redundant precoding filterbanks," *Proceedings of International Conference on Acoustics, Speech, and Signal Processing*, Istanbul, June 2000.

[20] K. S. Miller, *Multidimensional Gaussian Distributions.* John Wiley & Sons, New York, 1964.

[21] K. S. Miller, *Complex Stochastic Process — An Introduction to Theory and Application.* Addison-Wesley Publishing Company, 1974.

[22] J. Nocedal, S. J. Wright, *Numerical Optimization.* Springer-Verlag, New York, 1999.

[23] J. G. Proakis, *Digital Communications.* Third edition, McGraw Hill, New York, 1995.

[24] T. S. Rappaport, *Wireless Communications Principles and Practice.* Prentice-hall, New Jersey, 1996.

[25] A. Ruiz, J. M. Cioffi and S. Kastuia, "Discrete multiple tone modulation with coset coding for the spectrally shaped channel," *IEEE Transactions on Communications*, vol. 40, pp. 1012–1029, June 1992.

[26] S. D. Sandberg and M. A. Tzannes, "Overlapped discrete multiple tone modulation for high speed copper wire communications," *IEEE Journal on Selected Areas in Communications*, vol. 13, pp. 1571–1585, Dec. 1995.

[27] A. Scaglione, S. Barbarossa, and G. B. Giannakis, "Filterbank tranceivers optimizing information rate in block transmissions over dispersive channels," *IEEE Transactions on Information Theory*, vol. 45, pp. 1988–2006, Apr. 1999.

[28] A. Scaglione, G. B. Giannakis, and S. Barbarossa, "Redundant filterbank precoders and equalizers, Parts I and II," *IEEE Transactions on Signal Processing*, vol. 47, pp. 1988–2022, July 1999.

[29] M. Tomlinson, "New automatic equalizer employing modulo arithmetic," *Electronics Letters*, vol. 7, pp. 138–139, Mar. 1971.

[30] M. K. Tsatasnis and G. B. Gianakis, "Optimal linear receiver for DS-CDMA systems: A signal processing approach," *IEEE Transactions on Signal Processing*, vol. 44, pp. 3044–3055, Dec. 1996.

[31] P. P. Vaidyanathan, *Multirate Systems and Filter Banks*. Prentice Hall, Englewood Cliffs, New Jersey, 1993.

[32] Z. Wang and G. B. Giannakis, "Wireless multicarrier communications," *IEEE Signal Processing Magazine*, pp. 29–48, May 2000.

[33] X. Wang, W. Ku and A. Antoniou, "Constrained minimum-BER multiuser detection," *IEEE Transactions on Signal Processing*, vol. 48, pp. 2903–2909, Oct. 2000.

[34] J. J. Werner, "The HDSL environment," *IEEE Journal on Selected Areas in Communications*, vol. 9, pp. 785–799, Aug. 1991.

[35] K. M. Wong, J. Wu, T. N. Davidson, and Q. Jin, "Wavelet packet division multiplexing and wavelet packet design under timing error effects," *IEEE Transactions on Signal Processing*, vol. 45, pp. 2877–2890, Dec. 1997.

[36] G. Worne, "Emerging application of multirate signal processing and wavelet in digital communications," *Proceedings of the IEEE*, vol. 84, pp. 586–603, Apr. 1996.

[37] X.-G Xia, "New precoding for intersymbol interference cancellation using nonmaximally decimated multirate filterbanks with ideal FIR equalizers ," *IEEE Transactions on Signal Processing*, vol. 45, pp. 2431–2441, Oct. 1997.

[38] W. Y. Zou and Y. Wu, "COFDM: An overview," *IEEE Transactions on Broadcasting*, vol. 41, pp. 1–8, Mar. 1995.